# NOTE TO USERS

Université d'Ottawa • University of Ottawa

# Université d'Ottawa · University of Ottawa

FACULTÉ DES ÉTUDES SUPÉRIEURES ET POSTDOCTORALES

FACULTY OF GRADUATE AND POSTDOCTORAL STUDIES

GIRGIS, Elisabeth

AUTEUR DE LA THÈSE - AUTHOR OF THESIS

M.A.Sc. (Chemical Engineering)

GRADE - DEGREE

Department of Chemical Engineering

FACULTÉ, ÉCOLE, DÉPARTEMENT - FACULTY, SCHOOL, DEPARTMENT

TITRE DE LA THÈSE - TITLE OF THE THESIS

Fuel Devolatilization in Packed Bed Wood Combustion

William Hallett

DIRECTEUR DE LA THÈSE - THESIS SUPERVISOR

EXAMINATEURS DE LA THÈSE - THESIS EXAMINERS

J. Thibault .....

J. Zhang .....

.....

J.-M. De Koninck, Ph.D.

LE DOYEN DE LA FACULTÉ DES ÉTUDES SUPÉRIEURES ET POSTDOCTORALES — SIGNATURE — DEAN OF THE FACULTY OF GRADUATE AND POSTDOCTORAL STUDIES

# FUEL DEVOLATILIZATION IN PACKED BED WOOD COMBUSTION

**Elisabeth Girgis**

Thesis submitted to the
Faculty of Graduate and Postdoctoral Studies
in partial fulfillment of the requirements for the Master of Applied Science degree
in Chemical Engineering (Environmental)

Department of Chemical Engineering
Faculty of Engineering
University of Ottawa

*Your file Votre référence*
*ISBN: 0-494-01480-6*
*Our file Notre référence*
*ISBN: 0-494-01480-6*

# ABSTRACT

Packed bed combustion is the burning of solid fuel particles supported by a grate with the combustion air supplied from below. The combustion process is divided into four main stages: drying, devolatilization, volatiles combustion and char combustion. Biomasses proposed as renewal energy sources, such as wood, have a very high volatile content (~80%). Therefore mechanistic models developed for the prediction of bed characteristics during biomass combustion must include devolatilization and volatile combustion stages in order to correctly predict combustion behaviour for better emissions control and process efficiency. A novel *in-situ* sampling method for tar, a major pyrolysis product, was developed that allows its concentration to be measured at various heights within the packed bed and appears to work satisfactorily. A series of experiments on packed bed combustion were conducted in a laboratory 'pot' type combustor. Two different equivalent particle size diameters (2.8 cm and 3.2 cm) of untreated spruce wood and two different airflow rates (0.025 $kg/m^2s$ and 0.03 $kg/m^2s$) were tested at a 22 cm bed height. Although the experimental data show scatter, the measurements indicated that pyrolysis occurred primarily within two particle diameters of the top of the bed, with large amounts of tar and CO and somewhat less $CO_2$ being produced. This research also expanded a numerical model for packed bed combustion of solid fuels with the addition of a simple first order pyrolysis reaction, in which fixed proportions of the products were set as light volatiles of CO and $CO_2$ with the balance as tar. The model results compared well with bed temperature, particle size and density measurement throughout the bed and gas concentration (CO, $CO_2$, $O_2$, and $CH_4$) measurements in the reduction and oxidation zone.

# RÉSUMÉ

La combustion de solide en lit fixe consiste à brûler une source d'énergie solide sous forme de particules sur une grille en présence d'un courant d'air ascendant. La combustion de solide à l'intérieur d'un lit fixe est souvent décrite en quatre étapes: séchage, évolution des gaz, combustion des gaz et combustion du charbon. Les biomasses proposées comme sources d'énergie renouvelable, tel que le bois, contiennent un taux élevé de substances volatiles (~80%). Donc la prise en compte de l'évolution des volatiles dans la modélisation de ce procédé devient très importante pour permettre de prédire le comportement de la combustion afin de mieux contrôler les émissions et améliorer l'efficacité des systèmes. Puisque le goudron est un produit important de la pyrolyse de la biomasse, une nouvelle méthode d'échantillonnage permettant de mesurer la quantité de goudron produite à diverses hauteurs à l'intérieur d'un lit a été développée et s'est avérée à bien fonctionner. Des essais de combustion en lit fixe ont été accomplis dans un réacteur de laboratoire de taille moyenne avec des lits 22 cm de haut. Deux différents diamètres équivalents de particules de sapin vierge (2.8 cm et 3.3 cm) et deux différents débits d'air d'alimentation (0.025 $kg/m^2s$ et 0.03 $kg/m^2s$) ont été testés. Même si les données expérimentales ont montré une certaine dispersion, les résultats indiquent que la pyrolyse se fait surtout à l'intérieur de deux diamètres de particule de la surface du lit et que le goudron et CO sont les produits principaux avec une quantité un peu moins importante de $CO_2$.

Cette recherche a aussi amélioré un modèle numérique de combustion de solide en lit fixe avec l'ajout d'une réaction de premier ordre pour l'évolution des gaz dus à la pyrolyse duquel une proportion fixe des produits a été allouée au CO et au $CO_2$ avec le reste étant du goudron. Les résultats du modèle se comparent bien avec les données expérimentales de

température, grosseur et densité des particules à travers le lit ainsi qu'avec les concentrations de gaz ($CO$, $CO_2$, $O_2$, et $CH_4$) dans les sections d'oxydation et de réduction.

# ACKNOWLEDGEMENTS

The author gratefully acknowledges financial support from NSERC. The mechanical engineering technicians in the shop at the University of Ottawa are acknowledged for their precision machining, arc-welding and other skills required to construct the experimental apparatus. Louis Tremblay and Dr. R.L. Droste are acknowledged for their assistance and the use of the precision scale required for the proximate analysis and tar measurements. The assistance of Nicole Clark during some of the combustion runs is also acknowledged.

A special thanks and sincere gratitude is given to Dr. Hallett for his guidance and assistance throughout this project. His knowledge of the technical subject matter and enthusiasm for learning has allowed this process to be enriching and fun.

À ma famille et Jeff, je vous dois un remerciement profond pour votre aide et votre encouragement. Vous rendez la vie intéressante et me permettez l'indulgence de prendre le temps de mieux connaître au sujet des étincelles qui font briller le monde.

# NOMENCLATURE

| | |
|---|---|
| A | length of particle (cm) |
| A | pre-exponential parameter ($s^{-1}$) |
| $a_{BC}$ | fuel particle specific surface area ($m^2/m^3$) |
| b | height of particle (cm) |
| $B_t$ | thermal transfer number |
| $B_i$ | mass transfer number |
| C | mass fraction of char |
| c | width of particle (cm) |
| $c_p$ | specific heat (J/kgK) |
| d | equivalent particle diameters (cm) |
| $d_{macropore}$ | macro-pore diameter (m) |
| E | activation energy (kJ/mol) |
| G | rate of production char combustion ($kg/m^3s$) |
| $G_P$ | tar production rate ($kg/m^3s$) |
| $G_V$ | mass flux of pyrolysis gas from the particle surface ($kg/m^2$ surface/s) |
| h | heat transfer coefficient for convection ($W/m^2K$) |
| $h_{sg}$ | heat transfer coefficient from the gas to the solid ($W/m^2K$) |
| $h_{sgo}$ | heat transfer coefficient without mass transfer ($W/m^2K$) |
| $H_p$ | enthalpy of pyrolysis (kJ/kg) |
| $k_{eff}$ | thermal conductivity of the bed (W/mK) |
| $k_{Yi}$ | mass transfer coefficient for species i ($kg/m^2s$) |
| k | thermal conductivity (W/mK) |
| $k_{rad}$ | diffusive contribution from radiation heat transfer (W/mK) |
| Le | Lewis number of the gas |
| Pr | Prandtl |
| r | rate of production of gaseous species per unit volume ($kg/m^3$) |
| Re | Reynolds |
| $S_1$ | mass stoichiometry of the $C+O_2$ reaction |
| $S_2$ | mass stoichiometry of the $C+CO_2$ reaction |
| T | temperature (K) |
| $T_2$ | effective radiating temperature of the surroundings (K) |
| $X_F$ | volume fraction of fuel in the total solids (ash + fuel) |
| $Y_{PR}$ | fraction of tar at the particle surface |
| $Y_{i\infty}$ | mass fraction surrounding the particle |
| $Y_{iR}$ | mass fraction at the particle surface |
| $Y_W$ | mass fraction of unconverted wood in a particle |
| $Y_C, Y_{char}$ | char mass fraction |
| $v_S$ | superficial velocity of the solid phase in bulk |
| W | mass fraction of original fuel unconverted |

Symbols

| | |
|---|---|
| $\alpha$ | ash mass fraction of the original fuel |
| $^{\circ}$ | value of the variable at the beginning of the time step involved |
| $\varepsilon$ | void volume |
| $\varepsilon_g^{macro}$ | macro-porosity of the gas through the charcoal structure. |
| $\Delta$ | change in given value |
| $\rho_{F0}$ | initial fuel density ($kg/m^3$) |
| $\rho_W$ | density ($kg/m^3$) |
| $\rho_F$ | fuel density ($kg/m^3$) |
| $\sigma$ | Stefan-Boltzmann constant ($5.76*10^{-8}W/m^2K^4$) |
| $\delta$ | thickness of the boundary layer on the particle (m) |
| $\psi$ | emissivity |
| $\chi$ | fixed portion of pyrolysis products |
| $\zeta_C$ | char yield |
| $\xi_i$ | fixed proportion of species i in the pyrolysis gas |
| $\gamma_i$ | proportion of species I in the total mass flux from the surface |
| $v_F$ | superficial velocity of the fuel particles as they move down in the bed (m/s) |

Subscripts

| | |
|---|---|
| A | related to the 0.020 cm thermocouple |
| B | related to the 0.038 cm thermocouple |
| CO2 | carbon dioxide |
| CO | carbon monoxide |
| c | char |
| fuel | fuel (wood +char) |
| g | gas |
| n | node to the north |
| P | pyrolysis gas |
| P | node being solved |
| S | node to the south |
| T | tar |
| V | volatiles |
| w | wood |

# TABLE OF CONTENT

# LIST OF TABLES

# LIST OF FIGURES

# 1 INTRODUCTION

Packed bed combustion is the burning of a solid fuel supported by a grate through which combustion air passes. This type of process can be found on a small scale such as a home wood stove or on a larger scale such as a spreader stoker system used to burn waste wood at a pulp and paper mill. This technology is well suited for biomass, such as wood, as it allows the top layer of fuel to be dried before it travels to the burning zone lower in the bed. Biomass typically has higher moisture content than traditional fuels such as coal. However despite the fact that packed bed wood burning has been used for centuries to supply heat, the ability to model the process is limited.

## 1.1 Internal Process

Packed bed combustion can be performed on either a stationary or traveling grate with fuel fed from above or below and air is supplied from below. **Figure 1.1** shows a cross-section of a typical stationary overfeed packed bed combustor, which operates in counter-current mode. The fuel is supplied from above and is dried in the top section of the bed by the burning char below and hot combustion gases. Once the fuel is dried, the temperature increases, allowing the release of volatiles in a process referred to as devolatilization or as pyrolysis. Devolatilization is the release of volatiles upon heating of a fuel because of thermal decomposition. The volatiles released include CO, $CO_2$, $H_2O$, tars and hydrocarbons. After devolatilization char is formed and the volatiles and char is oxidized in the bottom part of the bed (combust), releasing heat. Overfire air is often injected over the bed to complete the combustion of gaseous products.

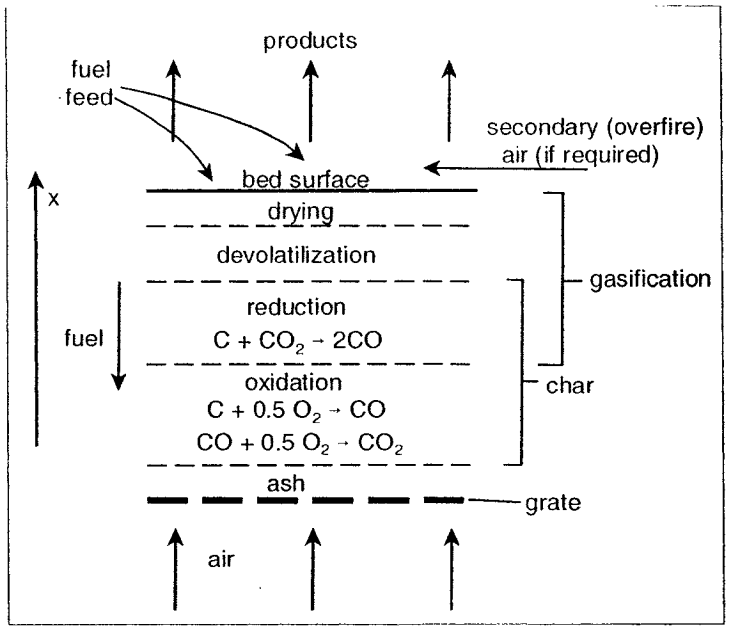


**Figure 1-1: Combustion Zones in an Overfed Packed Bed Reactor**

## 1.2 Need for Research

Packed bed combustion of biomass such as wood is relevant to two major environmental topics: renewable energy generation and waste management. Renewable energies are energy sources that allow the current generation to utilize energy without compromising the ability of future generations to meet their own needs. Based on various scenarios, up to 200-300 exajoules per year (EJ/year) of the 400 EJ/year worldwide energy demand could be supplied by biomass [Jones et al. (2000)].[1] Although perhaps ambitious, these figures indicate the significant potential of biomass in helping countries such as India and the European Union meet their renewable energy generation targets. Waste management strategies by the United States' Environmental Protection Agency and in the European Union have prioritized thermal treatment of

[1] 1 EJ = $10^{18}$J. This estimate includes adoption of genetic modification

municipal waste over landfilling because of reduced greenhouse gas emissions and the opportunity to collect energy [USEPA (1998), European Environment Agency (1999)]. In both areas, the ability to model the internal processes of solid phase biomass combustion will allow a greater control of the processes, thereby helping to reduce energy production cost and air quality impacts. The various after-treatment processes such as flares, scrubbers or adsorption columns will all benefit from a combustion process that can be properly modeled and controlled.

Combustor design and fuel characteristics will greatly affect whether the advantages outweigh the disadvantages of using biomass combustion as an energy source or waste treatment method. As volatiles compose about 80 wt% of the typical biomass fuel, the inclusion of devolatilization in a combustion process model is essential [World Bank (1999)].

## 1.3 Scope of Research

The main purpose of this work was to understand biomass combustion processes in a packed bed and make a first attempt at modeling them. Earlier work in this laboratory on packed bed combustion had focused on carbon combustion and ash processes; this work will focus on the additional process of pyrolysis, an essential part of the combustion of biomass or coal. Controlled combustion experiments were performed to obtain more detailed knowledge and information on volatile evolution during packed bed combustion of wood. This included the design, construction and testing of an in-situ tar sampling method to obtain data on volatile evolution at different heights within the bed. During this study a numerical discretization model developed by Cooper

(1996) and Ryan and Hallett (2002) was modified to include devolatilization. The main purpose of the experiments and modeling were to complete the following:

- To obtain data on the gas, temperature and tar profiles inside a packed bed of combusting wood;
- To develop a mechanistic model of combustion in a packed bed which included volatile evolution from the solid phase; and,
- To compare model predictions with experimental results.

A literature review of previous packed bed biomass combustion studies, methods of quantifying volatile (tar and gas) concentrations, and modeling approaches was completed and is summarized in the following chapter. Next, the combustion model and modifications made to include devolatilization are described. The following section describes the experimental apparatus, instrumentation, fuel characteristics and experimental procedures. This section also includes a description of the design criteria for the new in-situ tar sampling method. The experimental results are then presented and compared to the model modified to include devolatilization. Lastly, conclusions are drawn on the modeling results and the effectiveness of the tar sampling method, and areas for future research are recommended.

# 2 LITERATURE SURVEY

This section presents an overview of studies having a similar scope to this one in that they either attempt to mechanistically model and/or experimentally describe packed bed combustion of wood. First an overview of packed bed wood combustion experiments and previous attempts to model the process in the bed are presented. Next, studies which focus on individual particles are examined. The rate at which a particle devolatilizes depends not only on the reaction kinetics of pyrolysis, but also on heat transfer to and within the particle and other intra-particle effects. The main topics reviewed are the kinetic model, rate constants, heat of reaction, the effect of fuel composition and change in shape of single particles. A short discussion on the treatment of drying is also presented. This review provides a basis for the development of the mechanistic model discussed in **Chapter 3.0**.

The instrumentation and procedures of previous studies to measure tar and water concentrations in combustion gases are also presented. A review of these experimental studies provided the basis for the experimental operating conditions and design of sampling methods used in this study. The methods to measure temperature and concentrations of carbon monoxide, carbon dioxide, nitrogen and oxygen were based on work presented in Ryan's master's thesis (2000) and are not reviewed in this work.

## 2.1 Biomass Packed Bed Research - Modelling and Experimental Studies

The purpose of this section is to review experiments similar to the one proposed in **Chapter 1.0** and to determine what information on composition and temperature profiles in a bed is available that could be used to compare with a numerical model. Several experiments have been conducted on other different types of reactors such as fluidized

bed reactors, spouted bed and other novel reactor designs [Fjellerup et al. (1996), Löffler et al. (2002), Salzmann and Nussbaumer (2001), Bech et al. (1996), Park et al. (2002b), Bhattacharya (1998)] but these will not be examined here. There is more literature, much of it very old, on packed bed combustion of coal and coke, but this has been reviewed by Ryan and Hallett (2000) and by Cooper and Hallett (1998). However, relatively few studies have been conducted to understand the processes inside a packed bed of combusting wood.

Generally, biomass packed bed studies were found to include both experimental work and some modeling. Most of these studies deal with overfed combustion in a 'one-dimensional' bed, with fuel fed to maintain a constant bed height. A few papers have studied two-dimensional combustion on inclined or traveling grates. Much of this earlier work tends to ignore details of the pyrolysis process, concentrating on char combustion.

Huang (1987) studied the combustion of wood in 5 cm thick packed beds, measuring the temperature and gas fractions of $O_2$, CO, and $CO_2$ at different heights. The numerical model developed was based on simple energy and mass conservation equations which lumped gas and solid phases together and did not contain kinetics for devolatilization. However, the model did show good agreement with experimental results for a thin bed height. The packed bed model by Aganda et al. (1997) was simple as it adapted 1929 and 1952 models and did not include reaction kinetics of pyrolysis.

Kuo (1998) estimated the burning rate of biomass-based refuse by calculating the oxygen distribution in the combustion chamber with a one-dimensional model and compared the predictions to laboratory results. Fundamental energy, mass and momentum balances, porosity of the bed and underfire air rates were included in the model. The prediction of

the burning rate agreed well with various experimental studies on combustion; however, no information on the concentration of gaseous species other than oxygen was provided. When the thickness of a bed is large the combustion process becomes one of gasification. DiBlasi et al. (1999a, 1999b, 1999c) studied the gasification of various biomasses and reported numerous measurements of product gas heating values, ash properties and gas yields above the bed over time. These studies included variation of the oxygen supply rates.

Ignition and propagation of the reaction front within a packed bed was the subject of several papers. Typically the reaction front was located with thermocouples spaced the length of the reactor. In 1996, Bryden and Ragland modeled packed bed combustion with separate gas and solid phases and tied the pyrolysis to a scaled rate of char combustion reaction. The model assumed a linear decrease in particle diameter with motion down the bed, by an assumption made for larger particle sizes, 12-20 cm, because the study focused on overall burning rate and not on in-bed gas and temperature profiles. Comparison of the modeled burning rate with combustion of large hardwood logs (20 cm diameter) showed good results. Bech et al. (1996) studied the flame propagation in a 'cigar' burner on bales of hay. The model included separate gas and solid phases and a one-step pyrolysis reaction. Saastamoinen et al.'s (2000) study dealt with a "pot" furnace, essentially a one-dimensional bed and investigated heat conduction from the surface of the bed and convection from gas flowing though with larger particles treated as a semi-infinite slab. Gort and Brouwers (2001) and Xie and Liang (1997) also presented a theoretical model for propagation of a reaction front in a packed bed. Diffusion and convection are the main focuses of this model, which lumps together gas (including

pyrolysis products) and solids in the balance equations. The model does not include pyrolysis and uses an analytical solution.

A study of combustion of waste in an incinerator by Shin and Choi (2000) included separate gas and solid reactions and a one-step pyrolysis reaction. Their model, which simulates a travelling grate, is compared to an experimental one-dimensional packed bed with height diminishing with time. Thunman and Leckner (2001) investigated combustion of wet forest waste on an inclined reciprocating grate as well as in a "pot" furnace to conclude that with wet fuels ignition occurs at the grate. The model included heat conduction into the bed only.

Oman et al. (1999) studied packed bed combustion of wood chips in a novel two chamber reactor designed to understand combustion in a packed bed. Fuel was added in the lower chamber where it dried and devolatilized as it slowly travelled to the grate at the bottom of the chamber. By varying the inlet gas conditions, combustion of gases occurred separately in the upper chamber. This reactor was modeled for the lower chamber with several 1 cm high control volumes the width of the reactor and for the upper chamber with an additional control volume that included separate gas and solid heat and mass balances on the volumes. Pyrolysis was assumed to occur instantaneously. The model showed poor prediction of CO.

Van der Lans et al. (2000) used a 15 cm diameter by 137 cm long fixed bed reactor to study the effect of inlet air temperature, ignition front propagation and NO concentration on the outlet gas during straw combustion. Temperature was measured at 8 locations within the bed and outlet concentrations of $O_2$, $C_xH_y$, $NO_x$, $NH_3$ and $SO_2$ were measured. The results were modeled using a first order devolatilization reaction but predictions

compared poorly to measured gas concentrations. A CO gas phase oxidation reaction was not included in the model but mass transfer to the particle surface was.

A mathematical model for combustion of waste in a packed bed was proposed by Goh et al. (1998) and later tested by Goh et al. (2001) which focuses on the reduction of bed height. It neglects the interactions between air and gases within the voids of the bed. Gas and temperature profiles measurements in the bed were taken to test the model, but simplifying assumptions in the model, such as lumping all volatiles together as one product, were made due to a lack of kinetic knowledge. These were the only measurements reported from a full-scale incinerator.

Innovative attempts to model packed bed combustion of biomass have been proposed by Peters (1998) and Peters & Bruch (2001). Peters (1998) uses the Thiele modulus and the diffusion coefficient to classify bed combustion into two regimes: shrinking core and reacting core. However, the definition of Thiele modulus presented is different that than reported traditionally. The paper is partially based on earlier work on heat transfer and kinetics at low temperatures by Pyle and Zaror (1983). Peters and Bruch (2001) presented a novel numerical method for simulating the thermal decomposition of wood particles, which modelled each individual particle with a force balance to determine particle motion. It includes detailed reactions and heat and mass transfer for the individual particles, with transport of one or more reaction partners, adsorption at active sites, chemical reaction due to thermal decomposition, desorption of the products of the chemical reaction and transport of the products. Peters (2002) later expanded this model to study the effect of extinction. The model assumes the products of pyrolysis

immediately leave the particle and therefore there are no secondary reactions. The model is computationally very involved.

### 2.1.1 Conclusion

No studies were found that measured temperatures, gas concentrations and changes in particle volatility as a function of height in a packed bed. Most of the biomass packed bed modelling studies do not include particle consumption. Practical mechanistic models of biomass combustion and pyrolysis are often simplistic, may neglect such processes as multi-step reaction kinetics, heat transfer and diffusion inside the particle, secondary reactions and drying. Further information from within the bed on the gas and tar concentrations, particle sizes and density and temperatures may help clarify the pyrolysis behaviour within a packed bed.

## 2.2 Biomass Pyrolysis

The biomass packed bed studies reviewed above varied greatly in their approach to modeling devolatilization of the fuel. Biomass has a higher volatile fraction than coal, thereby significantly affecting factors such as ignition characteristics, flame behaviour, heating rate, products and quenching properties. Volatiles are the gaseous species, including hydrocarbons, tar, CO, $CO_2$ and moisture, which once released from a fuel due to thermal decomposition, leave behind a char residue. Proximate analysis of fuel using an ASTM standard test, such as the D1762-84 test for wood charcoal, is typically completed to determine the weight percents of moisture, volatiles, fixed char and ash of a fuel. These tests have shown that the volatile content of biomass is typically close to 85% compared to less than 31% for a medium volatile bituminous coal [Hallett, 1997]. Biomass also has a higher moisture content which can make it harder to ignite.

The following discussion will review the state of knowledge of the pyrolysis process itself and of the mechanistic models developed for pyrolysis.

### 2.2.1 Product Change with Heating Rate and Temperature

Establishing a universally acceptable kinetic pathway for pyrolysis has been complicated by the fact that pyrolysis products have been found to vary with temperature and heating rate. Antal (1983) in a review paper, notes that the products of pyrolysis at low temperatures (<250°C) have been found to be very different from those at high temperature (>750°C). At higher temperatures more CO and $CO_2$ are produced, while at lower temperatures more tar is produced.

A simple definition of the tar, a major product of this reaction, is all the condensable compounds of pyrolysis at ambient temperatures [Brage et al. (1996)]. Tar is the result of the depolymerization and fragmentation of the wood main structural components: cellulose, hemicellulose and lignin [Antal (1983)].

In the literature, tar is often referred to as pyrolysis oil or bio-oil when it is produced at high heating rates, and there have been recent efforts to produce this as a fuel source. Biomass-based pyrolysis oils are composed of water (15-30%), carboxylic acids, carbohydrates and lignin-derived substances. They are dark brown viscous liquids with an average molecular weight ranging from 370 to 1000 g/mol [Oasmaa (1999)]. In recent years, mainly due to increased commercial interest in use of bio-oil as an alternative energy source, detailed information on the tar component types and properties has also been published [Morf et al. (2002), Yu et al.(1997), Oasmaa and Czernik (1999), Sensöz and Can (2002)].

In 1996, Milosavljevic et al. published an extensive study on the effect of the heating rate on pyrolysis and concluded no thermal evidence existed that suggested different mechanisms of pyrolysis at high or low heating rates. However, numerous other studies have identified different products of pyrolysis and tar yield depending on the heating rate [Arseneau (1970), Cozzani (2000), Morf et al. (2002), Yu et al. (1997), Wu et al. (2002)]. Wu et al. (2002) investigated uncoated printing and writing paper at 25 degree intervals between 450 K to 950 K in a thermogravimetric analysis (TGA) with a mass spectrometer to conclude that the quantity of pyrolysis gases produced varied with temperature. Park et al. (2002a), using a tubular reactor, found that at reactor temperatures above 700°C, CO and $CO_2$ were the products of pyrolysis and oxidation accounted for 92% and more of the carbon mole balance. The other species were not identified. Also, the ratio of the $CO/CH_4$ was reported to vary between 0.4 and 0.74 for various woods and sawdust : while $CO/C_2H_4$ was found to vary between 0.79 and 1.36 [Antal (1983)].

### 2.2.2 Kinetic Models and Rate Constants

One of the key issues in properly modeling combustion is the form and parameters of the kinetics of devolatilization for which small samples are required to eliminate the effects of heat conduction on the particle. The majority of these small sample experiments were conducted by thermogravimetric (TGA) analysis and used single particles in the range of 1 mm diameter or smaller samples of biomass fibres with a total mass of less than 1 mg. The results of these tests are dependent on several factors as detailed by several studies: Cozanni et al. (1996), Reynolds and Burnham (1997), Antal et al. (1998) and Raafat et al. (2000), Liang and Kozinski (2000).

Antal and Varhegyi (1995) found sample sizes of cellulose of 1 mg or less are required for consistent kinetic measurements at moderate heating rates 100°C/min. Experiments have also been conducted with mass spectrometric methods [Chen et al. (1998)]. With either experimental apparatus, these tests are often conducted in order to define the reaction pathway and/or the kinetic rate constants since these methods minimize the effect of secondary reactions and vapour-solid interaction. With small samples the effect of heat transfer resistance is minimized, allowing kinetics to be the sole focus of the experiments.

The types of models developed through these tests and some modeling research can be divided into four categories: simple one-step first order, multicomponent models, multi-step parallel reaction models and more complex models.

### 2.2.2.1 Single Step First Order Reaction Model

A simple first order reaction of wood to a fixed percentage of tar according to an Arrhenius relationship is the most popular model [Chan et al. (1985), Antal et al. (1998), Grønli et al. (1999a), Liang and Kozinski (2000) and Rath and Staudinger (2001)]. A typical Arrhenius reaction is shown below:

Where r is the rate, A is the pre-exponential factor in $s^{-1}$, E is the activation energy in kJ/mol, R is the gas rate constant and T is the temperature in Kelvin.

$$r = -A \exp(-E/RT) \qquad (2.1)$$

In 1998, Antal et al. revisited in greater detail their previous work, as well as some of the models discussed later below, to understand the reasons for varying proposed pathways and difference in rate constants. The variable nature of biomass, the catalytic effect of ash and calibration procedures were all suspected to be involved. They concluded that a

simple, single-step, irreversible, first-order rate law with an activation energy of 228 kJ/mol describes well the pyrolysis of cellulose. Following the recommendations in that paper, Grønli et al. (1999a) conducted a "round-robin" TGA pyrolysis study to address this concern by testing cellulose at eight different laboratories. They fitted all the results with a single step first order model with an only slightly higher activation energy of 244 kJ/mol and a pre-exponential value of $10^{19}$ $s^{-1}$ at low heating rates.

### 2.2.2.2 Multicomponent Model

Unlike coal, biomass has a higher volatile content and is composed of several different components: cellulose, lignin, hemicellulose and water. Òrfao et al. (1999) conducted TGA of cellulose and proposed a model with separate first order reactions for cellulose, xylan and lignin. Grønli and Melaaen (2000) proposed a parallel reaction model for the different components with secondary tar decomposition. This model has also been used to model the pyrolysis of refuse-derived fuels including plastics using 4 components: cellulose, hemicellulose, lignin and polyethylene [Cozzani et. al. (1996), (2000)].

### 2.2.2.3 Multistep Parallel Reaction Models

Multistep parallel reaction models and variations thereof are another popular type of model [Chan et al. (1985), Koufopanos et al. (1991), Milosavljevic et al. (1996), Reynolds and Burnham (1997), Hastaoglu and Al-Khalid (2001) and Rath and Staudinger (2001)]. The majority of the studies referred to a model based on a pioneering work conducted by Broido (1965, as reported by Arseneau 1970) and Shafizadeh (1968). Because of the similarity in the models and the time they were developed, the models are usually referred to as the Broido-Shafizadeh (B-S) model. The Broido-Shafizadeh (B-S) mechanism for single particles of cellulose, which includes competitive reactions with

secondary tar decomposition, was the most popular model for various biomasses, including wood [Arseneau, 1970]. The kinetic pathways for the Broido reaction are presented below in **Figure 2.1**.

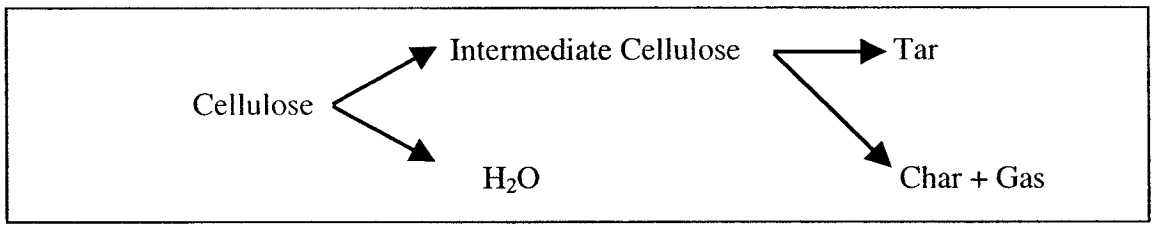


**Figure 2-1: Broido Reaction Pathway [Arseneau (1965)]**

Pyrolysis begins with an activation stage; followed by char formation accompanied by gas and tar release in three parallel reactions. Shafizadeh (1968) proposed a similar kinetic pathway model to the Broido one, as shown in **Figure 2.2** below:

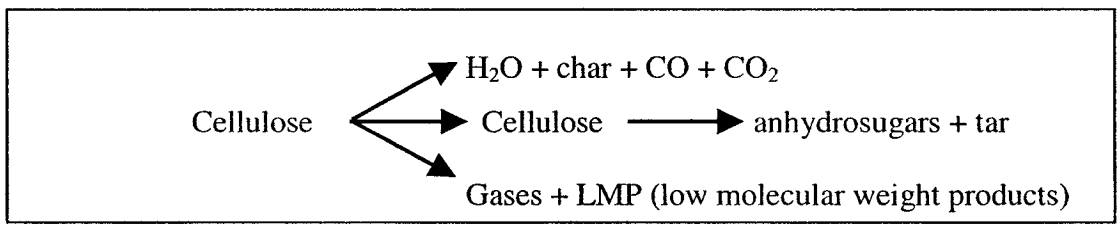


**Figure 2-2: Shafizadeh (1968) Proposed Kinetic Model**

After tar is formed it often undergoes secondary decomposition, forming more gases and char, and this is often added to the Broido-Shafizadeh mechanism as an additional step, as done in Varhegyi's (1993) proposed model that includes a secondary tar reactions.

The secondary tar cracking reactions during pyrolysis have been the subject of numerous studies, leading to several variations of the B-S model to be proposed. The kinetic rate constants for the single step of wood to tar in these models have been reported in **Table 2.1**.

Figueiredo et al. (1989) proposed parallel reactions for the production of tar, gas and char and further divided the gas into several first order reactions for $CH_4$ and other gas species. Brage et al. (1996) investigated secondary tar reactions and their effect on tar yield, focussing on small sample sizes and the effect of steam injection. Rath and Staudinger (2001) investigated secondary tar reactions using a TGA and divided the tars produced into three categories, of which two showed signs of secondary cracking. In Table 2.1, the A and E for multistep kinetic scheme are given for the step producing tar or the species assumed to be the main tar producing component.

#### 2.2.2.4 Complex Models Based on Fuel Chemistry

Much of the research in the past century on solid fuel combustion has focused on coal and therefore very detailed models based on the fuel chemistry have been developed. With the increased focus on biomass energy sources in recent years, several studies have attempted to use the complex chemistry-based devolatilization models developed for coal combustion to biomass with modifications for the higher volatile content of the fuel [Chen et al. (1998), Jones et al. (2002), Niksa (2000)]. More complex reaction models for biomass have also been proposed by Avni et al. (1985), Hajaligol (2001) and Biagini et al. (2002).

**Table 2-1 Kinetic Rate Parameters Reported for Small Particles**

| Author | Determination Method and Particle Description | Model Fitted | A $s^{-1}$ | E kJ/mol |
|---|---|---|---|---|
| Arseneau (1971) | TGA* and differential scanning calorimeter of cellulose | Broido (1965) | Not stated | 151 to 190 |
| Chan et al. (1985) | TGA, of pine | 1st order followed by 2nd reaction for tar | $2.0x10^{8}$ | 133 |
| Chen et al. (1989) | Mass spectrometry for populus deltoids | Complex based on molecular species with tar reaction | $4.88x10^{12}$ | 21.33 |
| Figueiredo et al. (1989) | TGA sample of saw dust | Multi parrallel with CO, $CO_2$, $CH_4$ and $H_2$. reactions (Rate for $CH_4$ reaction) | 0.0026 - 0.0107 | 19.13 |
| Koufopanos et al. (1991) | Modelling best fit (model includes a 2nd order term) | Broido (1968) with tar and gases for lignin, cellulose and hemicellulose. (Rate for lignin reaction) | $8.6x10^{-8}$ | 137.1 |
| Milosavljevic et al. (1996) | Review paper | Concluded too difficult to predict | | |
| Reynolds and Burnham (1997) | TGA for newsprint | Broido (1965) | $5x10^{12}$ | 180 |
| Antal et al. (1998) | TGA of cellulose | First order reaction | $1x10^{16.6}$ | 228 |
| Grønli et al. (1999a) | TGA of cellulose (round-robin) | First order reaction | $1x10^{19}$ | 244 |
| Ôrfão et al. (1999) | TGA of cellulose | Separate 1st order reactions for cellulose, xylan and lignin. Rate for cellulose reaction | $1.13x10^{15}$ | 201 |
| Liang et Kozinski (2000) | TGA sample of cellulose | First order reaction | 25 600 | 67 |
| Hastaoglu and Al-Khalid (2001) | TGA of wood | Variation of multi-step parallel reaction model by Shafizadeh (1968) | Average $1.56x10^{6}$ | 100.30 |
| Rath and Staudinger (2001) | TGA of spruce (0.5-1.0 mm) | First order reaction | $3.02x10^{18}$ | 320.2 |
| | | Variation of multi-step parallel reaction model by Shafizadeh (1968) | $8.2x10^{7}$ - $1.0x10^{14}$ | 117 to 197.5 |
| Biagini et al. (2002) | TGA using saw dust | Complex based on ultimate analysis | $3.9x10^{8}$ | 121 |

*TGA - Thermogravimetric analysis

As an example of the level of detail in some of these models a study by Avni et al. (1985) will be discussed, who modeled pyrolysis of lignin with 21 reactions. The model assumed that during pyrolysis the relatively weak bonds of C-O and C-C which bond phenylpropane (the basic unit of lignin) break, releasing tar composed of monomers, dimers, and trimers of pheylpropane subunits. Dependent on the structure of the original lignin, the model simulated the evolution of tar fragments which then crack into 'ring clusters' and light gases. The model allowed for different reactions at low and high temperatures. At low temperatures, the main products included $CO_2$ from carboxyl, $H_2O$ from hydroxyl, HC from aliphatic and methoxyl groups and CO from aldehydes while at higher temperatures the main products were $H_2$ from the aromatic hydrogen and CO from groups like diaryl ethers and phenols. Despite its complexity the model showed poor agreement in CO. This may be due to the fact that the particles were pretreated at 180°C for 48 hours prior to testing. (The effect of pre-treatment is discussed in **Section 2.2.4**.)

Chen et al.'s (1998) study modeled the depolymerization of the heavier aromatic compounds, which are found only in low or zero concentration in most biomass, with less attention paid to the more significant fraction of light hydrocarbons and moisture in found in biomass. This model showed poor agreement of water and carbon monoxide concentrations for the small sample tested. Jones et al. (1998) reviewed the use of a similar depolymerization modeling approach with the Functional Group Depolymerization, Vaporization Crosslinking (FG-DVG) model while the bio-Flashchain model was developed by Niksa (2000) from an earlier coal model (Flashchain). The results were not applied to a specific system such as a packed bed combustor, as modeling difficulties were noted due to the variable properties of different biomasses.

With both the Chen and Niksa models, modification of the coal devolatization model for biomass showed poor results.

In 1996, Hajaligol et al. (2001) investigated pyrolysis with different reaction rates for several aromatic hydrocarbon products to understand how they evolve from the biomass. An innovative study by Carsky and Kuwornoo (2001) modeled coal pyrolysis using a neural network to allow inclusion of knowledge from studies with differing activation energies and secondary reaction models. Adaptation of the model to fuel sources with a higher volatile content, such as wood, was not discussed. Models should therefore allow for inclusion of devolatilization and account for the higher volatile content of biomass fuels compared to coal.

#### 2.2.2.5 Summary of Proposed Models

As shown in **Table 2.1**, there is a wide range of proposed kinetic rate parameters because of the different kinetic pathways proposed. To address this general disagreement in the field, some clarification can be obtained by findings in a review by Antal and Varhegyi (1995). They proposed that kinetic rates could be accurately measured with a modern TGA, when external factors such as heat transfer intrusions, secondary reactions and substrate alteration due to pre-treatment have been accounted for in the design of the experiment. They concluded that for small cellulose samples a single first order high activation energy rate determining step is adequate to describe pyrolysis for commercial interests. They also noted the initial activation step proposed by Broido-Shafizadeh is not supported in that it either occurs too quickly to be measured or does not exist.

### 2.2.3 Heat of Reaction

The information published on pyrolysis of small samples is not in agreement with respect to the overall heat of reaction for a single first order reaction; however, there is general consensus regarding an initial endothermic stage followed by an exothermic secondary reaction. Koufopanos et al. (1991) was apparently the first paper to support this two step heat of reaction. For 20 mm particles, they found the reaction would be endothermic at low conversions but not for higher conversions. The author speculated that an initial endothermic phase during heat transfer to the core of the particle was involved, followed by an exothermic lignin degradation phase. Antal and Varhegyi (1995) and Miller and Bellan (1997) and DiBlasi et al. (2000) also supported a similar two-stage heat of reaction.

In a review paper Milosavljevic et al. (1996) reported heat of reaction values ranging from –2100 to 2500 J per gram. The papers published in the 1970's favoured an overall exothermic reaction whereas the majority of the papers published in the 1980's and 1990's tended to favour an overall endothermic reaction. The authors concluded from their testing that the endothermic heat of reaction is 538 J per gram of volatiles evolved but caution that the heat of reaction is a strong function of the heating rate and thus difficult to predict.

Models were also found that used an endothermic heat of reaction to describe the overall pyrolysis reaction [Hastaoglu et al. (2000), Oman et al. (1999), Kanury (1994)]. The Oman et al. (1999) model included a $CO+OH \rightarrow CO_2+H$ reaction step. The H remains unbonded without forming $H_2$ and was found to dictate the speed of pyrolysis. As this reaction is the rate limiting step, it may explain the highly endothermic heat of reaction.

### 2.2.4 Pre-treatment and Mixed Fuel Composition Effects

Recently small-scale[2] experiments have extended the pure cellulose research by Broido with an examination of the effect of mixed biomass sources. The effect of pre-treatment of fuel has also been studied, and individual components and additives shown to play a key role in determining the kinetic behaviour during pyrolysis and combustion.

With regards to pre-treatment, Zaror et al. (1985) found that salt impregnation of cellulose and wood samples would increase the char yield in the presence of an inert carrier for short residence times. However, this study found that a longer residence time of volatiles in the hot zone near the particle would increase char formation for untreated substrates, but under the same conditions that impregnation of samples with salt would impede char formation. The author raises questions as to whether the results may have been affected by fibre swelling or solid matrix deterioration during impregnation. Julien et al. (1991) determined that acid washing, although it changed the degree of polymerization and crystallinity of cellulose, had a smaller effect on pyrolysis than the ash content. DiBlasi et al. (1999) studied the effect of rain leaching in a 20 cm bed of straw in a nitrogen environment. These studies raised questions as to the benefit of pre-treating a fuel to obtain a consistent moisture content, since solid matrix deterioration may prove to be a greater variable that is more difficult to measure with available equipment.

With regards to mixed fuel studies, Cozzani et. al. (1996, 2000) used a multicomponent model for the pyrolysis of refuse-derived fuels with a polyethylene component. The experimental results showed excellent agreement; however, the model ignored diffusion

---

[2] Referred to operations processing less than 50 kg/wk or 50 kg/batch

and radiation heat transfer, and assumed a steady-state flow of volatiles. These simplifications may limit its transferability to other larger scale applications (bed height >2 cm) where mass transfer limitations within a bed become important. The reactivity of the cellulosic matter increased with PVC content, supporting the conceptual finding by Reina et. al. (1998). Reina et. al. (1998) studied the effect of different woods during pyrolysis: forest, demolition wastes, slot machine parts, furniture and pallets. The evolution of the components was found to be dependent on the volatiles content and therefore two additional reactions were added to the Broido Shafizadeh model. The rate constants were found to be different for each type of wood studied. A similar study aimed at reducing chlorine in combustion gases was conducted by Zenvenhoven et al. (2002).

Sorum et. al. (2001) investigated pyrolysis and kinetics of municipal solid waste which included plastics, wet organics, metal, glass and paper. The model used a parallel reaction model. In a study on the effect of fertilizer on straw pyrolysis Davidsson et al. (2002) concluded alkali release was two to four times higher when a chloride-rich fertilizer was used compared to a sulphate-rich fertilizer. Saade and Kozinski (2000) found that indenyl in sludge from the paper recycling de-inking process affected pyrolysis and may act as a catalyst for ignition.

### 2.2.5 Single Particle Pyrolysis

#### 2.2.5.1 Mass and Energy Transfer

With larger particles, heat conduction through the particle limits the pyrolysis rate and the pyrolysis gases interact with the decomposing wood as they exit the particle, thus affecting the ultimate char yield [Grønli and Melaaen (2000)]. Determining when and how wood particles change in size during combustion is the subject of debate and is greatly affected by the secondary reaction and by heat and mass transfer processes. The different kinetic rate parameters proposed for larger particles are presented in Table 2-2. Pyle and Zaror (1983) proposed a parallel reaction model for the different components with secondary tar decomposition. Kanury (1994) presented a classical shrinking core model for combustion of wood including heat transfer to the particle surface for ignition, and diffusion-controlled mass loss during char combustion. A shrinking core model assumes that the reaction occurs on the particle surface only, so the unreacted material becomes progressively smaller, leaving an annular region of reacted wood (char) as combustion progresses. The model assumed pyrolysis to be endothermic and its rate to be directly tied to the energy supplied to the particle in a process similar to evaporation. Pyrolysis reaction kinetics were not introduced.

**Table 2-2 Reported Kinetic Rate Parameters for Primary Tar Production Reaction for Large Particles**

| Author | Particle description | A $s^{-1}$ | E kJ/mol |
|---|---|---|---|
| Pyle and Zaror (1984) | 0.9 to 2.2 cm wood | 2 000 - 3 000 | 66 - 69 |
| Saastamoinen and Richard (1996) | 2 cm particles (modeled with a temperature dependant evolution of gaseous species) | 34 000 | 69 |
| Grønli et al (2000) | D=2.0,L=3.0cm wood | $2.00 \times 10^{8}$ | 133.1 |
| Larfeldt et al. (2000) | 30 x 2cm cylinders of wood | 10 700 | 133 - 198 |
| Peters et Bruch (2001) | Modeling of 4 cm wood particles | $4.12 \times 10^{6}$ | 112 |
| Morf et al. (2002) | Fir and spruce wood chips 1 to 4 cm | 40 000 | 76.6 |

Bettagli et al. (1995) studied the gasification of biomass to be able to calculate the gas composition at different operating conditions for particles of 5.5 mm, larger than what most believe to be the limit for diffusion-controlled pyrolysis. The results of this study showed a large concentration of $H_2$ (up to 0.4 mole fraction of products) but no tar. The model does include the basic steps of diffusion of reactant to the char external surface through the surrounding stagnant film, pore diffusion of gas inside the particle, adsorption, surface reaction, desorption on the pore walls and/or on the external surface, diffusion of products outside the pores, and, diffusion of products through the stagnant film. The model simply assumed gasification to occur 200-300 times slower than the combustion reaction according to a simple first order reaction because of difficulty in finding combustion kinetics for biomass.

Ouedraogo et al. (1997) also presented a shrinking core wood particle combustion model. They assumed pyrolysis occurred once a set temperature of 500°C was reached, so that pyrolysis is heat transfer controlled rather than by kinetic reactions. They allowed the moisture to evolve with the volatiles. Both these models assume that large particles lose weight on an external shell first while the core remains relatively undisturbed when inserted into a hot convective environment. Oman et al. (1999) also used a model in which the particle volume reduced during pyrolysis.

Khan and Bowen (1999) presented a fixed bed reactor model using a diffuse interface single pellet model. Despite the fact that this model allowed for several reaction zones within the particle, the authors concluded that the results of their work support a sharp change from reactant to product without secondary reactions. Morf et al. (2002) found for wood chips that secondary tar reactions became important around 650°C and they were coupled with an increased presence of CO, $CH_4$ and $H_2$ in the flue gases. They used an excess of nitrogen to reduce the effect of secondary reactions and allow pyrolysis to be modelled with a single first order reaction. Larfelt et al. (2000b) studied the effect of various heat transfer models on the prediction of pyrolysis for wood charcoal cylinder 30 cm long with a 2 cm diameter. They concluded that an assumption of constant thermal diffusivity agreed better with measured data than a temperature-dependant thermal diffusion model. At high temperatures (>1000°C) the effect of the change in structural shape of the particle will be more important in determining the effective thermal conductivity through the particle.

### 2.2.5.2 Particle Shrinkage

Dasappa et al. (1994) presented an empirical model for shrinkage of wood in which shrinkage was proportional to the conversion squared. The shrinkage coefficient was linked to a Taylor series expansion of the temperature and different coefficients were required for the longitudinal, tangential and radial directions. Pictures in the paper show that wood char has a relatively consistent geometric order unlike Dasappa et al.'s observations of coal, also shown in the paper.

Wornat et al. (1995) analyzed particle size change extensively using, among other techniques, scanning electron microscopy, dispersive x-ray spectroscopy and x-ray diffraction analysis. They found oxygen- and hydrogen- rich gases are released during devolatilization. A molten stage with silicon-rich beads around fibres was found at 48% conversion. They concluded that the shape of biomass particle fibres shrink during combustion but do not specify how this affects a large particle. Experimentally, DiBlasi et al. (2000) estimated a swelling of between 3 to 10%, mainly in the radial direction, for pine and Douglas fir wood. This was not observed for hardwood such as beech, which shrank about 15% in the radial direction. The authors hypothesize that swelling occurs due to gas overpressures during devolatilization. This effect of pressure generation during pyrolysis was also the subject of a study by Hastaoglu et al. (2000) and Agrawal and McCluskey (1985). The later studied the effect of pressure on newsprint pyrolysis using a single step model and found little correlation between the two above 350°C, whereas Hastaoglu et al. concluded pellet break-up could be due to the pressure build up.

Hagge and Bryden (2002) modeled particle shrinkage and examined the effect of the Biot number (internal heat transfer resistance /film resistance). They concluded that the shrinkage effect on tar yield was complex. At lower temperatures, shrinkage decreased

residence time in the particles and therefore secondary reactions. However, at higher temperatures more complete conversion to lighter hydrocarbons occurred. decreasing the impact of particle shrinkage.

Davidsson and Pettersson (2002) conducted experiments on particle shrinkage during rapid pyrolysis of birch wood in a furnace equipped with a video camera. Volume shrinkage was found to be between 45-70% and only occur in the longitudinal direction of the grain after about 60% mass loss. This volume shrinkage is significantly higher than those reported in the above works. Particles were found to swell in the direction traverse to the grain. These authors also present an empirical model for shrinkage.

### 2.2.6 Conclusion

In the past, difficulties in modeling biomass combustion appear to have occurred because of the volatile content and debate about the devolatilization mechanisms and their effect on gas concentrations. A single step $1^{st}$ order reaction should satisfy initial modeling requirements despite the presence of secondary reactions. The heat of reaction used in the model should be close to 538 kJ/mol endothermic, as found by the latest review paper [Milosavljevic et al. (1996)]. These studies highlight interactions observed in the presence of additives and mixed feed types, and therefore experiments performed to study the pyrolysis should avoid treated mixed medium fuels (e.g. wood/coal) until the basic mechanisms are known. Mass and heat transfer resistance were found to be important for larger particles and it is noted that these resistances will affect the rate of pyrolysis. Empirical relationships have been developed for particle shrinkage but there are reported contradictions with regards to change in particle shape. It was found to be dependent on the grain direction and difficult to predict for larger particles randomly

packed in a bed. The experimental studies on particle shape change also demonstrate how change in shape (~15vol%) is relatively insignificant in comparison to mass loss during devolatilization (~60wt%).

## 2.3 Drying

Many models used a simple one step wood to char and volatiles pyrolysis reaction model without a separate drying reaction, including water as a product with the volatiles. Chan et al. (1985) included a drying step in their model with water vapour evolving according to a simple one step Arrhenius equation with an activation energy of 87.9 kJ/mol and a pre-exponential factor of $5.13 * 10^6$ $s^{-1}$. Although drying is not a chemical reaction, an Arrhenius type rate for it has been used as a model by several authors. Saastamoinen and Richard (1996) modeled drying of the particle by assuming a layer of water of constant thickness attached to the pores of the particles. Their model included two competing reactions during pyrolysis. DiBlasi et al. (2000b) studied the interaction of moisture and pyrolysis and claimed that at high heating rates the two processes occur simultaneously.

## 2.4 Experimental Aspects and Measurements

This section presents previous experimental methods used to characterize biomass combustion and pyrolysis.

### 2.4.1 Tar Concentration Measurements

Recall that one goal of this work is to develop a mechanistic model including devolatilization in the combustion process. Therefore, a method to profile the volatiles concentration, of which tar is a major component, at various heights within the bed is an essential requirement of this work. Several researchers conducted studies on tar

measurement for the products leaving the bed using cold traps or solid phase absorption (SPA) methods, but they did not measure tar within the bed. These methods of sampling are generally conducted to measure air emissions leaving a stack to determine compliance with health and safety or environmental regulations using protocols such as Occupational Safety and Health Administration (OSHA) 58 from the United States Department of Labor. The probe is often not close to the combusting solids and samples are usually taken at a point where the majority of the secondary reactions have taken place. These methods will now be described to determine their adaptability to sampling for tar within a burning bed.

### 2.4.1.1 Cold Trapping

Cold trapping involves passing a gas through a liquid in impingers at a temperature kept low enough to condense the water vapour and, depending on the solvent selected, to absorb a specific species from the gas. After sampling the liquid can be analysed with a high performance liquid chromatograph (HPLC) or other methods to determine the concentration of the selected species. This technique is often used for stack testing of industrial sources using considerably larger air volumes and lower tar concentrations of gases than examined in the current study. Oesch et al. (1996) reported using a sample volume of 600 $m^3$ for tar sampling using cold traps with processes that produce between 0.1 to 0.5% by mass of tar in the flue gas. Cold trapping was also used to measure total tar production continuously from the combustion gases [Brage et al. (1996)]. Abatzoglou et al. (2000) also proposed a similar protocol using cold trapping.

A study by Simell et al. (2000) specifically proposed a sampling and analysis protocol for tar and particulates in the flue gas from large-scale biomass gasifiers. The method uses a

series of impingers, filters and a heated probe to avoid tar condensation in the sampling line. Dichloromethane is used to absorb the tar and then the sample is then analyzed with a gravimetric or HPLC analysis method. The gravimetric method measures the residue remaining in pre-weighed evaporating dishes after one hour at 105°C under a fumehood. Simell et al. (2000) proposed their sampling methods be used on the condition that the tar content in the sample gas remained below 10 $g/m^3_n$, which is about 20 times lower than that expected within the packed bed of wood based on TGA results by Chen et al (1985). However these protocols do not take into account a comment by Becker (1993): "Small soot particles undergo Brownian diffusion and tend to stick on sampling line walls. If the line is long enough to the point of removal of the soot by filtration, all the soot will be deposited in the sample line." These comments apply equally to the tiny droplets of tar that in part give wood smoke its characteristic opacity. The protocols do not provide an estimate of general precision or accuracy levels attainable. Collection of tar on the sampling train wall could therefore be considerable. Previous work [DiIorio (2001)] determined that the collection of tar in the sampling line makes cold trapping methods unacceptable due to clogging of the gas probe by tar. This collection may also falsify measurement, as capillary action may slowly entrain the tar from a previous sample into another one.

An option reported in the literature to reduce this collection in the sampling line during cold trapping was to maintain the temperature of the combustion gases in the probe above the condensation temperature until just after the gas cleaning system and then reduce the temperature to below 150°C [Abatzoglou et al. (2000)]. For measurement inside a packed bed this presents significant safety concerns : to electrically heat the probe above

the condensation temperature, around 150°C, wiring would need to be in relatively close contact with an open flame.

### 2.4.1.2 Solid Phase Adsorption

Another tar sampling method that has been used is solid-phase adsorption (SPA) on an amino phase from a free-fall reactor [Yu et al. (1997)]. This method involves collecting a sample on a solid phase extraction (S.P.E.) column with the use of a manually-controlled syringe to extract a fixed volume. The sample is then eluted with DCM and allowed to react for one hour prior to GC analysis. Total tar is determined by a gravimetric method after evaporation of the sample from a cold trap. Unfortunately, although this study uses both cold trapping and SPA, no comparison was done between the concentrations obtained from the different methods for a similar time period. Also, it did not mention cleaning of the syringe tip, allowing tar to collect near the syringe injection point. The syringe method is disadvantageous because of inaccurate volume measurement.

In 2000, Padban et al. published results on tar formation in pressurized fluidized bed air gasification of wood. They used four tar sampling methods with heated sampling lines. The first method ("LU") consisted of three stages: 1. cooling to collect water and polyaromatic hydrocarbons (PAH); 2. wire meshes to collect aerosols; and 3. a saw dust and silica gel dryer. The second and third methods were cold trapping and a combination of cold trapping and LU. The fourth method was SPA. The column used for tar sample analysis was a capillary with DB-Wax (DB-5). The authors did not state the precision or accuracy of the methods but did note that the LU and cold trapping methods agreed within 5%. The SPA concentrations of PAHs were found to be much lower than the

other methods. Unfortunately this study did not mention testing the sampling line for tar depositing before and after sampling.

One key design element in gas sampling is the ability to sample isokinetically. An isokinetic procedure will sample a gas at the same flow rate as the air surrounding the probe. This allows the particle samples to be representative of the surrounding environment since they were captured at a similar speed. Detailed discussion can be found in general texts on the subject including Wright (1994), and the importance of isokinetically sampling with tar has been highlighted by Abatzoglou et al. (2000) and Bechker (1993). The ability to sample isokinetically with SPA is difficult to predict since the syringe withdrawal is done once over a very short sampling period.

#### 2.4.1.3 Rinse Solvent

Irrespective of the sampling method used, due to the viscous nature of tar, a solvent is required to clean experimental equipment, and if desired analyse it in a liquid chromatograph. Many sources used dichloromethane (DCM) [Simell et al. (2000), Brage et al. (1996), Oesch et al. (1996)]; however, ASTM 1107-84 uses an ethanol and benzene solution. Abatzoglou et al. (2000) also reported isopropyl glycol and acetone as alternative solvents. A recent study on bio-oils, essentially wood tar, recommended the use of methanol to dilute the bio-oil [Oasmaa and Czernik (1999)]. Due to health concerns with DCM and benzene, methanol may be a more suitable rinse solvent choice in applications where tar deterioration for further analysis is not a concern.

### 2.4.2 Water Vapour

In pyrolysis packed bed studies, water vapour sampling was usually not conducted. Wu et al. (2002) pyrolyzed uncoated printing and writing paper at 25 degree intervals

between 450 K to 950 K in a TGA equipped with a mass spectrometer and two GC columns, a elemental analyzer, spectrometer and a psychrometer. They were able to measure gases (hydrocarbons and non-hydrocarbons), elemental analysis, heavy metals and $H_2O$ concentration; however, the psychrometer used is typically used for measuring ambient air conditions.

No reports were found that used a GC column to sample for water vapour and actually stated which type of column was used to detect the water vapour concentration. Experiments were not found that used a dry/wet bulb thermometer measurement in the sampling train. This is likely because the change in relative humidity with respect to the incoming air is expected to be very small and therefore requires a sophisticated measurement method.

### 2.4.3 Conclusion

No methods were found for sampling tar within a bed that could be safe and minimize tar collection in the sampling train. A new method for sampling tar is therefore required. Sampling for water vapour within a packed bed also appears not to have been successfully done. As much as possible the methods should sample isokinetically.

# 3 NUMERICAL MODEL

A computer program developed by Cooper (2000) and modified by Ryan (2002) simulates char (i.e. carbon) combustion in an overfeed packed bed. The following section outlines the main features of the model and describes the modifications made to simulate the present experiments conducted using wood. Changes made include addition of a simple first order devolatilization reaction and modifications to account for the different properties of wood versus the coke previously modeled. The FORTRAN code of the final numerical model is included in **Appendix A**.

## 3.1 Packed Bed Combustion Model

The model developed by Cooper (1996) and Ryan (2000) includes most of the relevant packed bed processes for char combustion, including ash sub-modelling, and does not contain the simplifying assumptions found in other models in the literature. It predicts the changes in gas and solid temperatures, gas concentrations ($O_2$, $CO_2$ and CO), fuel burning rate and fuel particle size as a function of bed height and with time. Differential mass, species and energy balances are used to describe temperature and gas concentration changes and are solved using the finite volume discretization techniques of Patankar (1980). Char is consumed as it moves down through the bed and the resulting particle shrinkage is accounted for through a particle number balance. The model includes all relevant processes: solid surface reactions (oxidation of C and reduction of $CO_2$); CO oxidation and reverse reaction in the gas phase; fuel particle char consumption (shrinking particle) and motion; ash layer build-up; heat conduction in the solid phase; heat conduction and diffusion in the gas phase; heat and mass transfer between the particulate and gas phases; properties variations; the effects of ash particles in the voids between fuel

particles on heat and mass transfer; and the effects of thermal boundary conditions such as the grate and the freeboard space above the bed. It can also account for non-spherical fuel and ash particles using the sphericity of the particle. Since all the transient terms have been included in the model, unsteady phenomena such as ignition and extinction can also be modelled. The model is one-dimensional, so radial variations are not taken into account. Also, since combustor beds are generally thin, pressure gradients have also been neglected.

In the present work, the model has been modified to include a volatiles evolution reaction and the changes in properties as wood is converted to char. Volatile combustion has not been included, and since the particles used in the experiments were nearly dry, moisture and drying were also neglected. The system modelled is an over-feed packed bed of fuel particles resting on a grate, through which air streams vertically upwards. Fresh fuel is fed to the surface to keep the level constant; devolatilization takes place in the top layer of the bed, and the volatiles burn above the bed with secondary air. (Only if the bed is less than two particles thick will oxygen from the primary air be available to burn volatiles within the bed.) The bed is assumed of large enough horizontal extent that it can be considered one-dimensional. Further details on the numerical solution method are presented at the end of this chapter.

## 3.2 Particle Solid Transport Equations

The pyrolysis of large pieces of fuel, such as are commonly fired in packed beds, is fairly complex. As previously discussed, the pyrolysis reaction itself is generally considered to be multi-step, resulting in gases, tar vapours and char as the products. With wood fuel each of the three main components (cellulose, hemicellulose, and lignin) may pyrolyze

differently. In addition to the chemical reactions, the processes of heat conduction into the solid, gas flow out of the solid, and drying are acknowledged to be important, particularly for large particles. However, as a first step in adding fuel pyrolysis to the existing model, the simplest possible pyrolysis model will be used: a one-step first order chemical reaction, with fuel particles assumed uniform in temperature and composition. Further studies may seek to include heat transfer inside individual particles in the model, however, for a first modelling attempt only a uniform particle temperature has been assumed.

The fuel is assumed to pyrolyze with a char yield of $\zeta_C$, as follows:

$$1\ kg\ fuel \rightarrow \ \zeta_C\ kg\ \ char + (1 - \zeta_C)\ kg\ \ pyrolysis\ gases \tag{3.1}$$

The char yield was determined experimentally from the ASTM D346-35 specification for selection of a representative sample and the ASTM D1762-84 test for wood charcoal proximate analysis.

The rate of production of pyrolysis gas per unit bed volume is

$$r_p = -(1-\varepsilon)(1-\zeta_C)\rho_W \frac{dW}{dt} \qquad (kg\ gas/m^3\ bed) \tag{3.2}$$

where W (= "wood") is the mass fraction of original fuel unconverted, $\varepsilon$ is void volume and $\rho_W$ is the density, and

$$\frac{dW}{dt} = -AW \exp(-E/RT) \tag{3.3}$$

As pyrolysis proceeds W will decrease and produce char, C. Char subsequently burns to produce CO and $CO_2$ and ash, plus tar and hydrocarbons.

Combustion and secondary reactions of pyrolysis gas within the bed are not considered at this time. A schematic of the pyrolysis process is shown graphically in **Figure 3.1**. The

wood particle enters the bed, and as it warms up it begins to pyrolyze, producing char. It was assumed that pyrolysis does not change the fuel volume and that unpyrolyzed wood does not react with $O_2$ and $CO_2$.

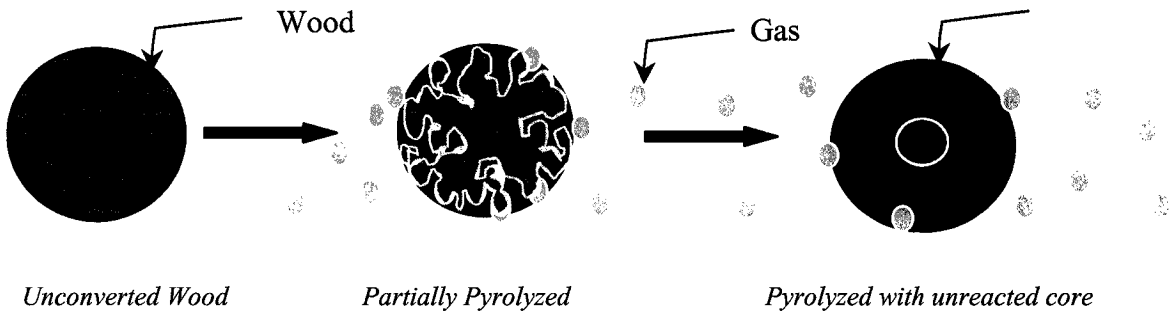


**Figure 3.1: Schematic of Wood Pyrolysis**

### 3.2.1 Extent of Pyrolysis

The mass conservation equation for a single fuel particle is given below:

$$\frac{\partial}{\partial t}[(1-\varepsilon)\,\rho_F\;X_F]+\frac{\partial}{\partial x}(\rho_F\,v_F) \;=\; -\,G\,a_{BC}(1+\alpha)-r_p \qquad (3.4)$$

where $\varepsilon$ is the void fraction in the bed, $\rho_F$ is the fuel density, $X_F$ is the volume fraction of fuel in the total solids (ash + fuel), $v_F$ is the superficial velocity of the fuel particles as they move down in the bed, G is the char combustion rate, $a_{BC}$ is the fuel particle specific surface area ($m^2$ surface/$m^3$ bed volume), and $\alpha$ is the ash mass fraction of the original fuel. This equation was developed by Ryan and Hallett (2002) and relates fuel motion to fuel consumption. To determine the rate of the pyrolysis the mass of unconverted wood must be known. Therefore, a new variable $Y_W$, which is defined as the mass fraction of unconverted wood in a particle was introduced, and a solid phase transport equation developed to track it. The change in wood mass in a slice of the bed is equal to the difference between the outflow and inflow of wood in the fuel particles leaving and

entering the slice, plus the conversion of wood mass to char by pyrolysis. This balance leads to the equation 3.5 shown below:

$$\frac{\partial}{\partial t}\left[(1-\varepsilon)\rho_F X_F Y_W\right]+\frac{\partial}{\partial x}(\rho_F v_F Y_W) = -\frac{r_p}{1-\zeta_C} \qquad (3.5)$$

The last term represents the conversion of wood by pyrolysis and is divided by (1- $\zeta_C$) because $r_p$ refers to the amount of gaseous products, while this equation is for wood as a whole. The fuel density $\rho_F$, volume fraction $X_F$, void fraction $\varepsilon$, and superficial fuel velocity $v_F$, can be calculated based on the bed conditions, and thus the mass fraction of unpyrolyzed fuel, $Y_w$, can be solved for. A finite volume method was used and details are provided at the end of this chapter

Equation (3.5) assumes that wood pyrolyzes only, and is not converted by contact with $O_2$ or $CO_2$ : only after wood has pyrolyzed and become char can it burn. The mass fraction $Y_W$ can be related to the unconverted wood fraction W in the pyrolysis rate expression by the relationship presented below:

$$Y_W = \frac{W}{W+(1-W)\zeta_C} \qquad (3.6)$$

This equation assumes that no char combustion occurs until devolatilization is finished. This assumption is approximately true, since the efflux of pyrolysis gases from the particle will tend to prevent $O_2$ or $CO_2$ from reaching the surface. The difference between W in the reaction rate expression and $Y_W$ is that W represents the fraction of the original fuel mass which remains unconverted, whereas $Y_W$ represents the mass fraction of wood in a given particle in its present state, with the remainder being char. Once the wood fraction is calculated it can be converted to W according to the following equation:

$$W = \frac{Y_W \zeta_C}{1 - Y_W (1 - \zeta_C)} \tag{3.7}$$

Note that since the wood itself does not burn, and since the pyrolysis reaction shown in equation (3.7) is assumed not to produce any ash, the rate of char combustion G is not required in the equation. If the same balance were written to track the char mass fraction $Y_C$, the carbon consumption rate G would need to be included in the equation leading to the mass conservation equation as shown below in 3.9. Ash is considered a separate solid component once it is released from the burning char particle. Details can be found in Ryan (2002). The char fraction is found using the simple relationship:

$$Y_{CHAR} = 1 - Y_W \tag{3.8}$$

Having determined the extent of pyrolysis and the wood mass, pyrolysis was accounted for in the conservation equations for the solid and gas phases in the bed.

For the solid phase (fuel and ash together), the overall continuity equation is given below [Ryan and Hallett (2002)]

$$\frac{\partial}{\partial t}\left[(1-\varepsilon)\rho_S\right] + \frac{\partial}{\partial x}(\rho_S v_S) = -G\, a_{BC} - r_p \tag{3.9}$$

where $v_S$ is the superficial velocity of the solid phase in bulk and G is the rate of carbon consumption due to char combustion.

This equation is solved for the total solids mass flux, $\rho_S v_S$. Ryan and Hallett (2002) have shown that this in turn is related to the fuel mass flux by

$$\rho_F v_F = \left(\frac{\rho_F}{\rho_S}\right) X_F\, \rho_S\, v_S \tag{3.10}$$

This flux can then be used to solve either the $Y_W$ or the $Y_C$ equation.

### 3.2.2 Gas Phase Transport Equations

The equation for overall gas phase mass conservation equation is

$$\frac{\partial}{\partial t}(\varepsilon \rho_G) + \frac{\partial}{\partial x}(\rho_G v_G) = G\, a_{BC} + r_p \qquad (3.11)$$

The pyrolysis products are assumed to consist of fixed proportions of $\xi_{CO2}$, $\xi_{CO}$ and $\xi_T$ for $CO_2$, CO and tar, respectively. The transport equation for tar vapour (subscript T) is thus given as shown below:

$$\frac{\partial}{\partial t}(\varepsilon \rho_G Y_T) + \frac{\partial}{\partial x}(\rho_G v_G Y_T) = \frac{\partial}{\partial x}\left(\rho_G D_{Peff} \frac{\partial Y_T}{\partial x}\right) + \xi_T r_p \qquad (3.12)$$

where $D_{P\,eff}$ is the effective diffusivity of tar in the gas phase, determined using the correlation of Dixon and Cresswell (1979). Corresponding equations are written for CO and $CO_2$ (Cooper and Hallett, 2000), with terms for the rate of production of each individual pyrolysis product added as:

$$r_{CO_2} = \xi_{CO_2} r_P \quad ; \quad r_{CO} = \xi_{CO} r_P \qquad (3.13)$$

### 3.2.3 Particle Surface Gas Concentration

At the particle surface, the net flux of a given species from the surface is given by the sum of mass transfer due to convection and diffusion as shown below:

$$G_i = \gamma_i(G + G_V) = (G + G_V)\, Y_{iR} + k_{Yi}(Y_{iR} - Y_{i\infty}) \qquad (kg/m^2 s) \qquad (3.14)$$

where $G_V = r_P / a_{BC}$ is the mass flux of pyrolysis gas (v = "volatiles") from the particle surface in kg/s.m$^2$ surface, $\gamma_i$ is the proportion of species i in the total mass flux from the surface, $k_{Yi}$ is the mass transfer coefficient for species i, $Y_{iR}$ is the mass fraction at the particle surface, $Y_{i\infty}$ is the bulk mass fraction surrounding the particle and G is the net flux of carbon from char combustion, so that the first term represents the total mass flux leaving the surface. The efflux of pyrolysis gases at the particle surface will reduce the

$O_2$ and $CO_2$ concentrations at the surface and thus suppress combustion while pyrolysis takes place. By combining this equation with the char oxidation and reduction reaction rates at the surface, the surface concentration of oxygen and other gases can be solved for $Y_{iR}$. An expression like this must be written and solved for the surface concentration of each gas phase component.

These expressions were developed by Cooper & Hallett (2000) for the earlier version of the model. They must be modified to account for the volatiles evolved as CO, $CO_2$ and tar. For CO, the mass flux at the surface of the particle is given by the following equation:

$$G_{CO} = (G + G_V) Y_{OR} + k_{YCO} (Y_{COR} - Y_{CO\infty}) \tag{3.15}$$

The CO flux is also given by reaction rates.

$$G_{CO} = (1 + S_1)(1 - x) G_1 + (1 + S_2) G_2 + \xi_{CO} G_V \tag{3.16}$$

The first two terms, containing $S_1$ and $S_2$, are the mass stoichiometry of the $C+O_2$ and $C+CO_2$ reactions and $\chi$ is the mass of carbon dioxide per kg of product ($CO + CO_2$) as per Cooper (1996), while the third is the CO from pyrolysis. Isolating for CO gas mass fraction we obtain the following:

$$Y_{COR} = \frac{(1 + S_1)(1 - x) G_1 + (1 + S_2) G_2 + k_{YCO} Y_{CO\infty} + \xi_{CO} G_V}{G + G_V + k_{YCO}} \tag{3.17}$$

Similarly for $CO_2$ we obtain the following:

$$Y_{CO_2R} = \frac{\left(\frac{1}{k_{YCO2}}\right)\left[x(1 + S_1) G_1 + \xi_{CO_2} G_V\right] + Y_{CO_2\infty}}{1 + (1 - k_{YCO_2})\left[G + G_V + \frac{S_2 G_2}{Y_{CO_2 Ro}}\right]} \tag{3.18}$$

The mass fractions of CO and $CO_2$ evolved per mass of volatiles, symbolized as $\xi_{CO}$ and $\xi_{CO2}$, respectively in the equation above were determined experimentally. Having removed the CO and $CO_2$ fractions from the gas at the particle surface, the tar production rate is obtained as shown below:

$$G_T = \left(1-\xi_{CO}-\xi_{CO_2}\right)G_V \tag{3.19}$$

and the fraction of tar at the particle surface can be derived as shown below:

$$Y_{TR} = \frac{\left(1-\xi_{CO}-\xi_{CO_2}\right)G_V + k_{YT}Y_{T\infty}}{G+G_V+k_{YT}} \tag{3.20}$$

### 3.2.4 Mass Transfer Coefficient Correction for High Transfer Rates

The mass transfer coefficient given by a mass transfer correlation is for low transfer rates, and needs to be corrected for the effects of high transfer rates. The mass transfer coefficient in equation 3.16 was corrected using a mass transfer number as shown below:

$$k_{Yi} = k_{Yio}\frac{\ln(1+B_i)}{B_i} \tag{3.21}$$

where $B_i$ is the mass transfer number, $k_{Yi}$ is the mass transfer coefficient and $k_{Yi0}$ is the initial mass transfer coefficient before correction. The expression for B can be derived by transforming equation (3.14) into the form shown below:

$$G+G_V = \frac{k_{yi}(Y_{iR}-Y_{i\infty})}{\gamma_i - Y_{iR}} = k_{Yi}B_i \tag{3.22}$$

or;

$$B_i = \frac{Y_{Ri}-Y_{i\infty}}{\gamma_i + Y_{Ri}} \tag{3.23}$$

The mass transfer number, B, was calculated previously for char combustion alone and did not account for the higher mass transfer that can be present during pyrolysis.

Therefore the definition of B was revised to include pyrolysis. If $B$ approaches 0, ln(1+B) approaches 0, and the correction was set to 1 to avoid a division by 0 in equation (3.21). If $B_i$ is low the mass transfer is low.

### 3.2.5 Particle Density

The fuel density will not be constant during pyrolysis. At any point in time the particle was modeled as composed of unpyrolyzed wood, and char, the ash being contained in the char until it is released by char combustion. The fuel particles are assumed not to change size during pyrolysis, so that the char density is $\rho_C = \zeta_C \rho_{F0}$, where $\rho_{F0}$ is the initial fuel density, and the fuel particle density at any time is given below:

$$\rho_F = \frac{1}{\left[\frac{Y_W}{\rho_{FO}} + \frac{Y_{char}}{\rho_C}\right]} = \rho_{FO}\left[W + (1-W)\zeta_C\right] \tag{3.24}$$

### 3.2.6 Start of Char Combustion

Char combustion is assumed to occur only after a very small thickness of char layer is formed outside the particle as shown in **Figure 3.1**. However, as the char combustion rate in the model is dependent on the oxygen concentration at the surface of the particle, attempts to model pyrolysis and combustion simultaneously from ignition created instabilities. Char combustion occurred prior to pyrolysis, giving unreasonable results and an unstable model.

Thus, to ensure char combustion could not occur prior to pyrolysis, the rate of char combustion was ramped up linearly from 0 to 100% based on the thickness of the developing char layer around the particle based on a given mass of wood converted to char. This assumption delays char combustion until 2% of the wood mass has been converted to char by devolatilization. Once a pre-set thickness was reached char

combustion was allowed to occur. As the model actually assumes a uniform particle composition, the thickness of the thin char layer required before char combustion could occur was simulated by a specified wood mass fraction. The equations used for char combustion reate G are:

$Y_W \geq Y_{W\,UPPER}$ : $G = 0$

$Y_{W\,UPPER} > Y_W > Y_{W\,LOWER}$ : multiply G by $\frac{Y_{Y\,UPPER} - Y_W}{Y_{W\,UPPER} - Y_{W\,LOWER}}$

$Y_{W\,LOWER} \geq Y_W$ : G unmodified.

After the thin char layer was formed ($Y_W < Y_{W\,LOWER}$), the full char combustion value was used and no explicit decision was taken as to whether or not char combustion would react during devolatilization. Once started the pyrolysis gases created reduce the oxygen concentration at the surface and both reactions can occur simultaneously as determined by the oxygen rate and extent of pyrolysis. $Y_{W\,UPPER}$ and $Y_{W\,LOWER}$ are currently set at 0.98 and 0.95.

## 3.3 Energy Equation

The energy equation for the solid phase including pyrolysis of a particle is:

$$\frac{\partial}{\partial t}(1-\varepsilon)\rho_S h_S + \frac{\partial}{\partial x}\rho_S v_S h_S = \frac{\partial}{\partial x}\left[\frac{k_{eff}\partial T_S}{\partial x}\right] + h_{sg}a_{BC}\Delta Hr_C + r_P\Delta H_P \qquad (3.25)$$

where $\Delta H_p$ is the heat of pyrolysis in kJ/kg gas produced. A $\Delta H_p$ greater than 0 indicates an exothermic reaction). $k_{eff}$ in the energy equations for the solid is the thermal conductivity of the bed determined from the thermal conductivity of the solid and the bed geometry using the Yagi and Kunii correlation as described by Cooper and Hallett (2000). The heat of reaction from pyrolysis is reported to vary greatly in the literature. Although currently the heat of reaction of pyrolysis has been set at -538 kJ/kg, based on Milosavljevic et al. (1996), the model allows a variation of the value of the heat of

pyrolysis to be conducted to study its effect on combustion. A discussion on the different values of heat of pyrolysis found in literature was given in **Section 2.2.3**.

The heat transfer coefficient from the gas to the solid $h_{sg}$ in the above was corrected for the mass transfer during pyrolysis using an equation similar to that for the mass transfer coefficient given earlier:

$$h_{sg} = h_{sgo} \frac{\ln(1+B_t)}{B_t} \tag{3.26}$$

where $B_t$ is the thermal transfer number and $h_{sgo}$ is the heat transfer coefficient without mass transfer. $B_T$ can be related to the mass transfer number $B_i$ by writing the relationship to the total mass flux from the surface in terms of $B_t$ and $B_i$:

$$G = \frac{\rho D_i \ln(1+B_i)}{\delta} = \frac{\lambda \ln(1+B_i)}{C_p \delta} \tag{3.27}$$

where $\delta$ is the thickness of the boundary layer on the particle. We then obtain the following equation:

$$B_t = (1+B_i)^{Le} - 1 \tag{3.28}$$

where Le is the Lewis number of the gas, defined as

$$Le = \frac{\rho D_i C_p}{\lambda} \tag{3.29}$$

This equation requires the use of gas phase thermal conductivity, specific heat and density. The gas phase energy equations and values are not changed from the earlier Cooper and Hallett (2000) model.

### 3.3.1 Thermal Conductivity

The thermal conductivity of the solid will vary as pyrolysis proceeds and the particle's density changes. The correlation presented by Koufopanos et al. (1991) was used to calculate the thermal conductivity of the wood, as shown below:

$$k_{wood} = 0.13 + 0.0004T \qquad (W/mC) \tag{3.30}$$

The program has been developed to allow a similar correlation presented by Gupta et al. (2003), where $k_{wood} = 0.035 + 0.000173T$ (K), to be used as an alternative if desired.

The model presented by Larfeldt et al. (2000b) was used to calculate the thermal conductivity of the char since it includes the effect of radiation in the larger pores. Within the temperature range of the experiments, this model provides reasonable values that are not negative or very high, unlike models proposed by Gupta et al. (2003):

$$k_{char} = k^0_{char} + \varepsilon\left(k_g[T] - k_g[T^0]\right) + k_{rad}[T] \tag{3.31}$$

where $k^{\circ}_{char}$ is the effective thermal conductivity at room temperature, given as 0.1 W/mK, $\varepsilon$ is the porosity, and $k_g$ and $k_{rad}$ are the gas phase conductivity and the diffusive contribution from radiation heat transfer, respectively. The $k_{char}^{\circ}$ value of 0.1 W/mK is close to the values of Grønli and Melaaen (2000) and Gupta et al. (2003).

The gas and radiation heat transfer model equations are given below:

$$k_g[T] = 9.0037x10^{-3} + 5.6263x10^{-5}T \tag{3.32}$$

$$k_{rad}[T] = 4\varepsilon_g^{macro}\sigma\psi d_{macropore}T^3 \tag{3.33}$$

where $\sigma$ is the Stefan-Boltzmann constant, $\psi$ is the emissivity set at 0.9 as per the Gupta et al. (2003), $d_{macropore}$ is the macro-pore diameter and $\varepsilon_g^{macro}$ is the macro-porosity of the gas through the charcoal structure. The macro-porosity and macro-pore diameter used

were 0.6 and 0.35 * $10^{-3}$, respectively, taken from Larfeldt et al. (2000b). For the partially pyrolyzed particles, the thermal conductivity was interpolated between that for char and wood using the wood fraction as shown below:

$$k_{fuel} = Y_W k_{wood} + (1 - Y_W) k_{char} \tag{3.34}$$

### 3.3.2 Specific Heat

The correlation proposed by Grønli et al. (1982) was used to calculate the overall specific heat $c_p$, of the wood:

$$c_{p-wood} = 5.46T - 524.77 \tag{3.35}$$

where T is in K and the units of $c_p$ are J/kgK

The correlation above was found to have a correlation coefficient of 0.995 between 300 and 400 K by the author. This correlation provides reasonable results in that the thermal conductivity of the wood is not very different to that of char at high temperatures.

The correlation proposed by Larfeldt et al. (2000b) was used to calculate the specific heat of the char:

$$c_{p-char} = 1430 + 0.335T - 7.32x10^{-2} \tag{3.36}$$

For the partially pyrolyzed particles the specific heat value was interpolated between those for char and wood using the wood fraction:

$$c_p = Y_W c_{p-wood} + (1 - Y_W) c_{p-char} \tag{3.37}$$

### 3.3.3 Tar Properties

As the model already included properties for CO, $CO_2$, $O_2$ and $N_2$, only tar properties needed to be added for gas phase computations. It was decided to use levoglucosan ($C_6H_{10}O_5$), which is essentially one unit of cellulose, as a representative substance on

which to base the properties of the tar vapour being evolved. It has been found to be compositionally similar to the products of pyrolysis by Oasmaa and Czernik (1999). Properties for levoglucoscan (thermal conductivity, specific heat and diffusivity) were estimated using correlations from Reid et al. (1987) as done earlier by Cooper and Hallett (2000) for properties of other gases.

## 3.4 Radiation Boundary Conditions

The previous model took into account radiation from the bed surface, the walls, and the lab outside, but not volatiles flame radiation. It assumed that the wall and surface above the bed were maintained at the same temperature as the incoming particles. Although not a serious concern for fuels with a low volatile content, with wood the combustion of pyrolysis reaction products above the bed can cause additional radiant transfer to the bed surface. Although convective and conduction heat transfer are included in the model, neglecting volatiles flame radiation could potentially overestimate the amount of heat lost above the bed, resulting in lower predicted solid temperatures.

Calculation of the effect of radiation above the bed has not been changed from the previous model. However experimental data, as described in **Section 4.5**, were taken to allow an analysis of the effect of radiation and to help determine if further model refinement is required.

## 3.5 Numerical Method

The governing equations were solved using the finite volume discretization techniques of Patankar (1980), the bed being subdivided into a number of slices and a balance being done for each slice. Discretization of differential equations results in linear algebraic equations that can be solved using matrix methods. Details of the discretization

employed have been described by Cooper (1996) and Ryan (2000). Discretization was also required to solve for the extent of pyrolysis given by the equation 3.5 in "Extent of Pyrolysis". In this study the control volumes were set to be evenly spaced as opposed to the exponentially increasing slices used by Cooper and Hallett (2000). A typical solution grid is shown in **Figure 3.2** below.

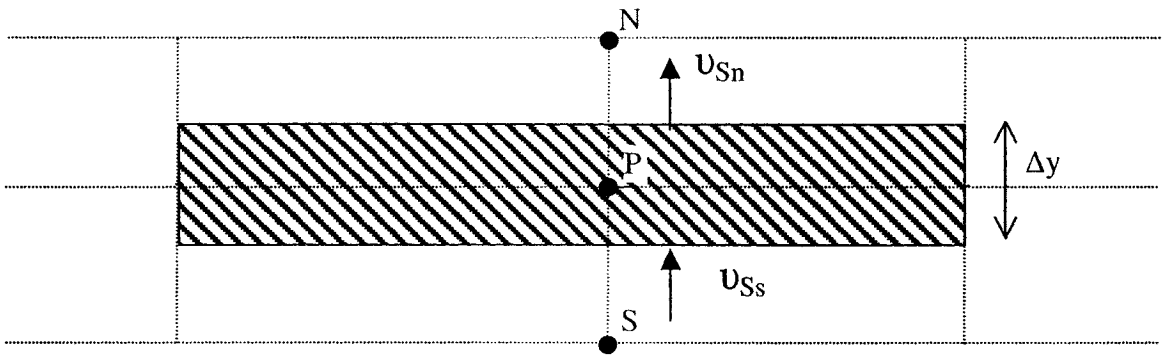


**Figure 3.2: Schematic of Typical Control Volume for a Generic Model**

Since the current model assumed radial variations to be negligible, there is no "east-west" variation. To solve the "extent of pyrolysis" equation for $Y_w$ the coefficients are given by the equation below:

$$a_p Y_{Wp} = b_N Y_{Wn} + c_S Y_{Ws} + S_C + S_P Y_{Wp} \tag{3.38}$$

where the subscripts P, N, and S refer to the node being solved, the node to the north and the node to the south, respectively:

$s_C = 0.0$

$s_P = - r_P \ / \ [(1-\xi_C) Y_{Wp}]$

$a_O = \rho_{Fn} x_{Cn} (1-\varepsilon)$

$$a_P = a_O - s_P$$

$$b_N = \rho_{FN} \ / \ \rho_{Sn} * x_{Cn} * v_{Sn}$$

$$c_S = \rho_{FS} \ / \ \rho_{Ss} * x_{Cs} * v_{Ss}$$

$$Y_W = \left(1-\varepsilon^0\right) x_c^0 \rho_c^0 Y_W^0 \left(L - L\Delta t\right)\left(\xi_N - \xi_S\right) - \left[ Ga_B \left(1+\alpha\right) - \frac{\xi_C r_p}{1-\xi_C} \right] \Delta t \left(\xi_N - \xi_S\right) + s_C \quad (3.39)$$

where ° refers to the value of the variable at the beginning of the time step involved.

# 4 EXPERIMENTAL ASPECTS

## 4.1 Experimental Reactor

The experimental combustor, shown in **Figure 4.1**, is of the overfed-bed type, in which the fuel is fed from above and the air supplied from below. It consists of four sections: a grate, the bed section, an afterburner and a canopy exhaust hood. The combustor is insulated with refractory lining to help prevent heat loss. It is also equipped with an afterburner and exhaust hood to burn off, dilute and remove combustion products. Ports in the combustor allow type B thermocouples to be placed radially at different locations in the bed. Two vertical traversing probes allow sampling for gas and tar concentrations. The probes may be used to sample radially if desired. A metal grate supports a 23 cm diameter bed with heights of up to 23 cm.

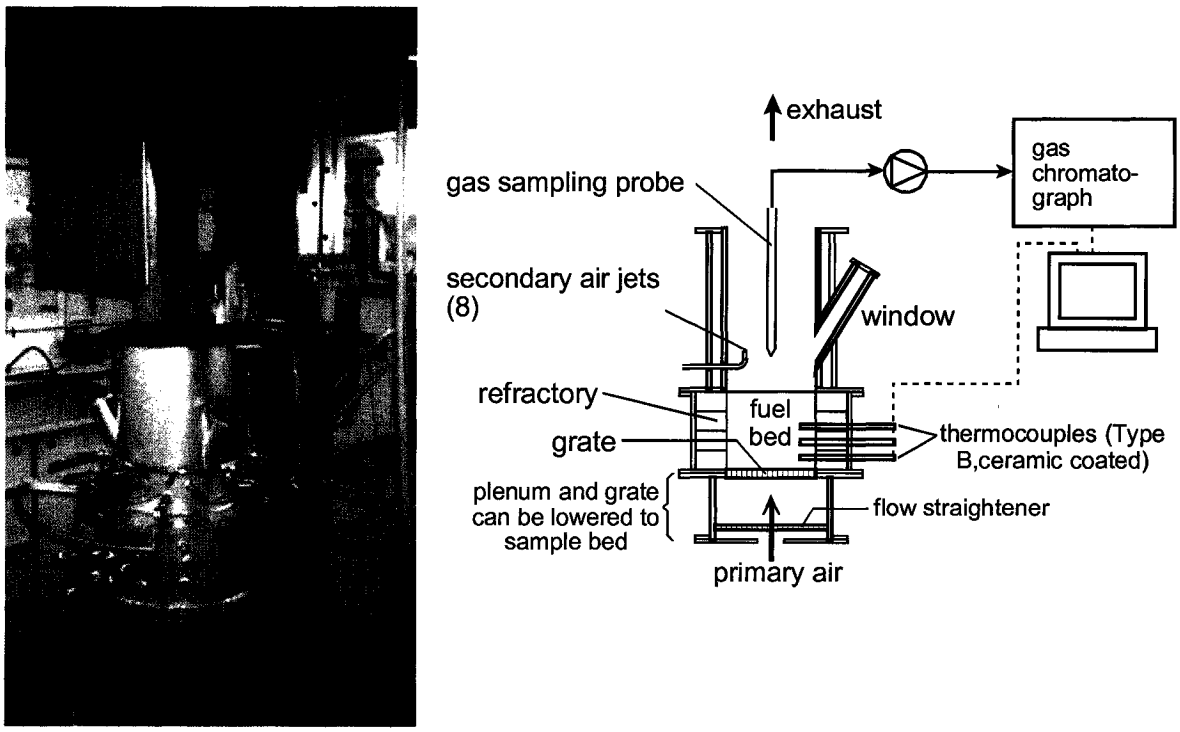


**Figure 4-1: Photo and Diagram of Packed Bed Combustion Reactor**

## 4.2 Experimental Procedure

An experiment was started by igniting between 200 g and 500 g of wood using a propane torch. Wet and dry bulb temperature measurements of the supply air were taken prior to ignition. The primary air rate was set, time noted and data acquisition started. Once an even distribution of flames was observed on this first layer of fuel, wood was added in 500 g increments until the desired bed height was reached. During this period when the desired height was being achieved overfire air and a propane torch were used to flare off the volatiles and reduce air emissions.

Once the desired bed height was achieved, fuel was added at 5 minute intervals to maintain a bed height that varied by only about +/- 2 cm, (approximately one particle diameter). At each wood addition the quantity was entered in the data acquisition system. The height of the bed was maintained between 19-23 cm during sampling. Two methods were used to verify that the bed was in more or less steady state operation. Firstly, the temperature profile of the bed was observed to obtain an estimate of the degree of steady state. Temperature variations at the top of the bed greater than 100°C were used as an indication of unsteady operation. Secondly, a specially designed rod with foot similar to a hoe used in gardening was used to monitor the bed height and ensure that it was uniform. Maintaining the bed height proved to be a labour intensive task requiring the fulltime attention of one person throughout the 4-5 hours of the experimental run while another would coordinate the tar and gas sampling. Temperature, tar and gas sampling are discussed in detail in the instrumentation section of this chapter.

At the conclusion of a run, the bed reactions were quenched by replacing the supply air with nitrogen. After approximately 10 minutes when the bed temperature readings were below 200°C, the nitrogen flow was reduced and the bed was allowed to cool for another

20 minutes. This extra cooling helped ensure that the char would not re-ignite during sectioning of the bed.

To obtain samples for particle size, density and ASTM analysis, the bed was sectioned in horizontal slices. This was accomplished by lowering the base of the combustor approximately 4 cm, inserting a sheet of metal in a specially designed holder to prevent the rest of the bed from falling, removing the particles and repeating the procedure for the remainder of the bed. Particles were non-friable and therefore they generally did not crush upon sectioning. Typically, the bed could be sliced into four sections.

## 4.3 Particle Size, Density and Proximate Analysis

After slicing the extinguished bed, representative particle samples from each slice were obtained following a modified ASTM D346-35 specification. This procedure consists of mixing, coning and quartering a pile of particles in order to retain a representative sample for laboratory analysis. This procedure was repeated for each slice until only 7 to 15 particles remained. These particles were then used in the particle size, density and proximate analysis determination.

Particle sizes and density for the feed fuel and the bed samples were determined using a caliper with a 0.01 cm precision and an electronic scale. Proximate analysis of these samples was carried out using the ASTM D1762-84 test for wood charcoal. The particles were ground using a mill and sieved to collect samples between 100 and 200 mesh sizes. To summarize the method, the moisture content was determined by the weight difference after heating at 105°C for 2 hours; the volatiles content by weight difference after heating at 950°C for 11 minutes; and the ash content by weight difference after heating at 750°C

for 6 hours. The weight measurements were taken using a Metler AJ150 scale with 0.1 mg precision.

## 4.4 Fuel and Run Conditions

Untreated spruce with a density of approximately 521 kg/m$^3$ (+/- 24 kg/m$^3$) was used for all experiments[3]. The fuel was cut into uniform parallelepipeds : this shape was found to ensure random packing yet allowed sphericity to be calculated easily. A photo and diagram of the particles is shown in **Figure 4.2**.

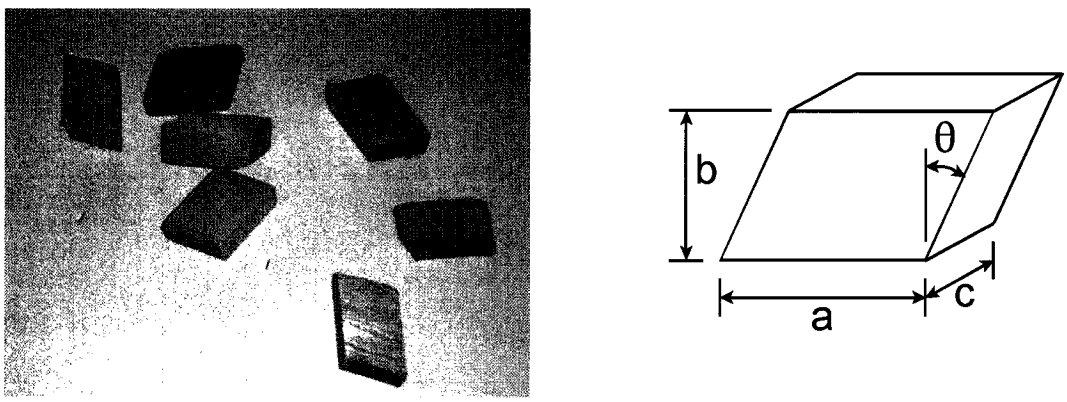


**Figure 4-2: Fuel Particles**

The equivalent particle diameter, angle and sphericity for the two fuel sizes used were 3.41 cm (+/- 0.07cm), 20° and 0.759, respectively for the larger particles and 2.82 cm (+/- 0.09m), 25°, 0.772, respectively for the smaller particles. The sphericity and equivalent particle diameter were calculated using the method proposed by McCabe et al. (1993)

[3] Unless otherwise specified all confidence intervals within this document are stated for 95% probability.

and discussed by Ryan et al. (1999). The equivalent particle diameter is the volume equivalent as shown below:

$$d = (6/\pi\ abc\ )^{1/3} \qquad (4.1)$$

where a, b and c are the lengths of the particle as shown in **Figure 4.2** above. The wood used was allowed to sit in the reactor laboratory room for at least two weeks prior to running an experiment to allow its moisture content to equilibrate with the laboratory environment.

**Table 4.1** summarizes the experimental operating parameters. All runs were conducted with a primary air flowrate of 107.7 kg/m$^2$h, except one run at 129.5 kg/m$^2$h. Runs lasted from 3.2 to 5.1 hours. Bed heights ranged from 19 to 23 cm.

**Table 4-1: Experimental Operating Parameters**

| **Variable** | **Experimental Range** |
|---|---|
| Primary air (kg/m$^2$h) | 108 or 130 |
| Measured average burning rate (g/min) | 50 to 71 |
| Test duration (h) | 4 to 5 |
| Bed height (cm) | 19 to 23 |
| Particle equivalent diameter (cm) | 3.41 +/- 0.07 or 2.82 +/- 0.07 |
| Sphericity | 0.76 |
| Fuel Type | Untreated spruce |
| Proximate analysis (wt% - dry basis) | Moisture: 5.7 % +/- 1.2 wt%;<br>Volatiles: 84 % +/- 0.7 wt%; and,<br>Ash: 0.36 % +/- 0.11wt% |

During the experiments, three types of measurements were taken: temperature, tar concentration and gas concentration. The following section describes the equipment used to obtain these measurements, the method used to analysis the results and the methods used to obtain representative readings.

## 4.5 Temperature

All the thermocouples used for these experiments were Type-B (Pt-30%Rh/Pt-6%Rh) and capable of withstanding temperatures up to 1700°C. These thermocouples are reported by the supplier, Omega Technologies, to have an accuracy of +/- 2°C. They were housed in ceramic tubes to provide durability and maintain the thermocouple tip at a known vertical height within 0.5 cm. Due to the lower temperature of wood combustion compared to coke combustion, no coating other than the ceramic tubes was used.

All of the thermocouple wires used were 0.008" (0.020 cm) in diameter except one used to measure the radiation effect above the bed, which was 0.015" (0.038 cm). The temperature readings were taken at a radial distance of 4 cm in from the reactor wall and at 3 cm, 6.5 cm, 12 cm and 14.5 cm above the grate. Temperature readings to quantify the radiation effect were taken at a height 24.5 cm above the grate using a special ceramic tube with four holes that allows the tips of a 0.008" and a 0.015" thermocouple to be within 3 mm of each other.

The thermocouples were connected to a National Instruments SC-2070 terminal board and National Instrument AT-MIO-16XE-50 data acquisition board. LabView software was used to record the temperatures at 10 seconds intervals.

## 4.6 Tar Sampling

Conventional tar sampling methods described in **Chapter 2.4.1** quantify tar concentrations in the flue gas leaving the combustion process and thus treat the combustion process as a black box. To allow comparison of the mechanistic model prediction of volatile evolution within the bed with actual data these sampling methods would not provide the required information. In this section, the design considerations for the newly developed tar sampling probe will be described followed by a description on the sample train, method of analysis and sampling method. With this method, the sample collection occurs directly at the location of volatile evolution.

### 4.6.1 Design Considerations

The main design considerations were the ability to measure local tar concentrations within the bed, flexibility and safety. This implied that the method would need to minimize tar collection in the sampling line before sampling the location and include a check for inefficient tar capture. The methods reported in **Section 2.4.1** for measurements of tar from stacks would likely lead to clogged probes and lines when sampling the higher concentration of liquid tar found within a bed. Based on TGA studies discussed in **Chapter 2.2**, it was estimated that about 0.36 g of tar is produced per gram of fuel burnt or less than 0.04g/min of liquid tar in a one cubic centimetre area for the operating conditions of these experiments. Since tar is a sticky and viscous it can easily collect in sample lines. It was therefore decided that a new method was required for sampling tar within a bed. The method also needed to have the flexibility to sample at various heights in relatively short periods of time and to allow for modification of the sampling conditions (flow control and some degree of control over sampling

temperature) to meet those of the combustor. The equipment therefore needed to allow for temperature and flow control. Another important consideration that restricted design options was safety. The temperature within a combusting bed of wood can reach 1200°C, thereby restricting the selection of material and construction method available. A search was conducted for materials that could capture condensing tar liquid and withstand high temperature. Glass wool, porous ceramic and a nickel chrome metal foam were found to be possible candidates. The nickel-chrome foam was selected for its heat transfer properties. It transfers heat at a faster rate than glass or ceramic, thus allowing for quicker cooling and slightly quicker response to change in cooling water temperature.

### 4.6.2 Probe Description

The nickel-chrome 'filters', probe tip, sampling train and probe installation designed are shown in **Figures 4.3, 4.4, 4.5** and **4.6** respectively. Constructed of stainless steel, the probe designed draws combustion gases from within the bed and cools them to approximately 150°C rapidly enough to condense the tar at the tip of the probe on a nickel-chrome metal 'filter'. Oesch et al. (1996) also used 150°C as their controlled condensation temperature for tar sampling. The custom-made tar filters, shown in **Figure 4.3**, are 3/8" (0.952 cm) diameter cylinders with a height of 0.55" (1.4 cm) cut from a sheet of Retimet metal foam made by Dunlop Ltd.. The very open structure of the foam allows for collection of droplets. The metal properties of the foam provide the required heat transfer properties to be achieved while maintaining the probe tip dimensions comparable to one equivalent particle diameter.

**Figure 4-3: Nickel-Chrome Metal 'Filter' (Regenerated on left, Filter After Tar Collection on right)**

The tar 'filter', held in place by a collet and sealing ring, can then be removed and replaced for the next sample as shown in **Figure 4.4**. Filters were machined to a close fit with the collet. The collet contracts around the filter as a ring is tightened to seal it in place. This also ensures good thermal contact as well as stopping tar from by-passing the filter. Precise metering of flowrate for a given time is needed throughout the sampling period. The probe tip was made of brass rather than stainless steel for good heat conduction.

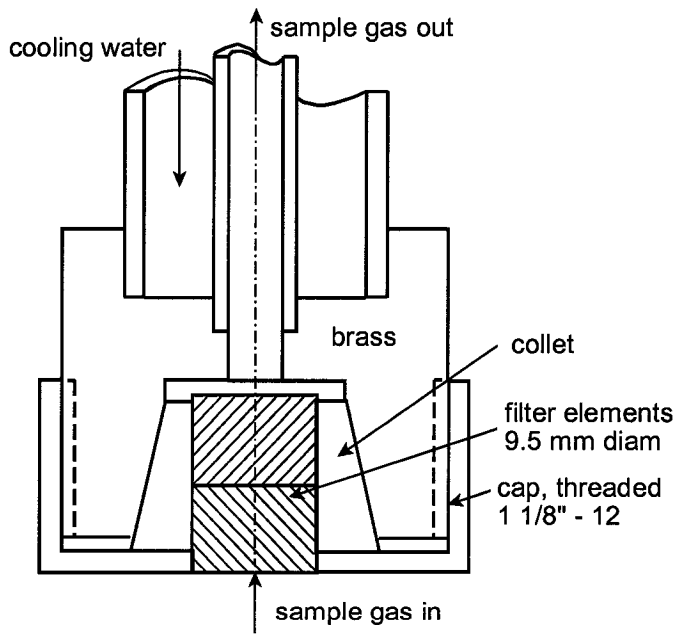


**Figure 4-4: Tar Probe Tip**

Cooling of the filter and probe is accomplished through 50°C water, supplied by a quarter inch 0.035" wall thickness tube terminating approximately 3 cm from the probe tip. The

cooling water, supplied at a minimum rate of 3.6 L/min, is return through a ¾" outer tube return which surrounds both the combustion gas and water supply tubing. The combustion gas sampling tube is ¼" diameter O.D. to help ensure that clogging would not be an issue. The gas flow is monitored and controlled with a flowmeter. Further details on probe design are provided in Appendix B.

### 4.6.3 Method of Analysis

The concentration of condensable volatiles (tar) is found by dividing the change in mass of the metal filter by the metered quantity of gas drawn through the filter. The sample gas flow was measured with a rotameter, whose readings were corrected for the sample temperature and pressure. There is some uncertainty in the temperature of the gas drawn through the probe: the gas leaves the probe at a temperature near the cooling water temperature, or 50°C, but it then passes through several meters of piping at the ambient temperature, which could vary from 15°C to 33° depending on the weather outdoors.

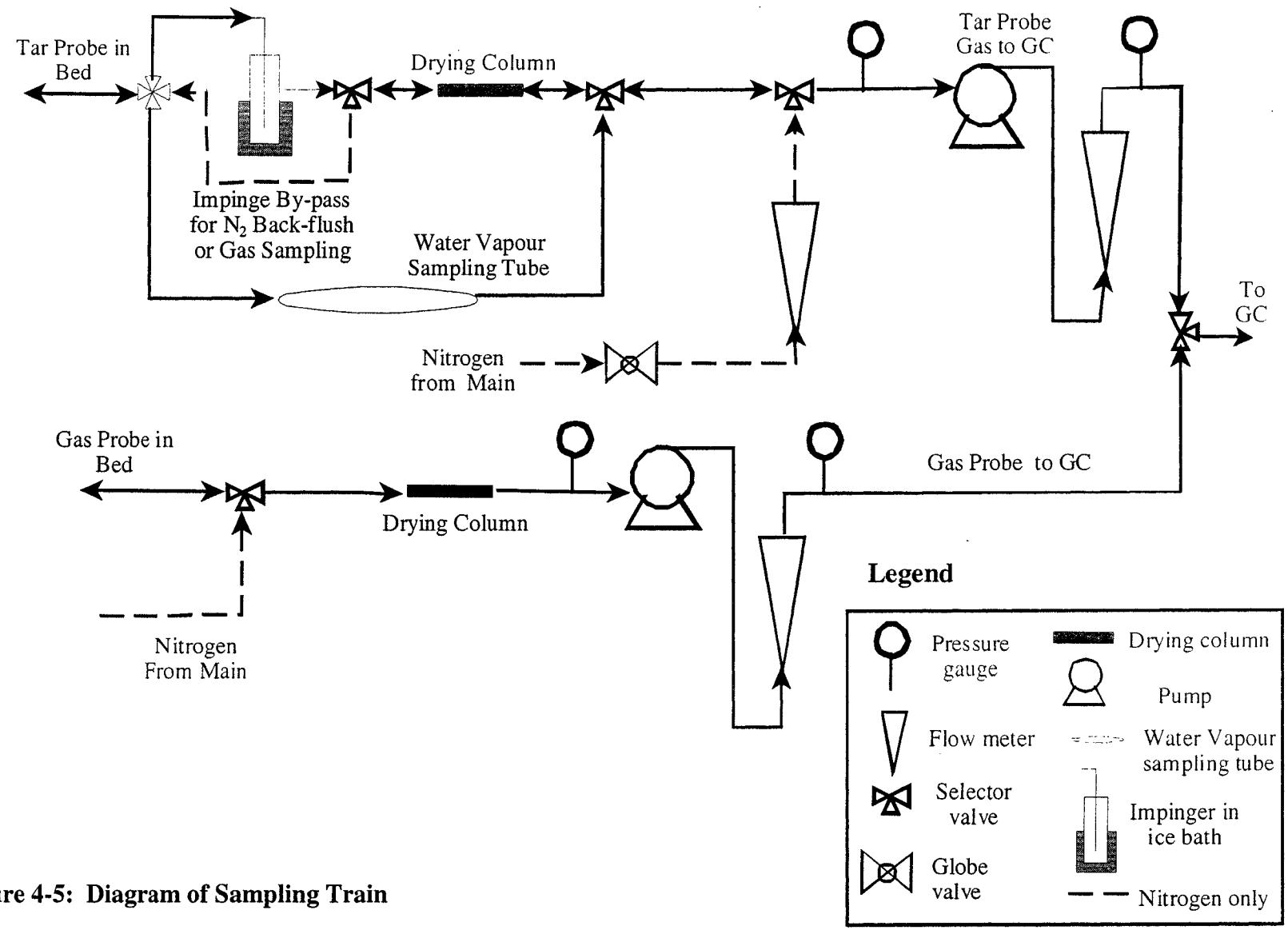


**Figure 4-5: Diagram of Sampling Train**

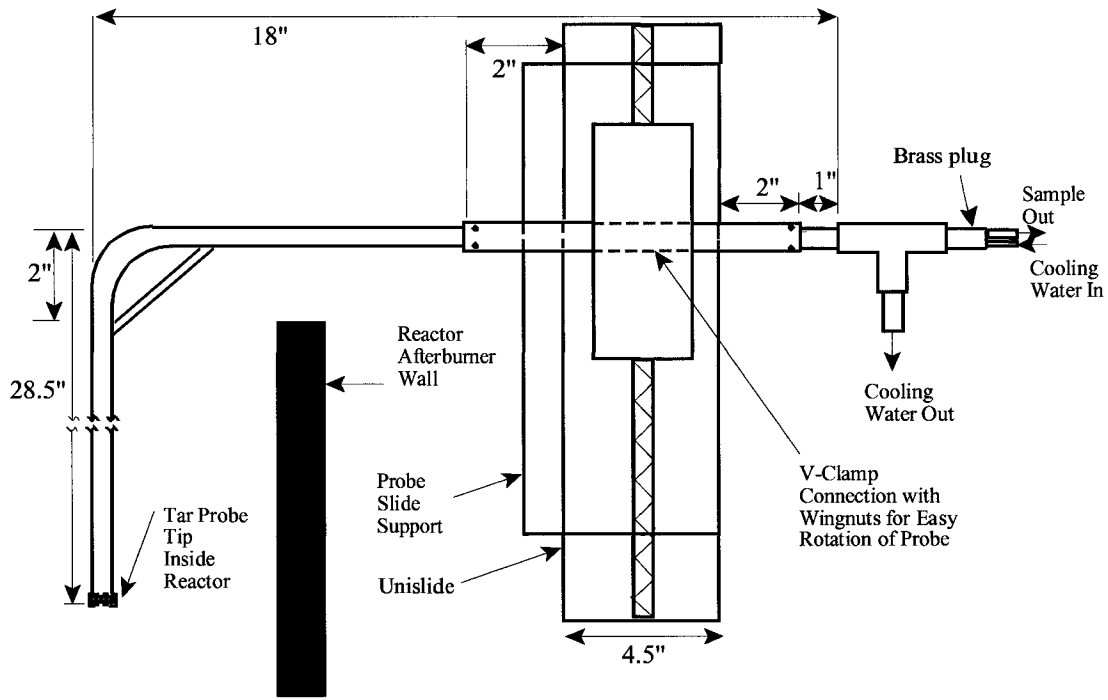


**Figure 4-6: Tar Probe Diagram**

### 4.6.4 Tar Sampling Method

To take a tar sample, the probe was lowered until the desired height in the bed was reached. A nitrogen back flow was used while lowering the probe in the bed to help prevent any accumulation of tar on the tip before the sampling began. Sampling began immediately once the desired height was reached, since preliminary tests as discussed in **Chapter 5.2.2.1** showed that leaving the probe in the bed without drawing gas through it could result in a collection of tar on the filter. The start of sampling was coordinated with the start of a wood feed to the bed.

Trial and error sampling was required to determine the length of the sampling time required at a given height without showing evidence of break-through in the filter. The sample time varied between 4 and 10 minutes with the average sample time lasting 6 minutes. After sampling the probe was raised quickly from the bed and the filter removed and replaced with a new one. The filters were then weighed to determine the approximate mass of tar generated over a known time at a specific location.

Since tar is darker than the grey colour of the metal, if tar breaks through to the top side of the filter a visual indication is provided that not all the tar was captured in the filter. At this point the filter could in theory be washed with a solvent and analyzed in an HPLC to obtain an approximation of the breakdown of species collected. However, currently only a quantification of the mass of tar collected and qualitative observations are done.

### 4.6.4.1 Flowrate Selection

The tar probe sampled approximately isokinetically so as not to disturb the flow in the bed[4]. To achieve this, the sampling flow was set to a rate equivalent to the superficial velocity in the bed based on the supply airflow rate to the reactor. This flowrate was not changed with location in the bed. In reality, the gas mass increases as one moves up through the bed, owing to products of combustion and pyrolysis being added to the stream. In theory, one could use changes in the $N_2$ fraction to calculate this increase; however, this information is not available until after a run when data are reduced. The sampling rate is therefore somewhat lower that isokinetic for many tar data points. However, deviations from isokinetic sampling are mainly a concern when sampling particulate, and since the sampled gas flow is low, departures from isokinetic conditions should not disturb the bed much.

### 4.6.4.2 Cooling Water Temperature

Near the top of the bed some moisture is evolved. To avoid condensation of the water vapour in the probe, the cooling water temperature was kept above the dew point, estimated as 40-45°C. An Omega digital thermometer with alarm was used to help ensure that the cooling water temperature was maintained between 47°C to 53°C during sampling. The water was heated using the recycled cooling water from the reactor jacket, and gas sampling probes. When required, the cooling water temperature was reduced using either a radiator for slow cooling or fresh tap water for rapid cooling. A diagram of the cooling water lines is shown in **Figure 4.6**.

---

[4] Isokinetic sampling is used to ensure that the gas being drawn through the end of a sampling nozzle is representative of that of the surrounding gas, and is achieved by ensuring the velocity the gas is being drawn into a probe at the same velocity as the surrounding gases. Isokinetic sampling is particularly important with particulate because if sampling at slower rate, the smaller particles will be follow the gas flow while the heavier particles will continue on a straight path into the sampling probe.

### 4.6.4.3 Cleaning

Since a tight seal is required to ensure the sample gas passes thought the metal filter the collet and nut were cleaned between every sample. Methanol was chosen as the cleaning solvent, instead of dichloromethane. Methanol is known to dissolve bio-oils [Oasmaa and Czernik (1999)] and dichloromethane is a health concern due to its low boiling point (40°C) and toxicity. Since the goal of the testing was to capture tar, and not at this point provide a chemical analysis of the tar, degradation of the species for further analysis was not a concern for these tests.

### 4.6.4.4 Metal Filter Regeneration

After a run the metal filters were washed in methanol and then heated to 275°C to remove the collected tars. The filters were heated for 3 hours, inspected for discoloration, and the process repeated until the colour or the filter appeared the same light grey as the unused metal foam. The colour difference between a used and regenerated filter can be seen in **Figure 4.3**. The process was then repeated at 350°C. Metal filters which appeared dented were not reused. One filter was sectioned as reassurance that when no colour appeared on the outside of the filter the inside was also relatively free of collected tar.

## 4.7 Gas Concentration Measurements

Gas samples were taken using a vertically-traversing water-cooled probe in addition to the tar probe. In the lower half of the bed a convection quench probe as described by Ryan [2000] was used and in the upper half of the bed the tar sampling probe described above in **Section 4.6** was used. The convection quench probe was used in the lower section of the bed, since at high temperatures and in the presence of $O_2$ and CO quenching is required to freeze the species concentrations. The tar sampling probe was used in the upper half of the bed since oxygen is no longer present, eliminating the

concern of secondary reaction in the sampling line, and since tar was found to frequently clog the 1.6 mm ID sample tubing of the gas probe. (During development of this sampling method tar clogging of the gas convection-quenching probe, sample lines and pump proved to be frequent occurrences.) Sampling the gas concentrations with the tar probe also allowed tar and gas samples to be taken from the same location, reducing uncertainty in comparison of the two measurements.

### 4.7.1 Analysis of Gas Concentrations

For both probes, the gas samples were drawn under vacuum through the probe and then pumped to a Varian 3000 gas chromatograph equipped with a Carboxen-1000 column and thermal conductivity detector for analysis. The sampling train is shown in **Figure 4.5**.

The gas chromatograph was connected to a National Instrument AT-MIO-16XE-50 data acquisition board. LabView software was used to calculate the gas concentrations and record the values. Methane, acetylene, ethylene and ethane were added to the DAQ system to allow these peaks to be integrated should they be present. The weighting factors were taken from Kaiser (1963) for these new compounds. Ryan's (2000) response factors for CO, Ar, $CO_2$, $O_2$ and $N_2$ were not changed. All response factors are shown in **Table 4.2**. A calibration gas of 10% CO, 10% $CH_4$, 15% $CO_2$, balance nitrogen was used prior to each run to check for leaks and proper operation of the gas chromatograph. Acetylene gas was also used to determine the peak location for $C_2H_2$.

**Table 4-2: Response Factors for Gas Chromatograph Analysis**

| Compound | Weighting Factor |
|---|---|
| $O_2$ | 1.293 +/- 0.002 |
| AR | 1.420 |
| $N_2$ | 1 |
| CO | 0.998 +/-0.003 |
| $CH_4$ | 0.86 |
| $CO_2$ | 1.298 +/- 0.01 |
| $C_2H_2$ | 2.29 |
| $C_2H_4$ | 1.71 |
| $C_2H_6$ | 1.70 |

### 4.7.2 Gas Sampling Method

When either probe was lowered into the bed a nitrogen back flush was used to avoid clogging and particle deposits. The tar sampling train is equipped with a three-way selector valve that allowed by-passing the impinger during nitrogen back-flushing and gas sampling. Once at the desired height, gas was then drawn through the probe for at least 3 minutes to ensure the gas sampled by the GC was representative of the gas at the specific bed location. It was estimated that the largest volume of gas between the tip of either probe and the GC was 0.2 litres. Therefore, at the lower gas sampling rate of 0.432 L/min the line should be more than sufficiently flushed after 3 minutes. For reasons previously discussed in **Section 4.6.3** gas samples were taken quasi-isokinetically.

# 5 RESULTS AND DISCUSSION

The following section presents and discusses the results of the experimental sampling and modeling, including gas and tar concentrations, particle density and size, proximate analysis and temperature. Next, the model predictions are discussed, investigating the effect of the kinetic rate constants, ratio of pyrolysis products and the effect of the radiation above the bed. Modeling results are then compared to experimental gas and tar profiles, particle density and size, proximate analysis, temperature and the air to fuel ratio. Finally, the section will conclude with a brief discussion on the observed effect of particle size and airflow rate on combustion conditions.

## 5.1 Fuel Bed Experiments

A total of 8 runs were conducted using the operating conditions are listed in **Table 5.1**. Experiments were conducted for a period long enough to obtain four tar samples at 2 cm intervals from the top of the bed plus at least one replicate tar sample per run. The first five runs were conducted as replicates in order to test the tar sampling method and its replicability. The bed height shown in **Table 5.1** was the nominal value maintained during the run; however, in fact feeding was intermittent (typically every 5 minutes) and the height could fluctuate by +/- ½ particle sizes, or between 19 and 23 cm. Proximate analysis and density measurements could not be taken for two runs (071102 and 081102) since the bed was not quenched properly. The concentration and temperature profiles obtained from these experiments are presented in **Figures 5.1-5.5** and **5.22-5.25**.

**Table 5-1: Run Conditions**

| Test | Bed Height (cm) | Particle Size L - LARGE S – SMALL (cm) | Air mass flux ($kg/m^2h$) | Measured average burning rate ($kg/m^2min$) | Test duration (h) |
|---|---|---|---|---|---|
| 071102 | 21 | L (no bed sample) | 108 | 1.24 | 4.5 |
| 072202 | 22 | L - 3.42 | 108 | 1.25 | 4.7 |
| 081102 | 22 | L (no bed sample) | 108 | 1.44 | 5.1 |
| 092502 | 22 | L – 3.29 | 108 | 1.40 | 4.2 |
| 121302 | 22 | L – 3.35 | 108 | 1.15 | 4.7 |
| 121802 | 22 | S – 2.80 | 108 | 1.27 | 4.2 |
| 010803 | 22 | S – 2.81 | 108 | 1.25 | 3.8 |
| 011303 | 22 | S – 2.71 | 130 | 1.56 | 3.2 |

The properties of the fuel used in the experiments are summarized in **Table 5.2** below. These properties were determined using the methods detailed in the **Chapter 4**.

**Table 5-2: Fuel Properties**

| Property | Value with 95% confidence interval |
|---|---|
| Average Diameter (cm) | Small: 2.77 +/- 0.09<br>Large: 3.36 +/- 0.07 |
| Particle density ($kg/m^3$) | 521 +/- 24 |
| Sphericity | Small: 0.772<br>Large: 0.759 |
| Void fraction char | 0.47 |
| Moisture content (wt%) | 5.7 +/- 1.2 |
| Volatile content (wt%) | 84 +/- 0.7 (dry basis) |
| Ash content (wt%) | 0.36 +/- 0.11 (dry basis) |

## 5.2 Experimental Results

### 5.2.1 Gas Concentration Profiles

Oxygen ($O_2$), nitrogen ($N_2$), carbon monoxide (CO), methane ($CH_4$) and carbon dioxide ($CO_2$) were found to be the main gaseous products of wood combustion. In one sample a trace of acetylene was also detected. **Figures 5.1** to **5.5** present the experimental data

along with model predictions. Run 072202 shown in **Figure 5.1** is typical of the concentration profile observed for each experiment. Oxygen, which enters through the bottom of the bed in the supply air, is rapidly consumed within 2 equivalent particle diameters from the grate. As the oxygen is consumed carbon dioxide is formed and peaks approximately at the same time as the oxygen has been consumed. Next, carbon monoxide is formed by reduction of $CO_2$ for approximately another 2 equivalent particle diameters.

At this point, unlike previous observations during coke experiments [Ryan (2000)] in which CO continued to rise slowly, the concentration of carbon monoxide slowly rises until approximately one equivalent particle diameter from the surface of the bed, at which point an increase in CO and a large increase in $CO_2$ concentrations is observed. Methane and tar are also observed at about 2 particle diameters from the bed surface. A sharp decrease in the nitrogen concentration from about 70 vol% to 50 vol% was also found at this height (not shown in figures), indicating an overall increase in combustion gas mass and the evolution of pyrolysis gases. The presence of methane is a sign of pyrolysis as reported by several authors such as DiBlasi et al. (1999c). Nitrogen, since it is inert, serves as a good indication of the overall quantity of gas in the bed, the falling $N_2$ concentration indicating the additional mass of pyrolysis and combustion products.

As mentioned in Chapter 2, the products of pyrolysis are numerous and secondary tar decomposition to lighter products was reported by many works in the literature. These data are consistent with these previous findings and suggest that CO, $CO_2$ and $CH_4$ are formed mainly near the top of the bed. Tar formation was observed deeper in the bed thus suggesting the gas concentration increase near the top of the bed are formed at least

partly by secondary reactions. All the experimental runs show these trends as shown in **Figures 5.1** to **5.5**.

Gas measurements from runs under the same conditions showed some scatter as can be observed mostly easily with samples near the grate for the large particle runs. At any one sample point the probe may have been above a particle for one sample but beside a particle for the next sample. The actual environment around the probe tip is thus continually varying and will cause measurement variations. In general, however, generally the gas concentrations measurements at the same height from different runs under the same conditions agreed within 8% for a given gas species with outliers occurring with roughly 10% of the measurements.

### 5.2.2 Tar Measurements

The tar sampling method designed and used in these experiments was not found to be reported elsewhere in literature. Therefore, this section will discuss the variables found to affect the tar sampling method, give observations of the tar collected, present results and analyze the results.

#### 5.2.2.1 Method Observations

The tar collected can generally be described as a viscous and very dark brown liquid as shown in **Figure 5.6**. Small quantities of the collected tar were found to give off a strong 'campfire' odour. A small sample kept in a closed vial was observed to thicken and clump with time. It is not known whether or not the solidification observed was due to an improperly sealed container (evaporation loss) or to the polymerization of the tar. The solidified tar was soluble in methanol. The mass of the tar sample collected on the

nickel-chrome filters was found to decrease by about 15% one day after sampling; hence tar samples were weighed as soon as possible after collection.

During the first run, it was found that if the collet and the holding ring of the tar probe (**Figure 4.4**) were not well cleaned and tightly sealed tar would collect between them. Methanol rinsing of the collet and sealing ring was done after each sample to clean them. It was found in the 1st run that if the probe cooling water temperature dropped significantly below 50°C, water would condense above the metal foam filter and drip out when the collet was removed. Measuring the cooling water temperature with an electronic thermometer with alarm was used in the following experiments to allow the water temperature to be more sensitively controlled.

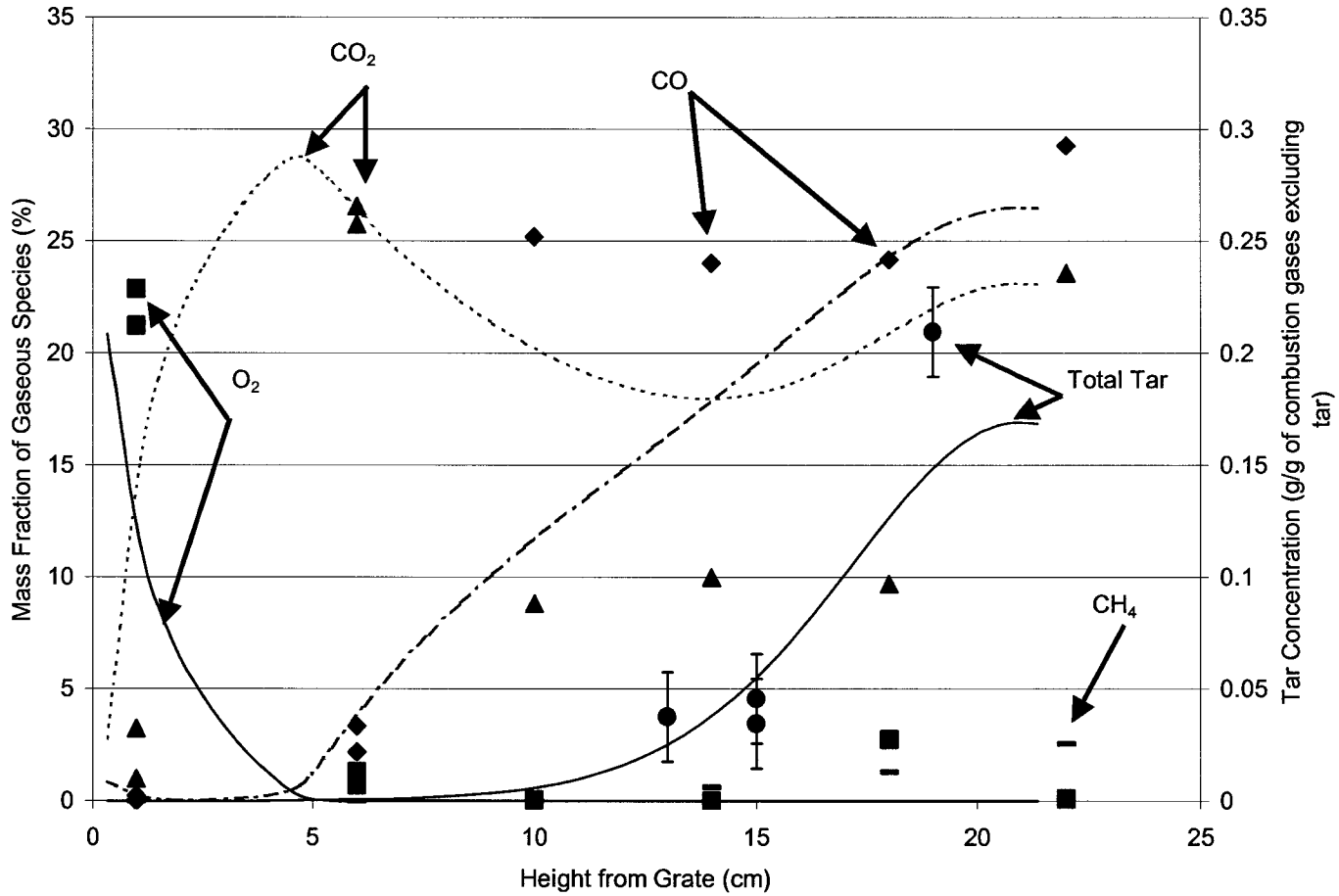


**Figure 5-1: Gas Concentration Profile for Run 0702202. Airflow 108 kg/m$^2$h, Particle Diameter 3.4 cm (■ $O_2$, ▲ $CO_2$, ♦ CO, ● Tar, - $CH_4$, _____ Predicted $O_2$, — · — Predicted CO ····· Predicted $CO_2$ — Predicted Tar)**

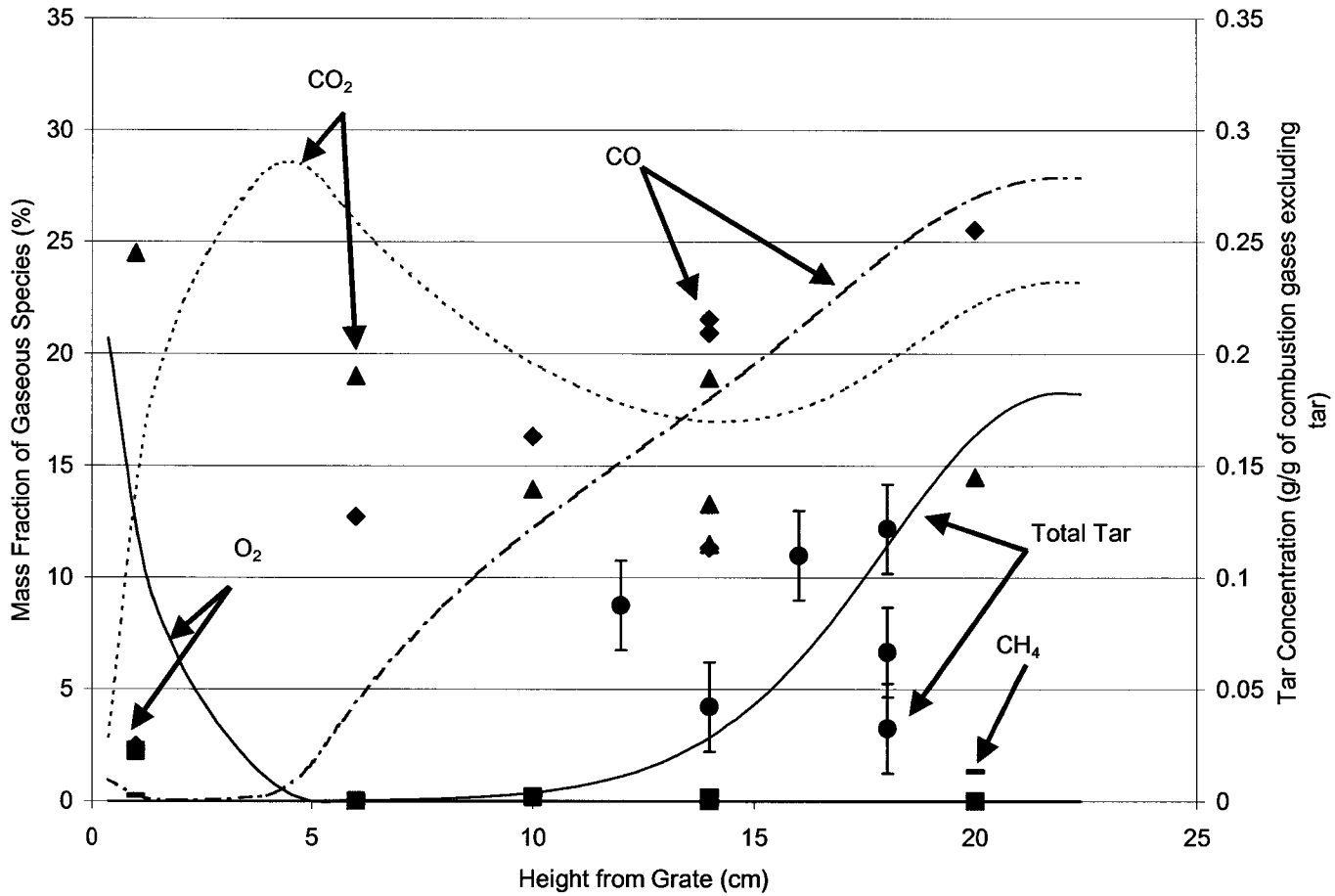


**Figure 5-2: Gas Concentration Profile for Run 121302. Airflow 108 kg/ $m^2$h, Particle Diameter 3.4 cm (■ $O_2$, ▲ $CO_2$, ♦ CO, ● Tar, - $CH_4$, _____ Predicted $O_2$, — · — Predicted CO ····· Predicted $CO_2$ — Predicted Tar)**

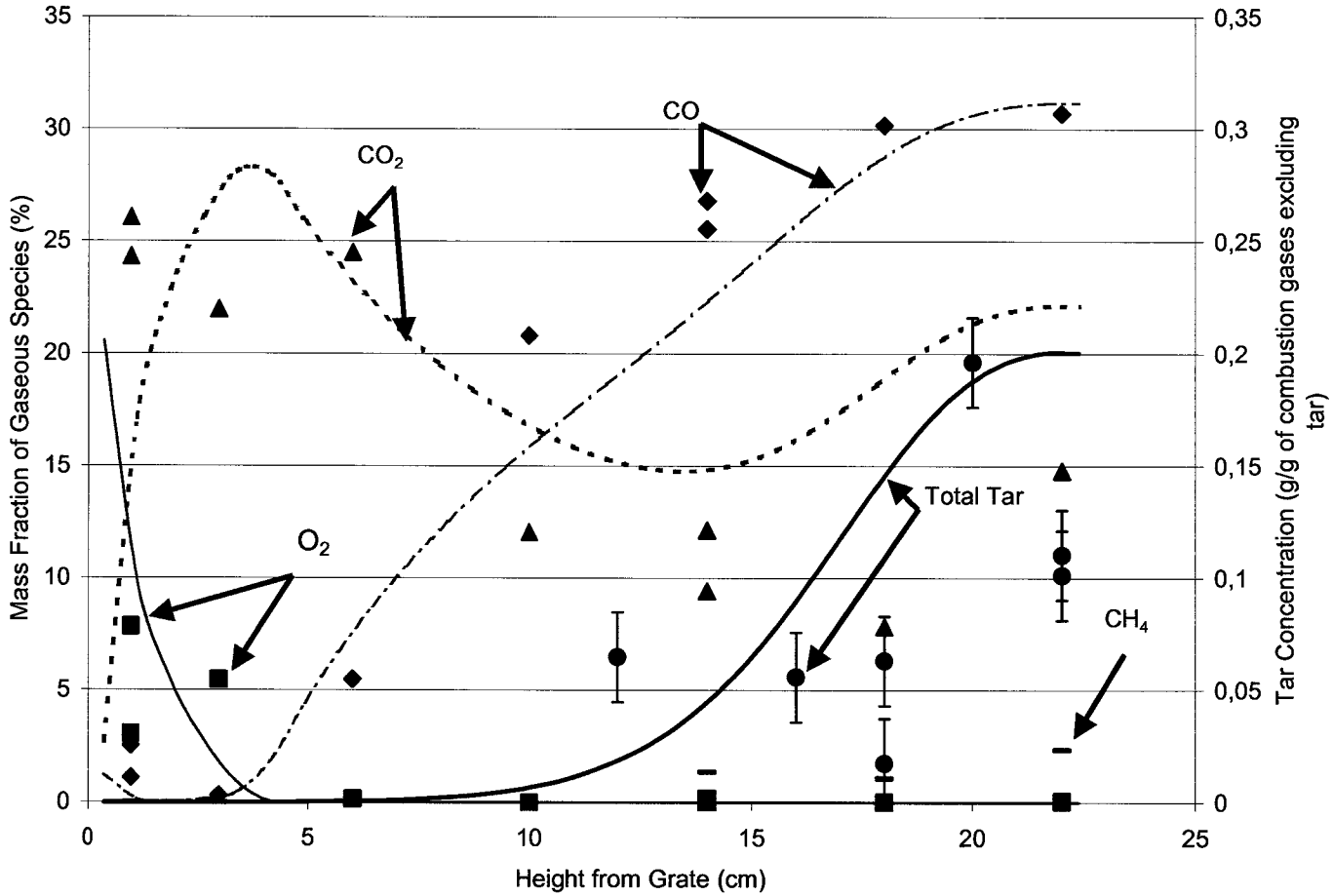


**Figure 5-3: Gas Concentration Profile for Run 121802. Airflow 108 kg/ $m^2$h, Particle Diameter 3.4 cm (■ $O_2$, ▲$CO_2$, ♦ CO, ● Tar, - $CH_4$, _____ Predicted $O_2$, — · — Predicted CO ····· Predicted $CO_2$ — Predicted Tar)**

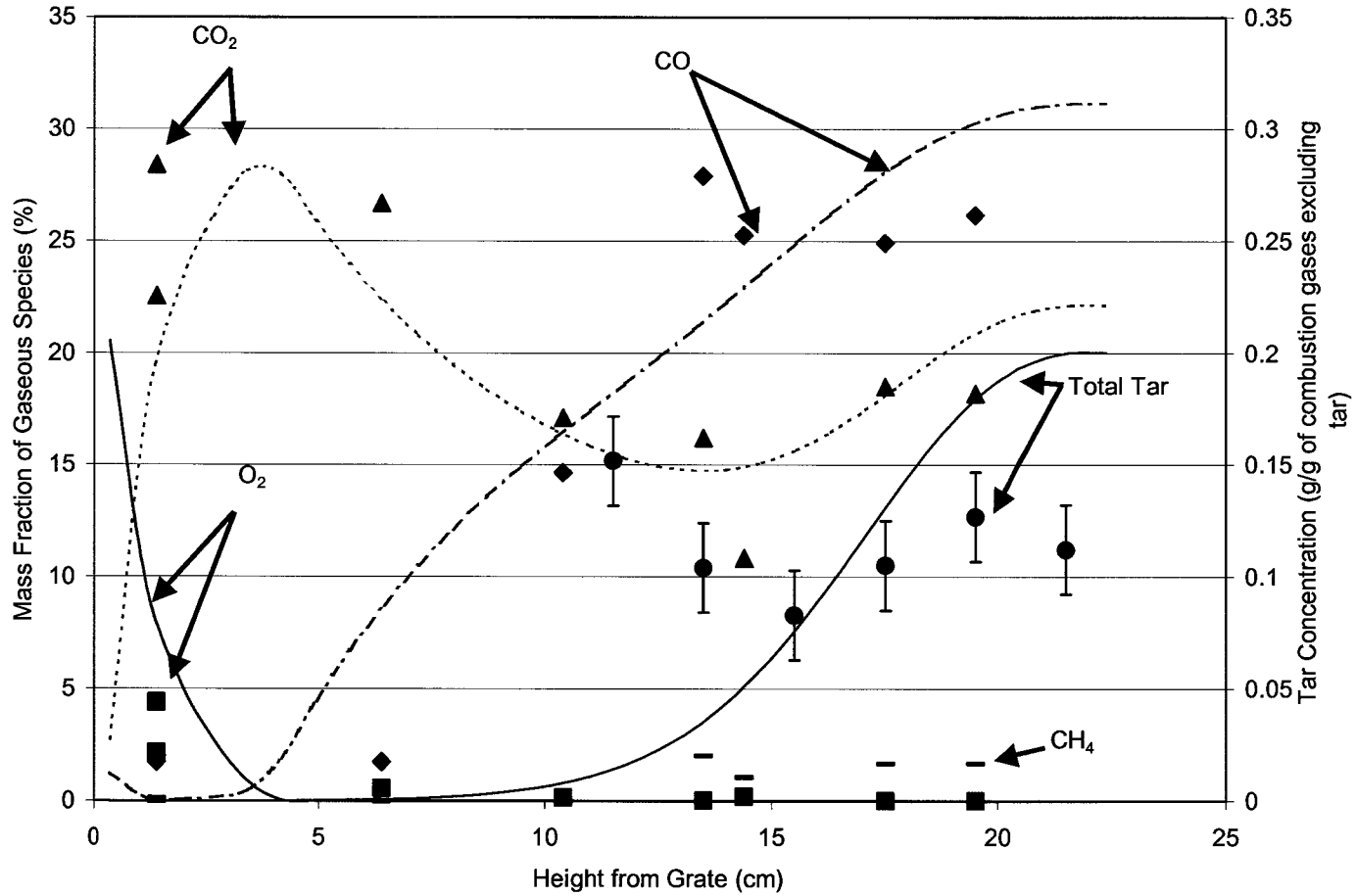


**Figure 5-4: Gas Concentration Profile for Run 010803. Airflow 108 kg/ $m^2$h, Particle Diameter 3.4 cm (■ $O_2$, ▲$CO_2$, ♦ CO, ● Tar, - $CH_4$, _____ Predicted $O_2$, — · — Predicted CO ····· Predicted $CO_2$ — Predicted Tar)**

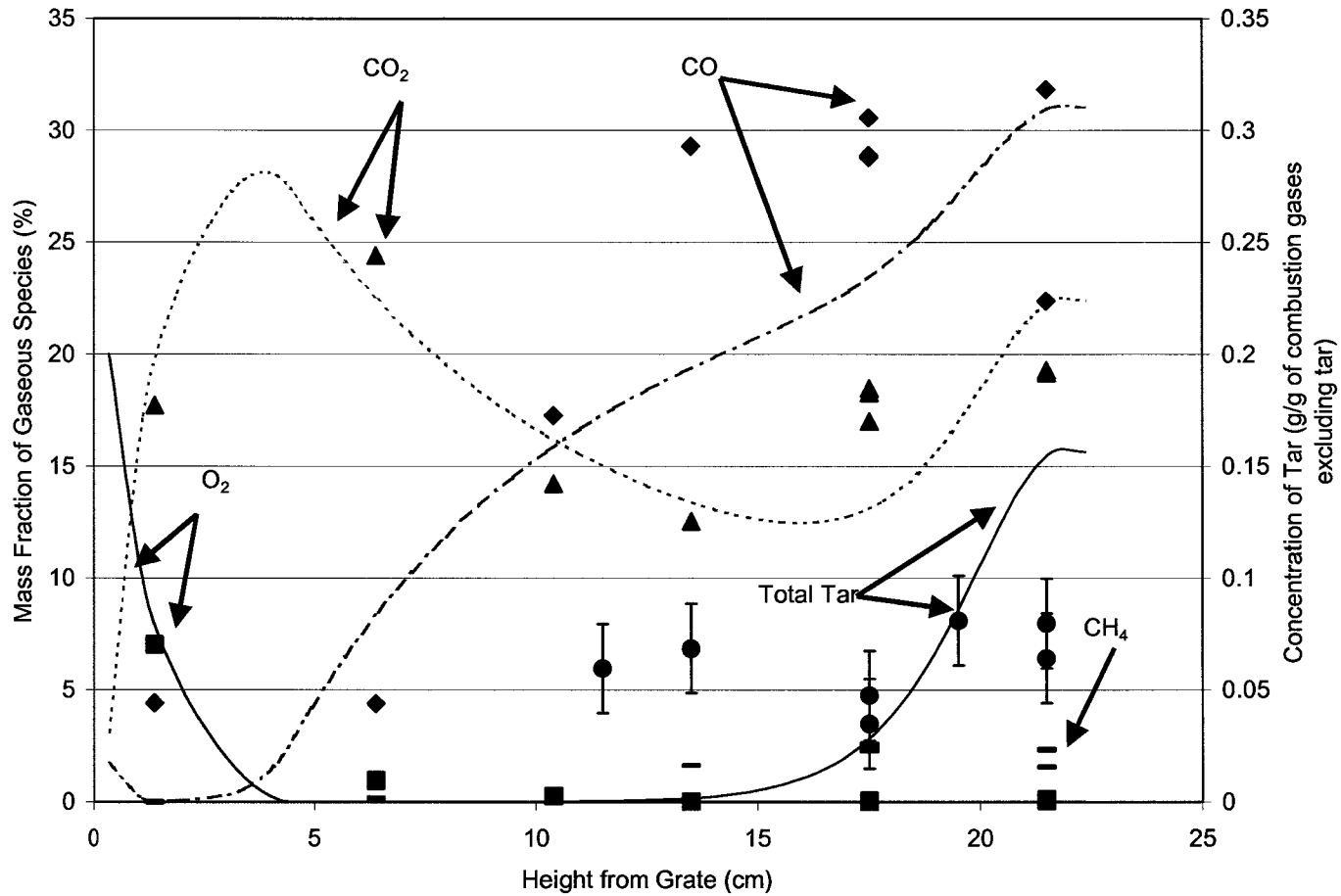


**Figure 5-5: Gas Concentration Profile for Run 011303. Airflow 130 kg/ $m^2$h, Particle Diameter 3.4 cm (■ $O_2$, ▲ $CO_2$, ♦ CO, ● Tar, - $CH_4$, _____ Predicted $O_2$, — · — Predicted CO ····· Predicted $CO_2$ — Predicted Tar)**

There was also concern as to whether or not the tar would break through the metal foam filters and collect in the sampling probe and sampling lines. In the first run, the amount of tar collected was greater than the anticipated quantity and breakthrough occurred, allowing some tar to collect in the sampling lines. The addition of an impinger filled with methanol in an ice-bath filled in the sampling train directly after the probe provided an immediate indication of tar in the sample gas. The methanol would change to a brown colour if tar broke through. However, since less than 0.1 g of the tar can turn 10 ml of methanol dark black, it is difficult to know with certainty whether the substance collected in the glass wool of the drying column after the first run was water or tar. With experience, the required sampling time was better estimated and breakthrough was prevented. It was found that typically when the cooling water temperature was well controlled around 50°C and the sampling time was below 10 minutes little or no colour change of the methanol would be observed. If breakthrough was observed the sample was rejected. Tar has been defined in this work as condensable below 100-150°C for reasons based on the probe design calculations discussed in **Appendix B**. It is noted that some light hydrocarbons, such as benzene, toluene, ethylene and xylene (BTEX), that are not condensed may also not be picked up by the gas chromatograph.

**Figure 5-6: Vial of Collected Tar**

During run 081102, the sensitivity of the tar sampling method was examined further with three tests. In the first test, the effect of leaving the probe above the bed for 3 minutes without any suction (ie. no sampling flow) was examined. This sample collected tar representing 6.8% of the metal foam filter mass or between 30% to 65% of the typical

mass of tar collected. The second sample was taken to test the amount of collection during lowering and raising the probe from the bed, with the probe being lowered again without suction to within 19 cm of the grate and quickly removed to simulate 0 residence time in the bed. The mass of tar collected was only 0.1% of the filter mass or less than 1% of the typical mass of tar collected. A third sample was taken to see if tar collection took place if the probe was left in the bed for 2 minutes at a height of 19 cm from the grate without any suction to test the effect of residence time in the bed without sampling. This sample showed a mass collection of only a 0.3% of the filter mass or between 1 to 3% of the typical mass of tar collected. This percentage is probably lower for actual samples since the probe was backwashed with nitrogen between sampling to prevent sampling from occurring before it should. (Nitrogen was not backwashed through the probe for these test samples once the probe was at the desired location.) A possible reason for the higher collection above the bed may have been dripping of volatiles condensation and dripping of tar from the upper part of the probe. Inside the bed, fuel particles contacting the probe and the higher local gas velocities may have prevented dripping. The collection of tar on the filter for the sample left above the bed for 3 minutes was considered to be significant and a sampling protocol of not leaving the probe above the bed for any length of time was strictly enforced for the subsequent runs. As well, after each test, the outside of the tar probe was wiped clean of tar between samples to minimize any possible dripping effect.

To sample isokinetically the sampling rate should have increased approaching the surface of the bed in accordance with the increase in total gas mass flow. However, calculating this flow rate before taking a sample was not possible and therefore a set flow rate was selected. With more data or model predictions, a selection of sample flowrate to more

closely approximate isokinetic sampling at various heights may be possible. However, since the stream being sampled from is not particle-laden the impact of not sampling exactly isokinetically is expected to be minimal. The rotameter reading precision was to +/- 11 ml/min which represents 2.6% of the gas flow measurement.

The tar concentration profiles collected have been included in the gas concentration profiles shown in **Figures 5.1** to **5.5** and are the mass of tar collected divided by the mass of tar-free gas drawn through the probe. The tar readings were found to range between 0.017 to 0.196 mg/mg tar-free gas. Unfortunately, due to the presence of condensate, tar collection by the collet due to improper sealing of the filter, breakthough of tar, significant change of bed height during the sampling and other noted experimental errors, many of the tar measurements from the first runs were discarded. However for the later runs, once the sampling method was better developed only 16% of the measurements needed to be discarded. These points have not been presented. The majority of these discarded measurements were from the first runs where this novel *in-situ* sampling method was being tested. However, five of the runs (072202, 1213802, 121802, 010803, and 011303) produced 4 or more tar measurements per run that were kept for repeatability analysis as discussed below.

The tar data did display some scatter when comparing runs with the same test conditions. As previously discussed scatter is known to be introduced because at any one sample point the probe may have been above a particle for one sample but beside a particle for the next sample. However by comparing **Figures 5.1** and **5.2** and **Figures 5.3** and **5.4**, sets of runs conducted at the same conditions show similar tar concentration magnitudes and trends with the exception of a few anomalies such as the high tar concentrations at 20 cm in **Figure 5.3**. Further discussion on the observed variability in bed conditions are

presented in **Sections 5.2.2.3** and **5.19**. The variability observed is also of the same order of uncertainty created by experimental errors in sampling rate and weight measurements discussed in **Sections 5.7.1** and **4.6.4**.

Replicate samples (two samples at the same position in the bed) were taken during each run. The difference between the two readings from one replicate pair was calculated. These differences were used to assess the repeatability of the sampling method. For all replicates taken, the average difference between samples at the same height was 0.02 mg/mg tar-free gas. This difference for the smallest measured tar concentration at 15 cm from the grate was 0.01 mg/mg (20% of reading) and for the largest measured tar concentration at 19.5 cm was 0.017 mg/mg (12% of reading). The error bound on the tar measurement calculated by combining using the errors of the tar mass and gas flow measurements was 12%.

### 5.2.2.2 Tar Profile

Results from the new tar sampling method, **Figures 5.1** to **5.5**, suggest a peak concentration at approximately 3 cm below the bed surface. The variation in concentration from the different runs followed the same trend. The peak concentration was found to be 0.196 mg/mg tar-free gas at 19 cm from the grate. Contrary to the experimenter's previous hypothesis speculating that pyrolysis only occurred within one to one and half particle diameters from the bed surface, tar was found to be collected below two particle diameters from the surface of the bed. The tar concentration profile, that is fairly level near the bed surface and shows a repeatable trend of decreasing at about 5 cm from the bed surface. Then below 5 cm the concentration gradually increases again till about 10 cm from the bed surface before it decreases again.

If tar was simply released from the fuel without any further reaction, one would expect a tar concentration rising continuously towards the top of the bed. Any decrease in tar concentration, as observed in runs 010803 and 011303, is likely due to secondary reactions of tar into other products. Reasons for this decrease with increasing height could also include the evolution of light gases or hydrocarbons not picked up by the gas chromatograph or compression of char particles below when lowering the probe into the bed. Unfortunately the sampling probe was not designed to allow sampling to the full length of the bed and thus a profile below 11 cm from the bed surface to confirm the cause of the increase near the 10 cm bed height was not possible. However, the observation of a tar concentration that dips is supported by findings from DiBlasi et al. (2000) who noted two different devolatilization rates due to the different biomass components and secondary tar reactions.

#### 5.2.2.3 Comparison of Gas Measurements Obtained Using the Tar Probe versus the Gas Sampling Probe

As discussed in the experimental methods, it was decided to use the tar probe to sample gas in the top section of the bed to avoid clogging of the small diameter tube in the gas probe and to obtain a gas sample taken exactly at the same location as a given tar sample, thus reducing experimental variables in comparing gas and tar behaviour at a given location.

To test whether the use of a different probe to sample gas would introduce significant error in the results, replicate gas samples (same location from the grate within one run) were taken with the gas and tar probes. A total of 4 and 5 replicate samples, for the large and small particle size runs respectively, were randomly taken with either the gas or tar sampling probe. An F-test comparison of the ratio of the sample variances for each of the

gas measurement methods was conducted. An F-test compares the variances of two sets of data to determine whether or not the variances are significantly different. This test showed that for each of the gas species, within a 95% confidence interval for both the larger and smaller particles, it was reasonable to assume the two sampling methods had the same variance.

For both particle sizes, the variability of the gas sampling results from run to run were found to be greater in the top 7 cm of the bed than that between the two different sampling probes. For example, the variability of the CO measurements taken at 14 cm from the grate from different large particle runs was 4.27 vol% compared to only 0.25 vol% when taken with the different sampling probes within one run. The higher variability of the gas probe measurements reflects the stochastic nature of variation in local bed conditions.

### 5.2.3 Density and Particle Size

#### 5.2.3.1 Observations

Quenching the combustion reaction at the end of a run with nitrogen and sectioning the bed into slices provided more information on the pyrolysis process. The following observations are based on inspection and analysis of the bed slices using the procedure outlined in chapter 4. Observations were made as to the change in particle shape and how pyrolysis appeared to have occurred (shrinking core or constant particle size). Several particles were sectioned. In the top slice darkening of the particle to a black colour (an indication of char formation) seemed to occur first on one side, probably the side next to the hot bed. In the second slice from the top of the bed the particle appears to be a dark black throughout. Since the volatile content of the particles, discussed below,

show that not all the volatiles have left the particle within the top 8 cm of the bed, this suggests that visual observations of particle colour change alone do not provide as much information as the proximate analysis test results. Particles at the edge of a slice (presumably those near the wall inside the reactor) appeared to be pyrolyzed slightly less than those in the rest of the layer, and therefore were not included in the proximate and particle size analysis.

### 5.2.3.2 Profile of Density and Particle Size Change Across the Bed Height

The particles appeared to swell in the direction across the grain and shrink in the direction of the grain. With some particles, swelling and splitting of the particle was observed as shown in **Figure 5.7** for the particle at 12.5 cm. By the time the particle had reached the bottom 4 cm of the bed, the particle shape had changed enough that the direction of the grain was the only method to determine which side was originally the longest.

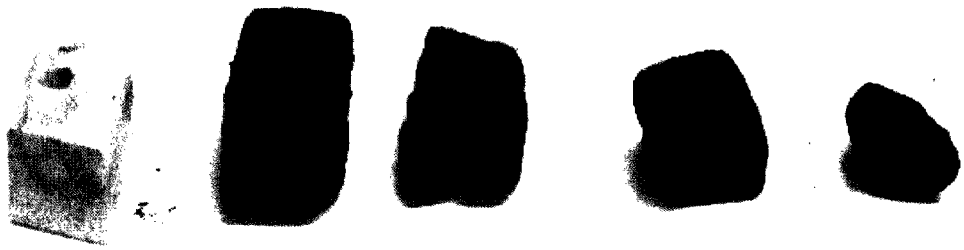

**Figure 5-7: Particles at Different Heights from Top of Bed to Grate (Left to Right: Feed, Heights of 18cm, 12.5 cm, 7 cm and 2.5 cm)**

The measured equivalent particle diameters and densities runs are presented in Figures 5.8 to 5.12 below. A sharp drop in density was observed in the top 10 cm of the bed, which is just over 2 equivalent particle diameters. The difference in density within each of the approximately 5 cm slices of the bed was further investigated using a paired comparison t-test for the large particle runs. A paired t-test compares the difference of

means from two groups of data, allowing a reduction in the extraneous sources of variation such as those caused by the stochastic nature of these packed bed experiments. Here the fuel densities are more likely to share common conditions with the bed slice above in an experiment conducted the same day than with tests conducted on different days with different run times. Pairing was thus done by comparing the mass per unit volume from one bed slice to the slice above it. The % decrease in mass per unit volume compared to the feed, for the large particle run, were found to be 70%+/-6%, 74%+/-9%, 63%+/-4% and 54%+/-26%, for the slices at approximately 2.5 cm, 7 cm, 12.5 cm and 18 cm from the grate respectively, within a 95% confidence interval. The higher variability in the 18 cm sample is representative of the greater degree of change particles undergo at the top of the bed in comparison to the lower sections. Data from the smaller particle experiments suggest similar results.

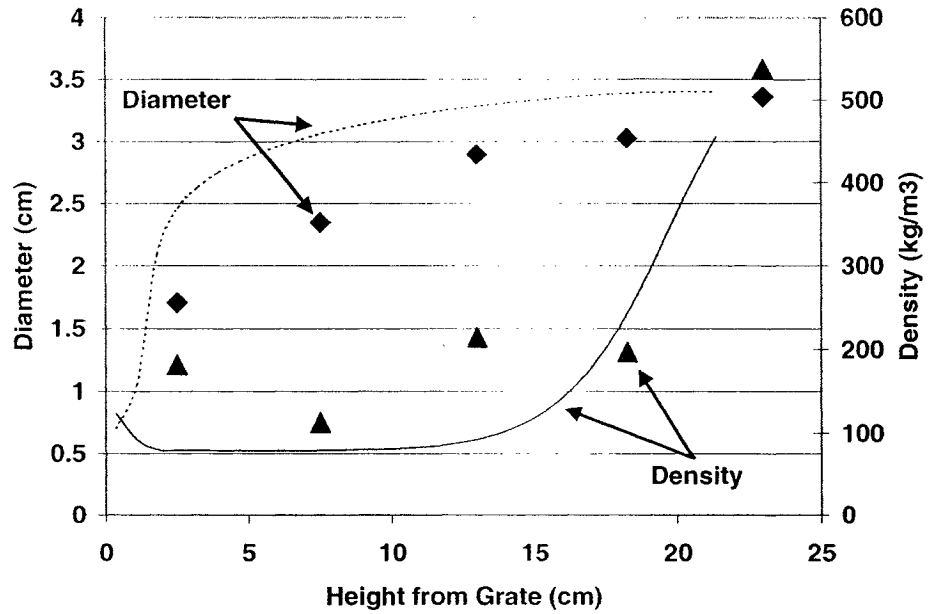


**Figure 5-8: Change in Particle Diameter and Density for Run 072202. Airflow 108 kg/m$^2$h, Particle Diameter 3.42 cm**

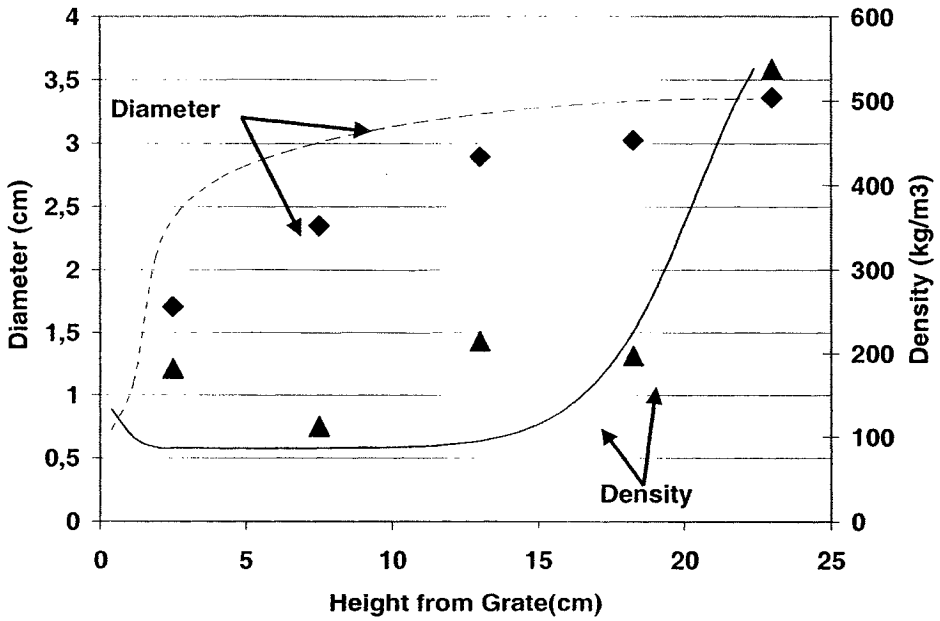


**Figure 5-9: Change in Particle Diameter and Density for Run 121302. Airflow 108 kg/m$^2$h, Particle Diameter 3.35 cm**

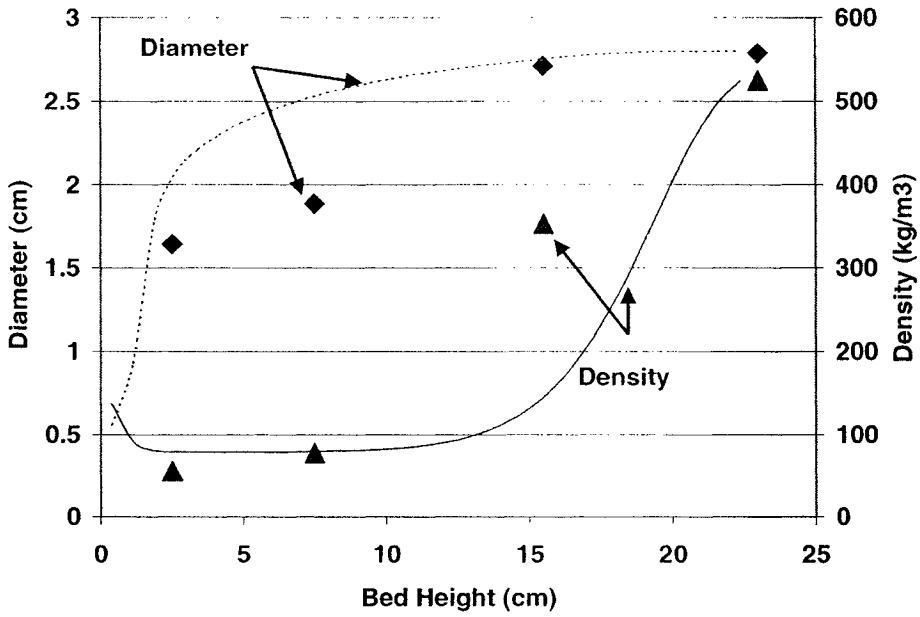


**Figure 5-10: Change in Particle Diameter and Density for Run 121802. Airflow 108 kg/m$^2$h, Particle Diameter 2.80 cm**

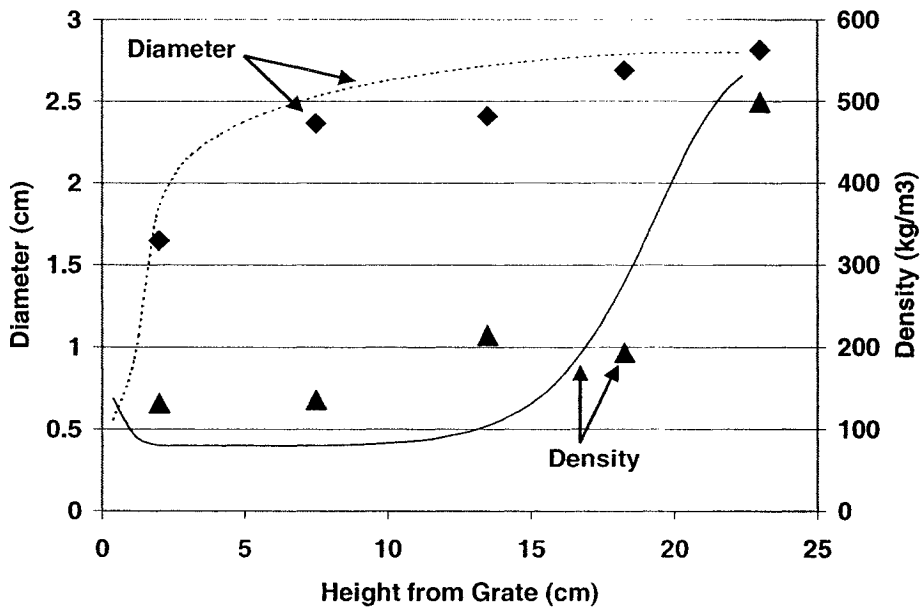


**Figure 5-11: Change in Particle Diameter and Density for Run 010803. Airflow 108 kg/m$^2$h, Particle Diameter 2.81 cm**

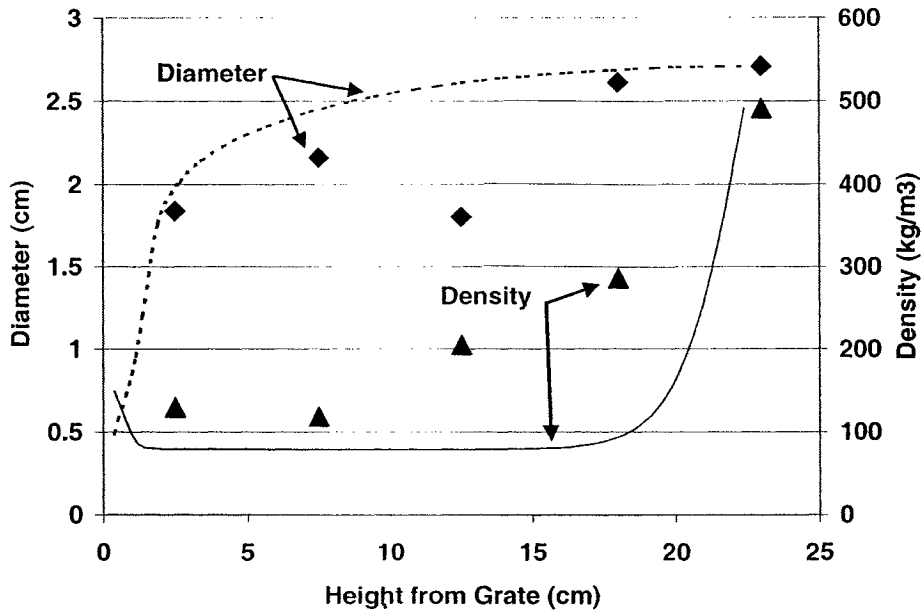


**Figure 5-12: Change in Particle Diameter and Density for Run 011303. Airflow 130 kg/m$^2$h, Particle Diameter 2.71 cm**

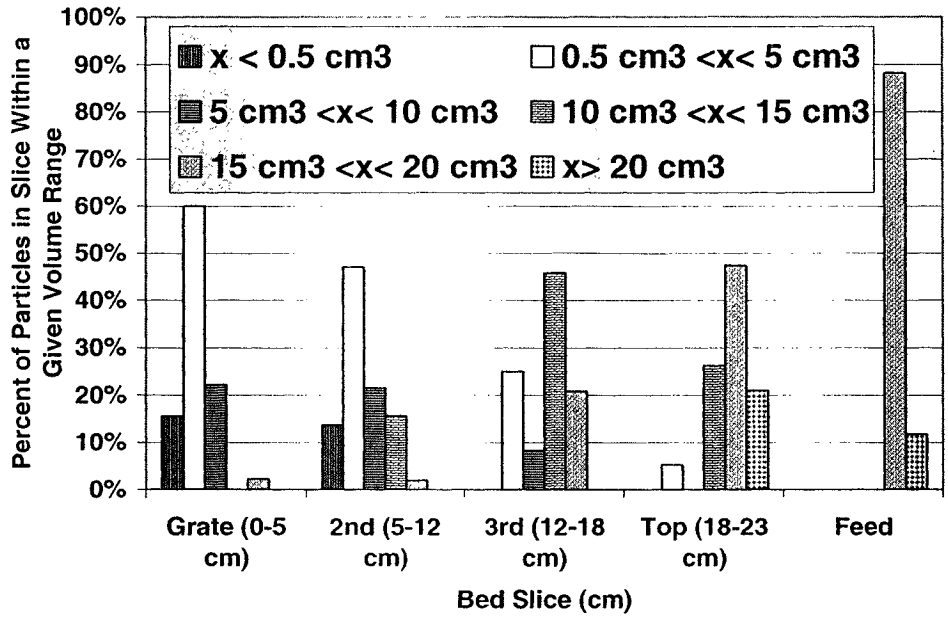


**Figure 5-13: Particle Volume Distribution for Run 092502. Airflow 108 kg/m$^2$h, Particle Diameter 3.29 cm**

Contrary to the change in density, the equivalent particle diameter was observed to drop gradually from the top of the bed to the grate. This gradual drop in particle diameter was investigated further by creating a particle volume distribution plot for run 092503 shown in **Figure 5.13**. At least 25 particles were measured per slice. The values for the grate sample shown do not include particles with a size smaller than 1 mm in any direction since at that scale differentiating between ash and wood char was difficult. These data show significantly different distributions for each slice of the bed. After simultaneous swelling and shrinking being observed in the top 10 cm of the bed, the data suggest a gradual decrease in particle size.

### 5.2.4 Moisture, Volatiles and Ash Content

A significant change in particle volatile and moisture fractions was observed within the top 10 cm of the bed. Although the data show no statistically significant difference between runs of small and large particles, a consistent change in composition with respect to the feed was observed for all runs. **Figure 5.14** to **5.18** show the change in proximate composition. Results are summarized in **Table 5.3**

Analysis of the proximate results was conducted using a paired comparison t-test of the feed composition with the char from various heights within the bed for runs at 108 $kg/m^2h$ and the larger particles. Pairing was done by comparing the mass loss from one bed slice to the slice above it. The results are summarized in **Table 5.3**. They show, as expected, that the most significant mass loss of volatiles, 38.9% +/- 14%, occurred in the top 5 cm slice of the bed. However as the particle travels down through the bed an additional 8.7 %, 23.3 % and 5.4 % mass loss of volatiles was observed in each of the sections at 12.5 cm, 7 cm and 2.5 cm, respectively, compared to the slice directly above

it. This suggests, contrary to expectations, that some devolatilization still occurs in the lower sections of the bed below two equivalent particle diameters from the top of the bed. although at a lower rate.

**Table 5-3: Comparison of Proximate Analysis of Feed with Different Bed Heights for Runs Conducted at 108 kg/m$^3$h with 3.35 cm Diameter Particles, with 80% Confidence Region**

| Approximate Centre of Bed Slice (cm) | Difference Between Feed and Value at Slice (Mass %) | | |
|---|---|---|---|
| | Moisture | Volatiles | Ash |
| 18 | 3.9 +/- 1.6 | 39 +/- 14 | Not significant |
| 15 | 3.7 +/- 2.1 | 48 +/- 20 | -0.55 +/- 0.35 |
| 7 | 4.2 +/- 2.0 | 71 +/- 16 | -1.26 +/- 0.34 |
| 2.5 | 4.6 +/- 2.0 | 76 +/- 3.0 | -24 +/- 4.0 |

A comparison of the change in ash fraction did not show any statistically significant difference between feed and samples from the top slices of the bed and only a small increase in ash fraction until the slice directly on the grate at ~2.5 cm was reached. The relatively small ash content down to the layer 5 cm from the grate is a result of the small initial fraction of ash in the original fuel (less than 0.5 mass %). The large increase in the slice at 5 cm from the grate, where the ash fraction was found to increase by 23 %, is representative of the fact at that this point most of the fuel will been burnt.

The moisture concentration was found to decrease by 3.9% in the first slice of the bed representing approximately 64% of the mass of moisture in the feed (the average feed moisture is 5.8%). This finding supports the theory that drying will occur when the particles first enter the bed. However, surprisingly, a trace of moisture is still present in the particles near the grate. This moisture could have been absorbed from the ambient environment while conducting the proximate analysis.

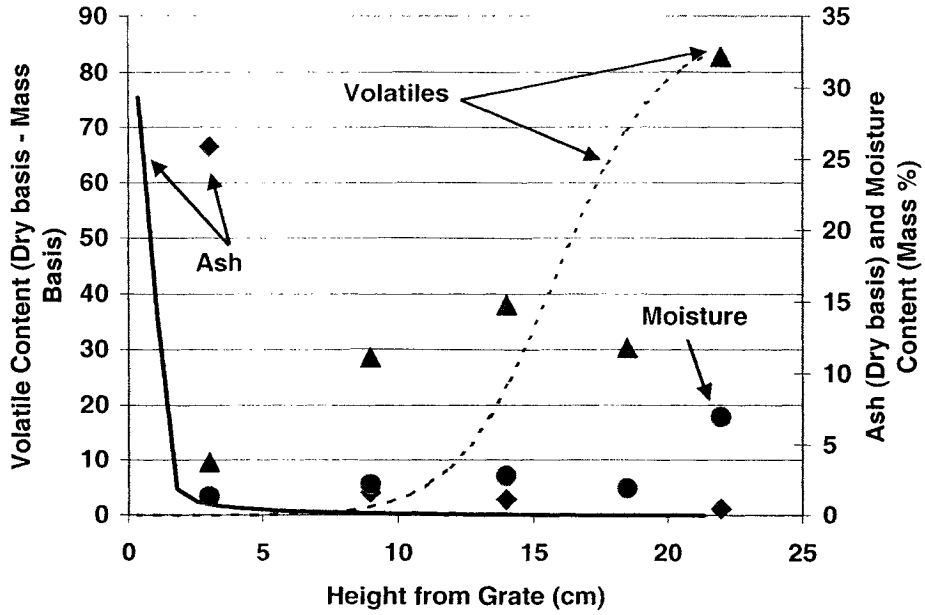


**Figure 5-14: Solid Phase Mass Fractions as a Function of Height from the Grate ▲volatile content • moisture and ♦ ash content for run 072202. Airflow 108 kg/m$^2$h, Particle Diameter 3.42 cm**

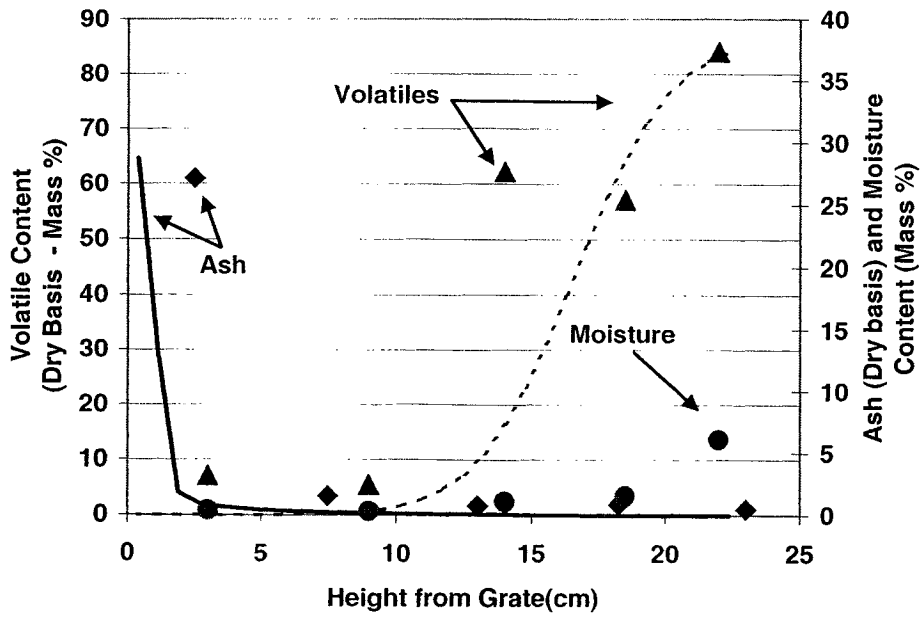


**Figure 5-15: Solid Phase Mass Fractions as a Function of Height from the Grate ▲volatility, • moisture and ♦ ash content for run 121302. Airflow 108 kg/m$^2$h, Particle Diameter 3.35 cm**

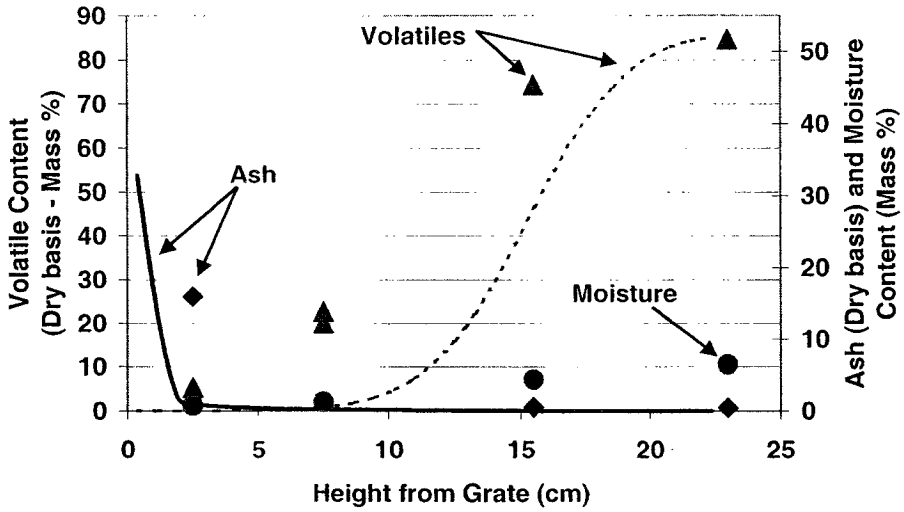


**Figure 5-16: Solid Phase Mass Fractions as a Function of Height from the Grate ▲volatile content • moisture and ♦ ash content for run 121802. Airflow 108 kg/m$^2$h, Particle Diameter 2.80 cm**

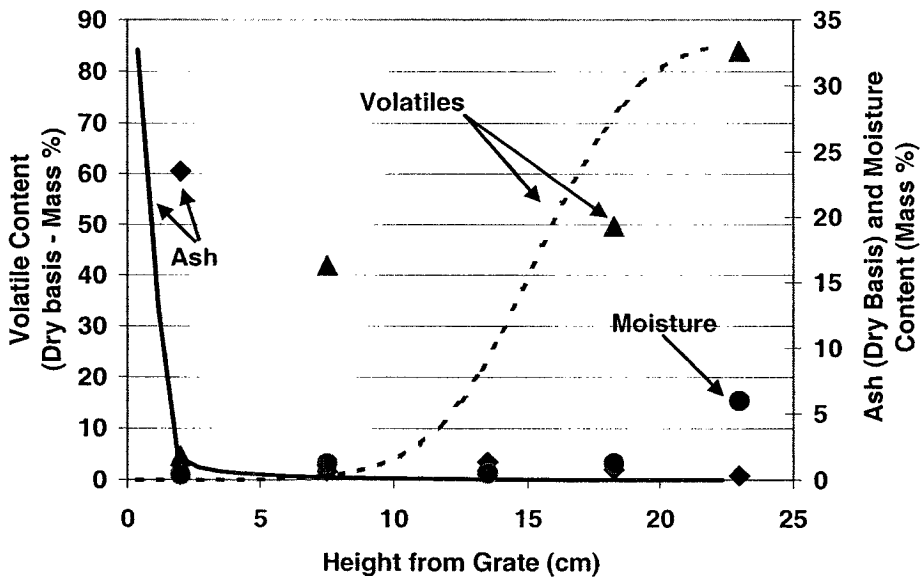


**Figure 5-17: Solid Phase Mass Fractions as a Function of Height from the Grate ▲volatile content, • moisture and ♦ ash content for run 010803. Airflow 108 kg/m$^2$h, Particle Diameter 2.81 cm**

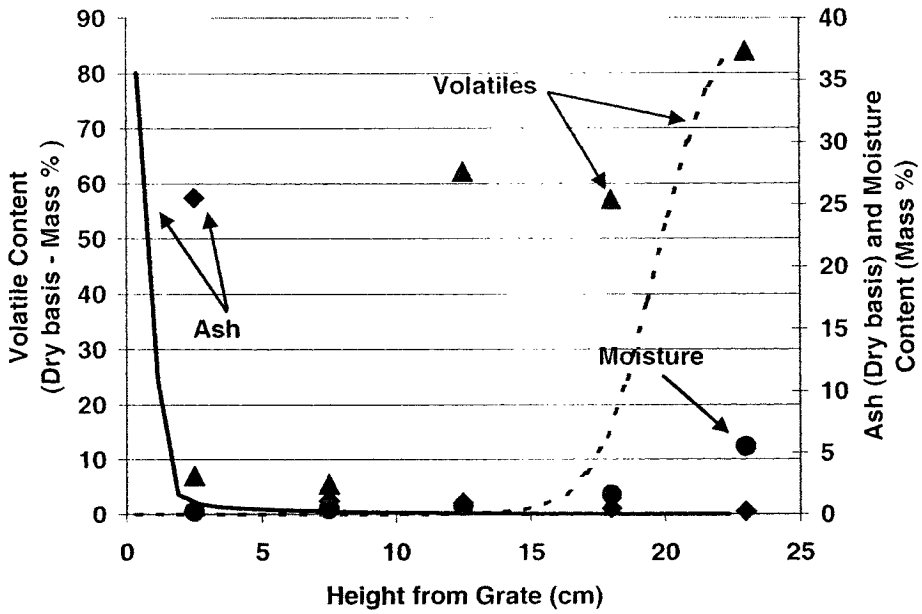


**Figure 5-18: Solid Phase Mass Fractions as a Function of Height from the Grate ▲volatile content, • moisture and ♦ ash content for run 011303. Airflow 130 kg/m$^2$h, Particle Diameter 2.71 cm**

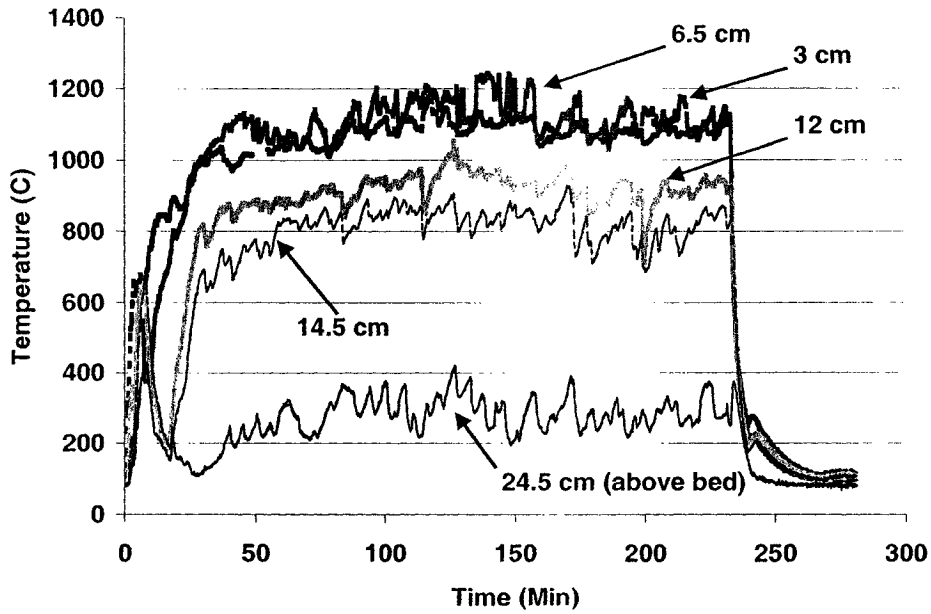


**Figure 5-19: Typical Records of Temperature versus Time at Different Heights in the Bed for Run 010803. Airflow 108 kg/m$^2$h, Particle Diameter 2.81 cm**

### 5.2.5 Temperature Results

A typical temperature record for run 010803 is shown in **Figure 5.19** temperature profile. The maximum temperature readings in the bed were observed at 6.5 cm from the grate and were in the 1150°C range. The temperature decreased approaching the top of the bed to about 850°C. The temperatures at the 12 and 14.5 cm heights fluctuated by about 100°C over a 5 minute period, with some larger fluctuations. This time of 5 minutes also coincided with the average feeding time. Similar fluctuations in temperature were also observed at the lower thermocouples but these were not observed to be tied as much to the feeding. The variable nature of processes within the bed is shown in **Figure 5.19**.

#### 5.2.5.1 Radiation Above Bed

Readings from the two different diameter thermocouples just above the bed were taken during each run, just above the surface of the bed to estimate the radiation effect. The radiating temperature is dependent on the sidewall temperature (~50°C), the temperature of the laboratory environment at the reactor outlet (varied between 6°C in winter to 30°C in the summer), the gas temperature (non-uniform, includes some volatiles flame radiation) and the temperature of the bed surface (not uniform). **Table 5.4** includes the temperature reading of the two thermocouples, the calculated actual gas temperature after correcting for radiation and the calculated effective radiating temperature for the various runs. (The effective radiating temperature is an average temperature representing the radiation exchanged by the thermocouple with the environment, including the cool combustor walls, the hot bed surface and the gas-phase volatiles flame above the bed.) Details on the calculation method to analyze the radiation effect above the bed are presented in **Appendix C.**

A maximum gas temperature of 622 K, and a minimum of 361 K were recorded. The measured temperature above the bed for the smaller particle runs was generally higher, than with the larger particle. It is suspected that the lower temperature with the larger particles may be due to a longer heat up time for these particles, thus creating more 'cold spots' at the bed surface. The lower temperature readings may also be due to channelling of cooler air up the wall.

**Table 5-4: Radiation Temperature Measurements**

| Run | Ratio of Mass of Gas at Top of Bed to Incoming Air Mass | 0.020 cm Thermo-couple Reading (K) | 0.038 cm Thermo-couple Reading (K) | Calculated Gas Temperature (K) | Calculated Effective Radiating Temperature (K) |
|---|---|---|---|---|---|
| 081102 | 1.90 | 524 | 546 | 524 | 1290 |
| 092502 | 1.06 | 367 | 373 | 367 | 804 |
| 121302 | 1.31 | 361 | 366 | 361 | 810 |
| 121802 | 1.47 | 558 | 567 | 557 | 1031 |
| 010803 | 1.42 | 612 | 622 | 611 | 1082 |

Radiation appears to have had the effect of giving thermocouple readings higher than the actual gas temperature. However, this difference is very small, accounting for less than 1% of the thermocouple reading for the 0.020 cm thermocouple. Physically this indicates that the radiating surface provides heat to the thermocouple which then transmits a little heat to the gas.

Unlike previous experiments by Ryan and Hallett (2002), the effective radiating temperature appears to be significantly different from the gas temperature. The radiation temperatures calculated were on average 2.1 times greater than the gas temperature. These results suggest that flame radiation may play a significant role in wood combustion.

## 5.3 Process Modeling

### 5.3.1 Kinetic Rate Constants

The model requires fitting of four parameters for the pyrolysis reaction: the activation energy E, the pre-exponential factor A, and the proportions of CO and $CO_2$ in the products of pyrolysis. Tar is assumed to be the balance of the pyrolysis products. Methane has been included with the total tar in the model. The reduction reaction kinetics have not been changed from those given by Ryan and Hallett (2002). However, it is acknowledged that model refinement may seek to adjust these reduction values, since they are based on coke, and wood char is structurally quite different.

As discussed in Chapter 4, the kinetic rate constants given for a simple first order pyrolysis reaction varied greatly in the literature. In the model, the rate constants were found to affect the depth to which pyrolysis would occur as well as the concentrations of the gas species. Most of the reaction rates proposed by authors in **Table 2.1** led either to conditions where the bed could not ignite or extinguished well before the actual experimental time. The maximum pre-exponential factor and activation energy for the run conditions of these experiments to maintain program stability were found to be near 0.35 $s^{-1}$ and 30 000 J/mol, respectively. This lack of fit with reported rates was likely due to the fact that the model does not include heat conduction within the particle or secondary reactions. The reaction rates proposed in this work, therefore, represent an effective rate, which includes heat transfer, pyrolysis and secondary reactions, unlike those in the literature which focused on the rate of the pyrolysis reaction alone.

Formal fitting of the kinetic reaction rate parameters was not attempted for the following two reasons. Firstly the model currently ignores important features in the real process

such as heat conduction through the particle, secondary tar reactions and evolution of known pyrolysis products such as methane. Secondly, due to the scatter in both the tar and gas data, fitting routines might try to fit physically unrealistic profiles.

Although no detailed analysis was conducted to determine the best fitting kinetic rate constants, parameters of A = .05 $s^{-1}$ and E = 20 000 J/mol were found to provide reasonable results. The $CO_2$ reduction reaction rate constants were not modified from those of the previous coke experiments. **Figure 5.20** and **5.21** present the model results for the $CO_2$, CO and tar profiles for these kinetic rate constants. As well as the results with A= 0.15 $s^{-1}$ and E = 20 000 J/mol and A = 0.05 $s^{-1}$ and E = 10 000 J/mol parameters are shown to provide an indication as to the effect of the pre-exponential factor and the activation energy. The model without inclusion of the pyrolysis reaction is also presented on these figures to allow assessment of the effect of changing rate constants as well as to separate the effects of pyrolysis from those of char combustion alone.

Decreasing the activation energy resulted in pyrolysis occurring closer to the top surface of the bed as did increasing the pre-exponential factor. Modelling without a pyrolysis reaction resulted in CO and $CO_2$ concentrations that levelled off near the bed surface, and of course no prediction of tar production.

In most runs in the lower half of the bed the CO concentration is slightly higher than the measured concentrations, an indication that the $CO_2$ reduction rate needs to be adjusted. Determination of the reduction reaction rate constants for wood char was not possible because the pyrolysis reaction zone was bigger than expected and overlapped with the $CO_2$ reduction zone. Comparing the results of modelling with and without pyrolysis in Figures 5-20 and 5-21 show very clearly how much extra CO and $CO_2$ is contributed by pyrolysis.

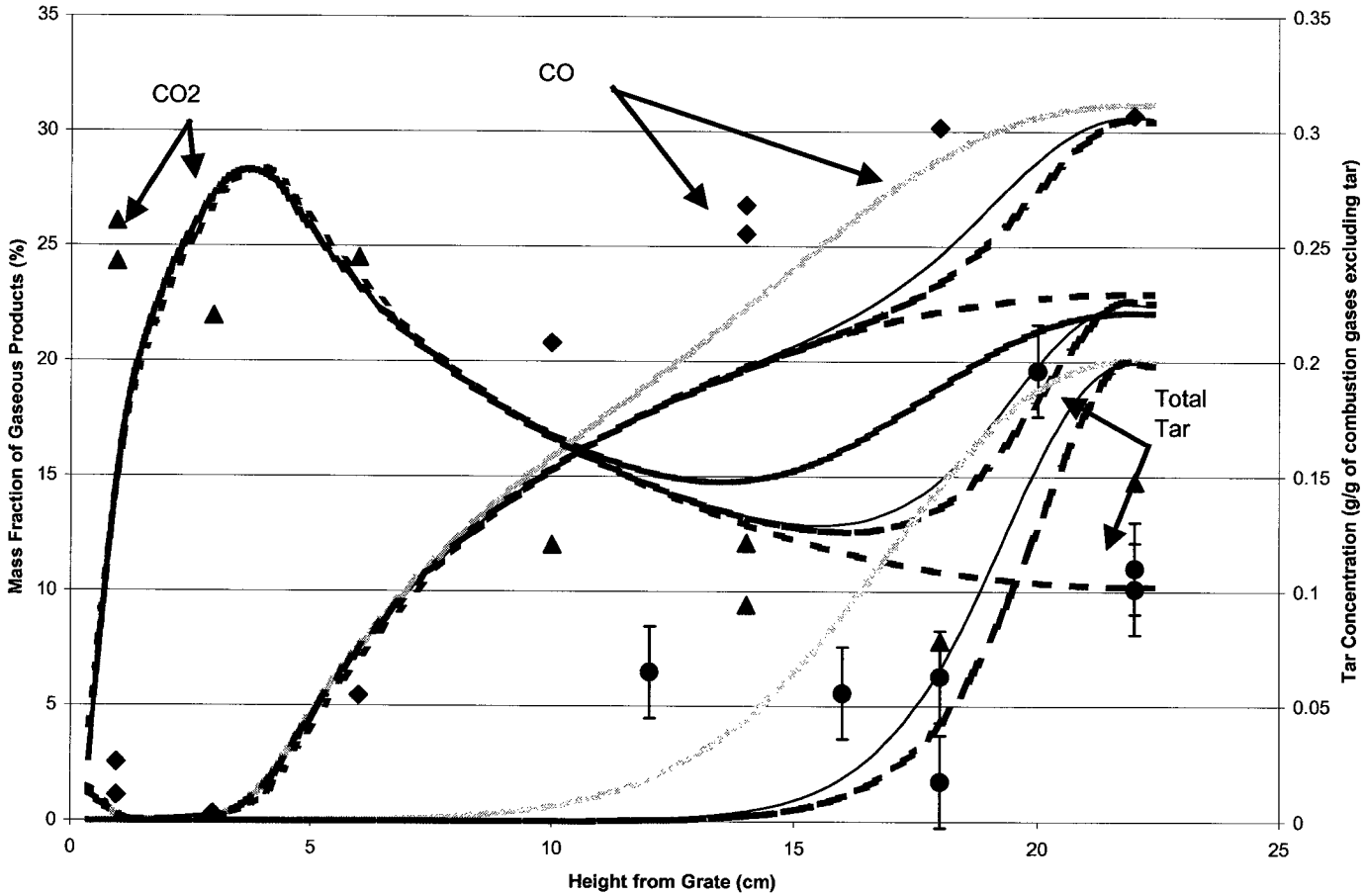


**Figure 5-20: Gas Concentration Profile for Run 121802. Airflow 108 kg/m$^2$h, Particle Diameter 2.81 cm (▲$CO_2$ ♦ CO ● Tar, - - - - no pyrolysis reaction, — — — A=0.05 $s^{-1}$ E = 10 kJ/mol ▒ A=0.05 $s^{-1}$ E = 20 kJ/mol ___ A=0.15 $s^{-1}$ E =20 kJ/mol)**

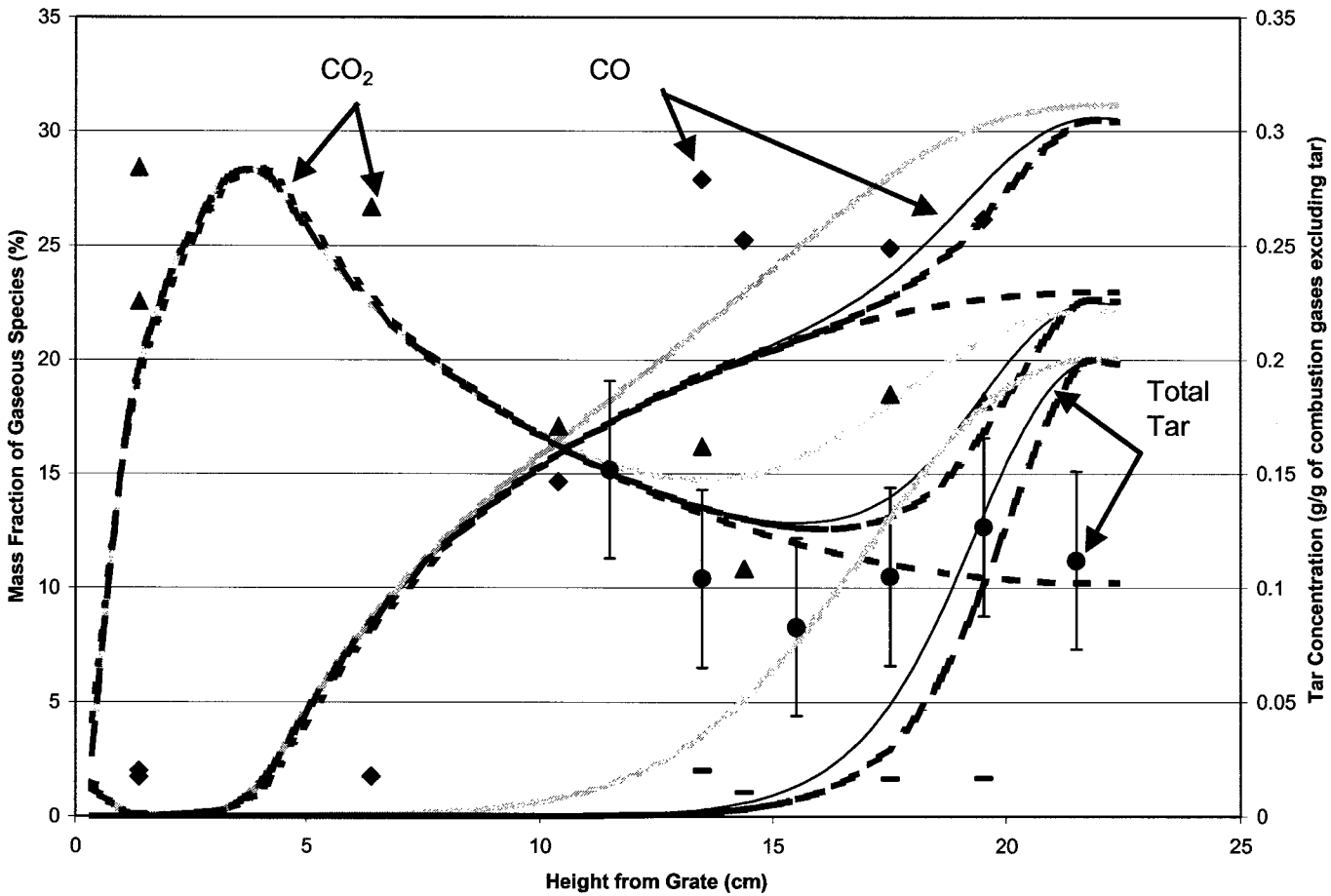


**Figure 5-21: Gas Concentration Profile for Run 010803. Airflow 108 kg/m$^2$h, Particle Diameter 2.81 cm (▲$CO_2$ ♦ CO ● Tar, - - - no pyrolysis reaction, — — — A=0.05 $s^{-1}$ E=10 kJ/mol ▒ A=0.05 $s^{-1}$ E=20 kJ/mol ____ A=0.15 $s^{-1}$ E =20 kJ/mol)**

### 5.3.2 Composition of Pyrolysis Products (CO, $CO_2$ and Tar)

Many authors have noted CO and $CO_2$ to be products of pyrolysis. Thus, as discussed in Chapter 3, the products from the pyrolysis were fixed to set mass fractions of CO and $CO_2$ with the balance being tar. (The char fraction was determined from previously discussed proximate analysis tests). Morf et al. (2002) found experimentally, using wood chips between 1 to 4 cm, that the conversions by pyrolysis of the original fuel to $CO_2$, CO and tar at 750°C were 13, 13 and 73 mass %, respectively for all products of pyrolysis except the char. Of the total products, 20% were identified as important precursors of secondary reactions from tar that form soot, CO or $CO_2$ but these are not currently modelled. Grønli and Melaaen (2000) found a similar tar conversion for large wood particles (D = 20 cm, L =30 cm), with 40 to 61% (mass of tar/mass of wood) from a model that included the porosity of the wood, chemical reactions, as well heat and mass transfer on the particle. The mass fraction of pyrolysis products used in the present model were set to 40% tar and the balance equally split between CO and $CO_2$; this proportion gave reasonable results, although improvements are probably possible with some adjustment of these numbers. The TGA gas composition values by DiBlasi and Branca (2001) are lower (~15%) but were for particles much smaller (< 0.3 cm) than those used here and reacted under flash pyrolysis conditions. Other gases discussed in the literature such as $H_2$ and methane are currently not modelled, and are only present to a few percent.

Increasing the amount of a gas species in the pyrolysis products increased the predicted mass fraction of that gas near the surface of the bed.

### 5.3.3 Comparison of Model with Experiments

Model predictions are compared with actual conditions in the bed in **Figures 5.1-5.5** and **5.8-5.25**. In all figures, points represent sampling data and lines show modelling results. The measured gas concentrations, **Figure 5.1-5.5**, agreed reasonably well with model predictions in the oxidation and reduction zones considering the scatter in the measurements. The oxygen concentration in the top 10 cm of the bed was essentially zero, since $O_2$ is totally consumed by char oxidation at the bottom of the bed. Therefore little or no volatiles combustion occurs in the bed itself. (The combustion gases flow up, thus not allowing the oxygen required for char combustion and the pyrolysis products to contact each other.)

Comparison of measured tar concentrations and model predictions indicates agreement at a height near 14 cm. However the sharp increase in tar concentration near the bed surface was not supported by the experimental results. This may be due to the lack of modeling heat conduction in the particle, which would slow pyrolysis near the bed surface, or to secondary tar reactions which may be more rapid than pyrolysis at a given point in the top portion of the bed. Secondary tar reactions would decrease the amount of tar and increase the amount of other products.

The comparison of particle density and size prediction and model results are shown in **Figures 5.8-5.12**. The void fraction of the fuel used was that of Ryan et al. (1999) determined by volume displacement. The greatest mass loss was found to occur within 2 equivalent particle diameters from the surface of the bed. Although the particle density decreased significantly, the equivalent particle diameter remained relatively constant until 10 cm from the grate where the reduction reaction begin. Simultaneous particle swelling

and breaking was observed in the samples from the 12.5 cm slice. These data suggest that mass loss occurs without significant change in particle size in the top section of the bed.

The changes in volatile and ash content compared to the model are shown in **Figures 5.14-5.28.** The predicted volatile concentration shows very good agreement with sampling results, although slightly lower at 7.5 cm. The predicted volatile concentration decreases significantly in the top 6 cm of the bed from 83% in the feed to 30% in the sample. The ash content prediction follows a similar trend as the experimental data in that it only becomes significant near the grate. (Drying is currently not included in the model.) These data support the conclusion that devolatilization occurs in the top portion of the bed.

Excellent agreement was also found between the model results and the experimental temperature readings. The model currently takes into account radiation from the bed surface, the walls and the laboratory temperature outside the reactor but not volatile flame radiation. The experimental results are found to fit between the temperature predictions of the combustion gas and solid particle temperature estimate, although closer to the solid temperature predictions than the gas temperature. Predictions have been shown in **Figures 5.22** to **5.25**. The points on these figures at 24.5 cm, often overlapping, are the readings from the thermocouple pair above the bed. Because of experimental difficulties with the thermocouples during run 011303, temperature predictions and experimental data plots are not presented for that run.

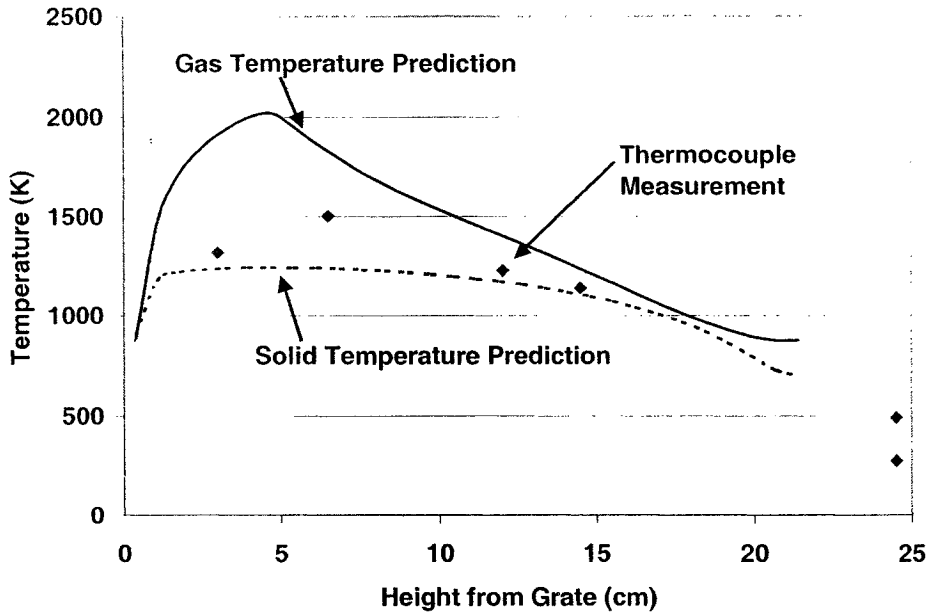


**Figure 5-22: Temperature Profile for Run 072202. Airflow 108 kg/m$^2$h, Particle Diameter 3.42 cm (♦ Thermocouple reading, - - - - - Solid Temperature Prediction, — Gas Temperature Prediction)**

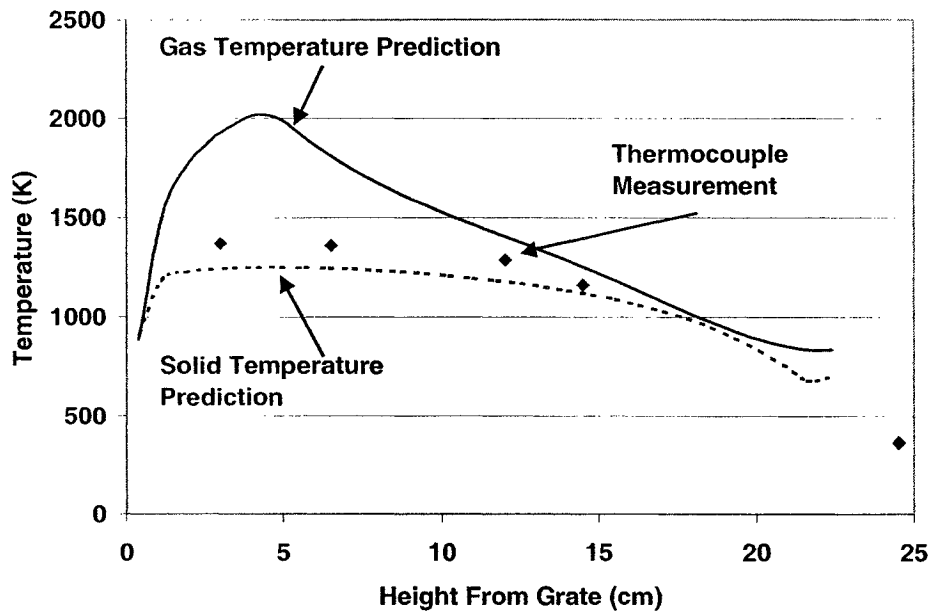


**Figure 5-23: Temperature Profile for Run 121302. Airflow 108 kg/m$^2$h, Particle Diameter 3.35 cm (♦ Thermocouple reading, - - - - - Solid Temperature Prediction, — Gas Temperature Prediction)**

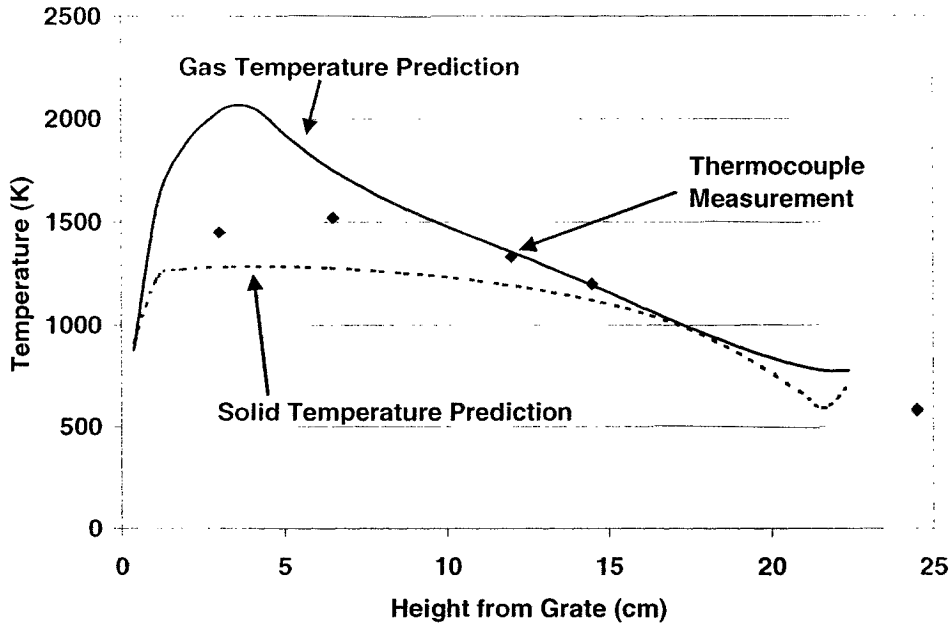


**Figure 5-24: Temperature Profile for Run 121802. Airflow 108 kg/m$^2$h, Particle Diameter 2.80 cm (♦ Thermocouple reading, - - - - - Solid Temperature Prediction, — Gas Temperature Prediction)**

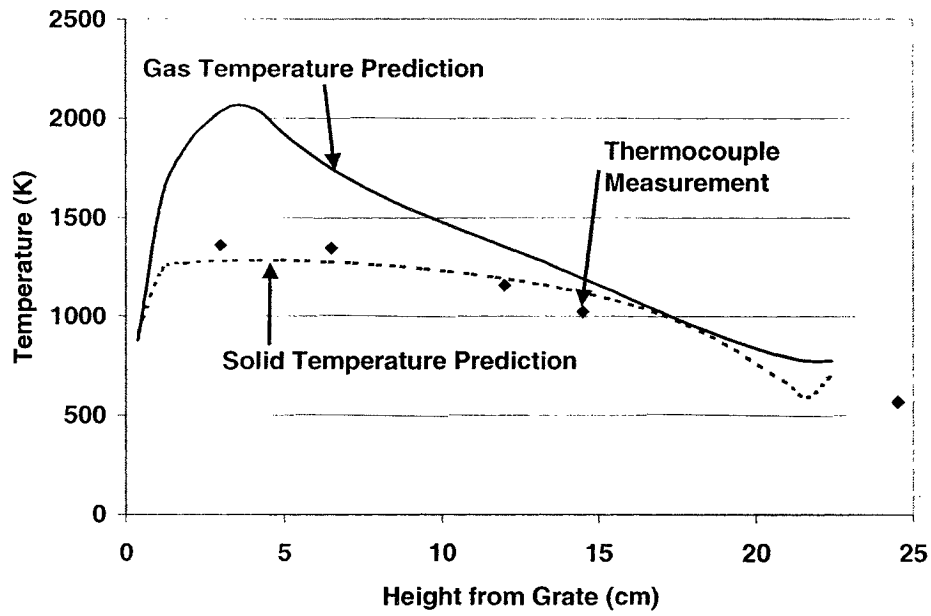


**Figure 5-25: Temperature Profile for Run 010803. Airflow 108 kg/m$^2$h, Particle Diameter 2.81 cm (♦ Thermocouple reading, - - - - - Solid Temperature Prediction, — Gas Temperature Prediction)**

### 5.3.3.1 Air to Fuel Ratio

Measured and predicted airflow rates are presented in **Table 5.5**. The actual air to fuel ratio was calculated by dividing the measured primary airflow rate into the reactor by the measured fuel addition rate once the bed had reached steady state (typically after 45 minutes). The predicted air/fuel ratios are lower than the actual ratios measured by up to 54%. (The predicted air/fuel ratio was calculated using the predicted burning rate at the time the bed was extinguished. The predicted burning rate decreased slightly with longer run times and therefore the predicted air/fuel ratio for runs under the same conditions are higher for the longer runs.) The reason for this difference is probably a wall effect which results in two phenomena that can affect the air to fuel ratio.

**Table 5-5: Predicted and Measured Air/Fuel Ratio and Estimate Thickness of Inert Wall Boundary Layer**

| Run | Measured air/fuel | Predicted air/fuel | Excess at Measured Airflow Over Predicted Value (%) | Calculated Thickness of Wall Boundary Layer with No Reaction (cm) |
|---|---|---|---|---|
| 071102 | 1.45 | 0.91 | 54 | 2.37 |
| 072202 | 1.44 | 1.28 | 16 | 0.64 |
| 081102 | 1.25 | 1.28 | 7 | 0.31 |
| 092502 | 1.28 | 0.91 | 37 | 1.81 |
| 121302 | 1.56 | 1.17 | 39 | 1.56 |
| 121802 | 1.42 | 1.03 | 39 | 1.70 |
| 010803 | 1.44 | 1.03 | 40 | 1.77 |
| 011303 | 1.38 | 1.11 | 27 | 1.19 |

The first phenomenon is the fact that the void fraction near the wall is greater than in the centre of the bed because particles do not fit the wall as well as they fit each other. The wall is flat, allowing for a smaller number of packing combinations than packing of particles between the voids of other similar size particles. The different packing near the wall will result in a larger void fraction near the wall, and thus the air will have less

resistance to flow through by the wall than the centre of the bed, resulting in channelling. The airflow across the bed will be non-uniform and higher near the wall. The actual airflow in the centre of the bed where most of the fuel combustion occurs will thus be lower than that measured by the rotameter.

The other phenomenon affecting the predicted air to fuel ratio is that the air which travels by the wall will be exposed to less fuel surface area than in the rest of the bed, resulting in less conversion of fuel per unit of air. Here channelling has the effect of decreasing fuel conversion per air quantity supplied to the reactor.

Schwartz and Smith (1953) and Chandrasekhara and Vortmeyer (1979) have examined flow distribution in packed beds noting similar findings of channelling. Schwartz and Smith (1953) noted that if the diameter of a pipe, which here is analogous to the reactor diameter, was less than 30 times greater than the particle diameter, important velocity variations would exist across a packed bed. The peak velocity was observed to occur approximately one particle diameter from the wall. For the data presented in **Table 5.5**, an attempt was made to estimated the magnitude of this effect by using predicted and measured air/fuel ratios to calculate the thickness of wall boundary layer equivalent to the amount of excess air noted in the measurements. Assuming the predicted air flow rates to be correct, the amount of air by which the measurements were in excess of this was first calculated. Next, assuming a uniform air velocity, the thickness of wall layer corresponding to this flow was calculated.

The thickness of wall boundary layer near the reactor wall averaged 1.3 cm for the large particle and 1.6 cm for the small particle runs. This represents approximately ½ particle thickness; this is exactly the thickness of the zone where the channelling effect becomes

important, lending support to the explanation of the discrepancy between predicted and measured air flows. For this work the reactor to particle size ratio was about 7. Thus the wall effect is greater in this work than previous work presented by Ryan and Hallett (2002) where the ratio of reactor diameter to particle size was between 22 and 30. As experiments were not conducted to measure the velocity profile across the bed and the model is currently only one dimensional, the magnitude of this flow distribution non-uniformity can currently only be described qualitatively. The airflow rate of a truly uniform bed would be somewhere between the measured airflow rate, which is too high, and that corresponding to the measured fuel consumption rate, which is smaller than that for a truly uniform bed.

Thus the burning rate is reduced. The presence of a wall effect was supported by observations of slower pyrolysis in particles near the wall as discussed in **Section 5.2.3**.

To test the effect of the airflow rate on the model prediction, the model was run with the measured air supply rate and with an airflow rate selected to make the model match the measured fuel consumption rate. An iterative process was required to find the airflow rate that would produce a combustion rate similar to that measured. The results showed, for the four last runs, that an airflow about 30% lower than the measured flowrate was required to meet the actual consumption rate. However, the temperature and gas concentration profiles did not show significant differences. This last observation suggests that the bed conditions are not a strong function of the airflow rate within the range tested and thus that errors in the input airflow should not greatly affect the model predictions of temperature and concentration profiles.

## 5.4 Effect of Operating Conditions on Combustion

### 5.4.1 Particle Size

The effect of particle size can be observed by comparing the results of runs 072202, 092502 and 121302 (3.3 cm particles) to 121802 and 010803 (2.8 cm particles). These tests had the same airflow rate but different particle sizes. A lower burning rate for the larger particles was predicted with the model but the measured average burning rate for the large particle run of 1.26 $kg/m^2h$ slightly higher compared to 1.25 $kg/m^2h$ for the smaller particles. Considering the stochastic variation of packed bed combustion, this is not a significant difference between the two particle sizes. The gas and solid temperature predictions near the bed surface are slightly higher for the larger particles as shown in **Figure 5.26**. This is likely because the effective thermal conductivity of the bed of larger particles is higher, allowing more heat transfer from the hotter lower regions of the bed. (Smaller particles have a larger number of voids between them, which act as radiation shields and reduce the effective conductivity.) However, the larger particle size reduces the surface area available to transfer heat into the particles, and should result in slower devolatilization, in spite of the higher temperature.

### 5.4.2 Airflow Rate

The effect of airflow rate can be observed by comparing the results of runs 121802 and 010803 with an airflow rate of 0.03 kg/m$^2$s to run 011303 with an airflow rate of 0.036 kg/m$^2$s. These tests had the same particle size. The average burning rate for the lower flow rate run was 130 kg/m$^2$h compared to 108 kg/m$^2$h for the 20% higher flow rate. For these airflow rates variations in model predictions for gas concentration and temperature were not large. Therefore the effect of modelling using a larger difference in airflow rates on gas concentration and temperature predictions is shown in **Figures 5.27**and **5.28**. The effect of $CO_2$ reduction reaction decreased slightly with a higher flow rate. The gas and solid temperature predictions both increased slightly with a higher air flow rate. This is likely because higher the burning rate release more radiant heat that is absorbed by the bed, increasing the bed temperature.

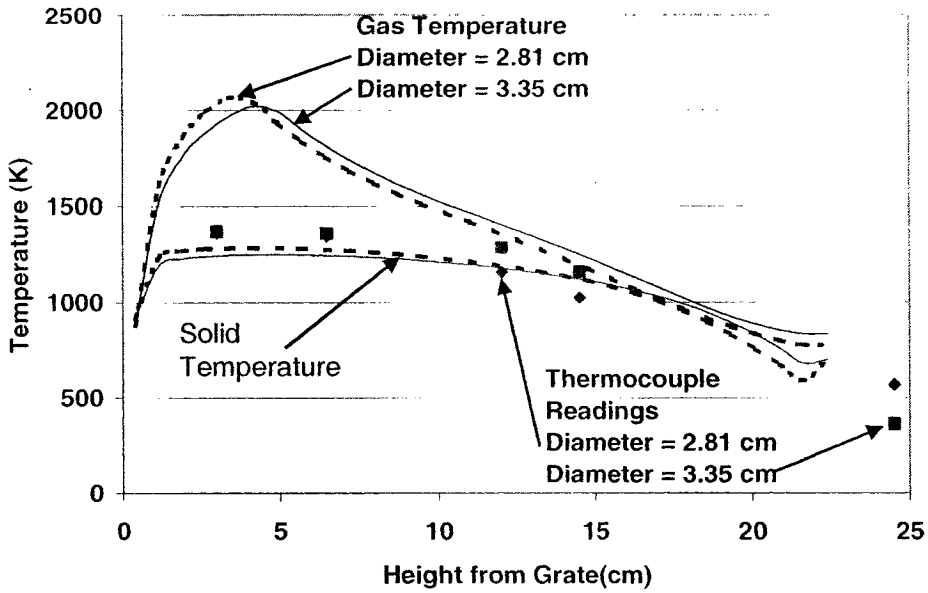


**Figure 5-26: Effect of Particle Diameter on Temperature Profile for Run 010803. Airflow 108 kg/m$^2$h, Particle Diameter 2.81 cm (♦ Thermocouple reading d = 2.81 cm, ■ Thermocouple Reading d = 3.35 cm - - - - - Temperature Prediction d = 2.81 cm, — Temperature Prediction d = 3.35 cm)**

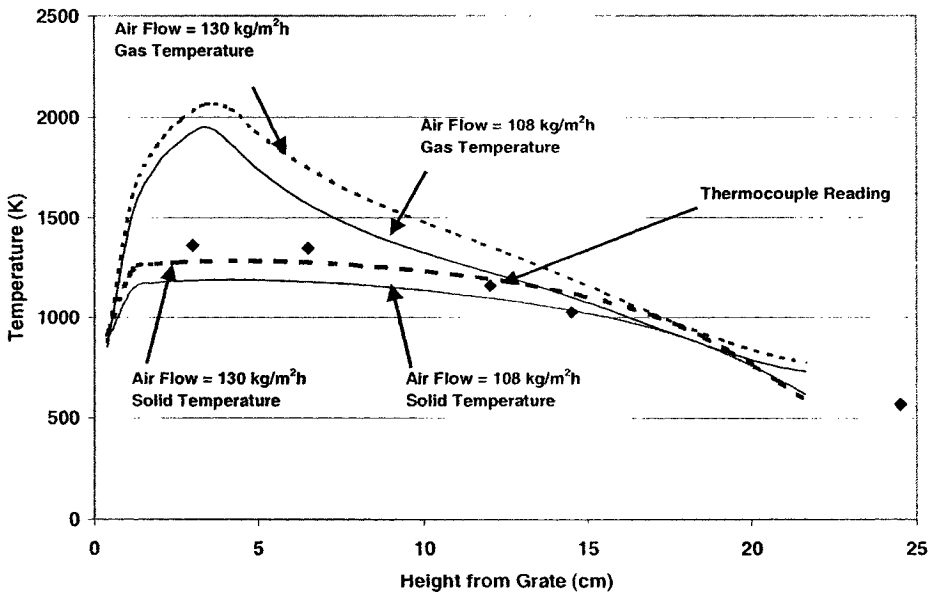


**Figure 5-27: Effect of Airflow Rate on Temperature Profile for Run 010803. Airflow 108 kg/m$^2$h, Particle Diameter 2.81 cm (♦ Thermocouple reading, - - - - - Temperature Prediction with Airflow Rate = 108 kg/m$^2$h , — Temperature Prediction with Airflow Rate = 130 kg/m$^2$h)**

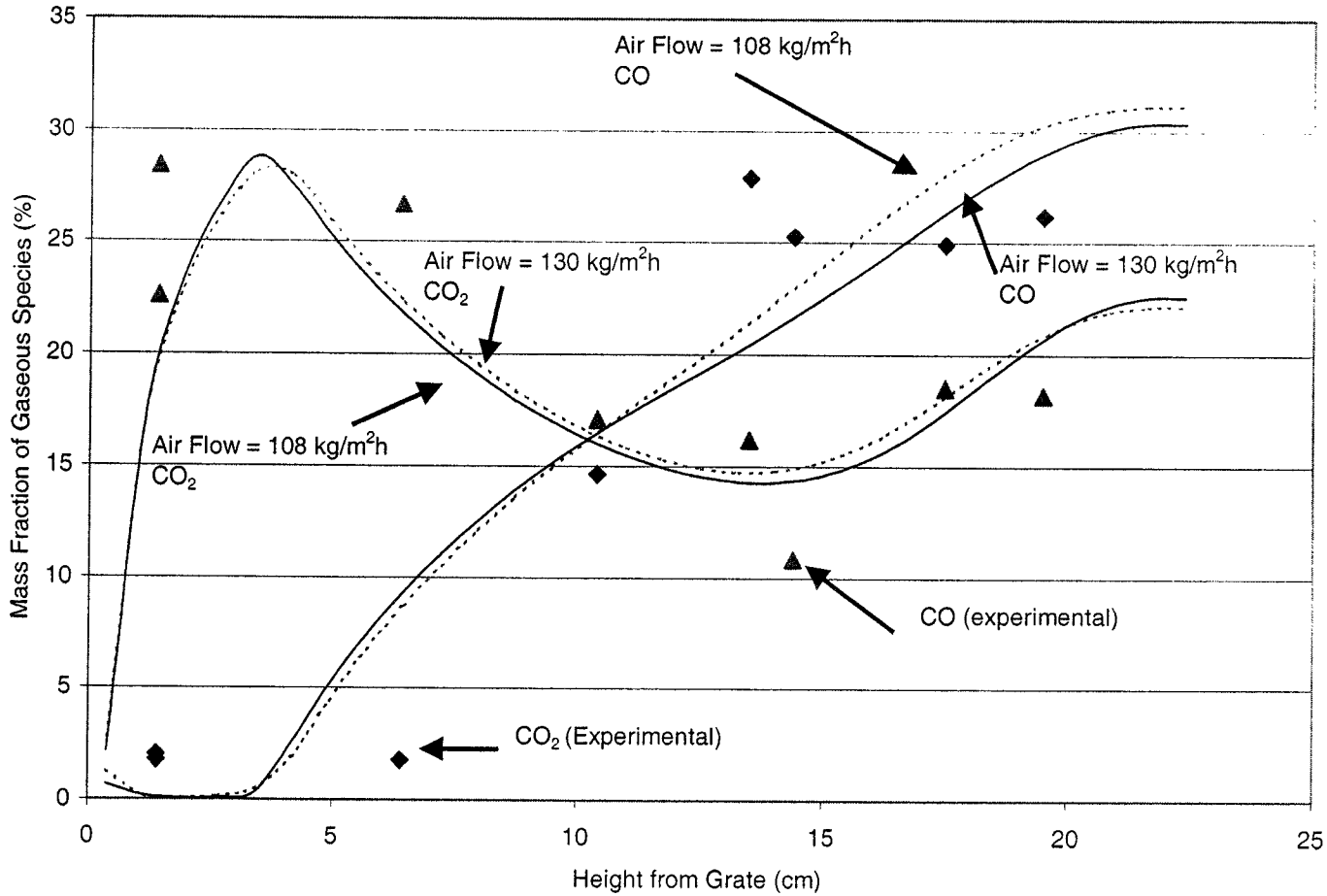


**Figure 5-28: Effect of Airflow Rate on Gas Concentration Profile for Run 010803. Airflow 108 kg/m²h, Particle Diameter 2.81 cm (♦ $CO_2$ Experimental Data, ▲CO Experimental Data, - - - - - Prediction with Airflow Rate = 108 kg/m²h , — Temperature Prediction with Airflow Rate = 130 kg/m²h)**

# 6 CONCLUSION

A series of experimental measurements on wood combustion in an overfeed packed bed and comparison to a detailed numerical model has been presented. The experimental method included the design and testing of a novel method to obtain tar concentrations at various heights in the bed. The model included the effect of a 1$^{st}$ order volatile evolution reaction with heat and mass transfer within the bed.

1. Data collected on gas concentration ($N_2$, $O_2$, CO, $CO_2$ and $CH_4$), temperature and particle properties (proximate analysis, density and size) profiles were typical of the pattern for packed bed combustion: at the bottom rapid consumption of $O_2$ and production of $CO_2$ with char oxidation, then reduction of $CO_2$ to produce CO, and near the top of the bed rapid production of pyrolysis products (observed here as mainly tar, CO and $CO_2$);
2. An in-situ tar sampling method was developed and appears to work satisfactorily in that the data, although displaying scatter, were consistent in replicate experiments. The method requires a knowledge of the expected tar concentration range to ensure that the sampling time does not allow tar break-through of the metal foam;
3. The temperature, gas and tar concentration measurements displayed some scatter. Most of this was believed to be due to stochastic variations in local conditions within the bed;
4. The tar sampling results suggest the presence of tar within two particle diameters from the bed surface.
5. Although the particles were observed to shrink with the grain, they expanded in the direction across the wood grain. Modelling, which assumed that pyrolysis occurred at

constant particle volume while char combustion occurred at constant density with a shrinking particle, compared reasonably well with particle samples from experiments.

6. Volatile flame radiation above the bed appears to play a significant role in determining the overall effect of radiation above the bed;
7. A simple first order reaction for devolatilization was included in the mathematical model. Pre-exponential factor, activation energy, and CO and $CO_2$ mass fractions in the pyrolysis products used were Av = 0.05 $s^{-1}$, Ev = 20,000 kJ/mol, 30% and 30%, respectively. The pyrolysis products were released more quickly and closer to the top of the bed in the model than in the experiments.
8. The model results compared well with bed temperature and particle properties (size, proximate analysis and density) throughout the bed and with gas concentrations (CO, $CO_2$, $O_2$, and $CH_4$) measurements in the reduction and oxidation zone. The total volatiles (tar) species prediction appeared to need refinement; and,
9. The air to fuel ratio was under predicted by the model likely due to the wall effect;

# 7 RECOMMENDATIONS

1. Smaller particles should be used to allow the oxidation, reduction and pyrolysis zones to be more clearly separated to allow a better determination of rate constants. This should also reduce the wall effect and the influence of intra-particle heat conduction, thus creating a bed which is closer to the model assumptions;
2. A tar probe that allows sampling the full length of the bed should be developed to confirm the region where pyrolysis stops. The new design may also consider a cone tip to the probe to minimize the compaction of fragile wood char particles in the lower section of the bed;
3. More data should be obtained on the moisture content in the combustion gas at various heights within the devolatilization to allow drying and secondary tar reaction involving water to be modelled;
4. Modelling heat trasfer within the particle may improve prediction of tar and gas concentration in the devolatilization zone; and,
5. Several more experiments should be performed at various bed heights and air flow rates to further test model accuracy and allow an analysis of the data that takes into account the stochastic variability of packed bed combustion.

# 8 REFERENCES


Abatzoglou, N., N. Barker, P. Hasler, and H. Knoef "The development of a draft protocol for the sampling and analysis of particulate and organic contaminants in the gas from small biomass gasifiers" Biomass and Bioenergy **18**, 5-17 (2000)

Aganda, A., P. Murray and S. Kionga-Kamau "Temperature Profiles in a wood packed bed heated by hot inert gases" Trans IchemE **75**, Part A, 677-684 (1997)

Agrawal, R. and R. McCluskey "Effect of pressure on the pyrolysis of newsprint" Fuel **64**, 1502-1504 (1985)

Antal, M. J. "Biomass pyrolysis: A review of the literature Part I – Carbohydrate pyrolysis" Advance in Solar Energy, American Solar Energy Society, pp. 61-111 (1983)

Antal, M. and G. Varhegyi "Cellulose Pyrolysis Kinetics: The Current State of Knowledge" Ind. Eng. Chem. Res. **34**, 703-717 (1995)

Antal, J., G. Varhegyi, E. Jakab "Cellulose Pyrolysis Kinetics: Revisited" Ind. Eng. Chem. Res. **37**, 1267-1275 (1998)

Arseneau, D. "Competitive Reactions in the Thermal Decomposition of Cellulose" Canadian Journal of Chemistry **49**, 632-638 (1971)

Avni, E., R. Coughlin, P. Solomon and H. King "Mathematical modelling of lignin pyrolysis" Fuel **64**, 1495-1501 (1985)

Bech, N., L. Wolff and L. Germann "Mathematical Modeling of Straw Bale Combustion in Cigar Burners" Energy & Fuels **10**, 276-283 (1996)

Becker, H. "Physical Probes" in Instruments for Flow with Combustion A.M. Taylor, Ed. Academic Press, England pp. 53-112 (1993)

Bettagli, N., U. Desideri and D. Fiashi "A Biomass Combustion-Gasification Model: Validation and Sensitivity Analysis" Journal of Energy Resources Technology **117**, 329-336 (1995)

Bhattacharya, S. "State of the Art of Biomass Combustion" Energy Sources **20**, 113-135 (1998)

Bhattacharya, D. and D. Pei "Heat Transfer in Fixed Bed Gas-Solid Systems", Chemical Engineering Science **30**, 295-300 (1975)

Biagini, E., F. Lippi, L. Petarca and L. Tognotti "Devolatilization Rate of biomasses and coal-biomass blends: an experimental investigation", Fuel **81**, 1041-1050 (2002)

Brage, C., Q. Yu and K. Sjöström "Characteristics of evolution of tar from wood pyrolysis in a fixed-bed reactor" Fuel **75**, no. 2, 213-219 (1995)

Bryden and Ragland "Numerical Modeling of a Deep, Fixed Bed Combustor" Energy & Fuels **10**, 269-275 (1996)

Chan, W., M. Kelbon and B. Krieger "Modelling and experimental verification of physical and chemical processes during pyrolysis of a large biomass particle" Fuel **64**, 1504-1513 (1985)

Chandrasekhara, B. and D. Vortmeyer "Flow Model for Velocity Distribution in Fixed Porous Beds Under Isothermal Conditions" Wärme- abd Stoffübertragung **12**, 105-111 (1979)

Chen, Y., S. Charpenay, A. Jensen, M. Wöjtowicz and M. Serio "Modeling of Biomass Pyrolysis Kinetics", Twenty-Seventh Symposium (International) on Combustion/The Combustion Institute, 1327-1334 (1998)

Cooper, J. "A Numerical Model for Char Combustion in Packed Bed Reactors", M.A.Sc. Chemical Engineering Thesis, University of Ottawa (1996)

Cooper, J. and W. Hallett "A numerical model for packed-bed combustion of char particles" Chemical Engineering Science **55**, 4451 (2000)

Cozanni, V. "Reactivity in Oxygen and Carbon Dioxide of Char Formed in the Pyrolysis of Refuse-Derived Fuel" Ind. Eng. Chem. Res. **39**, 864-872 (2000)

Cozzani, V., C. Nicolcella, M. Rovatti and L. Tognotti "Modeling and Experimental Verification of Physical and Chemical Processes during Pyrolysis of a Refuse-Derived Fuel" Ind. Eng. Chem. Res. **35**, 90-98 (1996)

Dasappa, S., P. Paul, H. Mukunda and U. Shrinivasa "The gasification of wood-char spheres in $CO_2$-$N_2$ mixtures: Analysis and experiments" Chemical Eng. Science **49**, no. 2, 223-232 (1994)

Davidsson, K. and J. Pettersson "Birch wood particle shrinkage during rapid pyrolysis" Fuel **81**, 263-270 (2002)

Davidsson, K., J. Petersson and R. Nilsson "Fertiliser influence on alkali release during straw pyrolysis" Fuel **81**, 259-262 (2002)

DiBlasi, C., C. Branca "Kinetics of Primary Product Formation from Wood Pyrolysis" Ind. Chem. Res. **40**, 5547-5556 (2001)

Di Blasi, C., C. Branca, A. Santoro and E. Hernandez "Pyrolytic Behavior and Products of Some Wood Varieties" Comb. Flame **124**, 165-177 (2001)

Di Blasi C., E. Hernandez and A. Santoro "Radiative Pyrolysis of Single Moist Wood Particles" Ind. Eng. Chem. Res. **39**, 873-882 (2000b)

Di Blasi, C., G. Portoricco, M. Borrelli and C. Branca "Oxidative degradation and ignition of loose-packed straw beds" Fuel **78**, 1591-1598 (1999b)

Di Blasi, C., G. Signorelli and G. Portoricco "Countercurrent Fixed-Bed Gasification of Biomass at Laboratory Scale" Ind. Eng. Chem. Res. **38**, 2571-2581 (1999a)

Di Blasi C., G. Signorelli, C. Di Russo and G. Rea "Product Distribution from Pyrolysis of Wood and Agricultural Residues" Ind. Eng. Chem. Res. **38**, 2216-2224 (1999c)

Dixon A., and D. L. Cresswell "Theorectical Predicion of Effective Heat Transfer Parameters in Packed Beds", AIChE Journal **26**, 663-668 (1979)

Eckert, E. and R. Goldstein Measurements in Heat Transfer, Hemisphere Publinshing Corporation, Toronto (1976)

European Environment Agency "Environment in the European Union at the Turn of the Century – Chapter 3.7 Waste generation and management" European Environment Agency Report (1999)

Figueiredo, J., C. Valenzuela, A. Bernalte and J. Encinar "Pyrolysis of holm-oak wood: influence of temperature and particle size" Fuel **68**, 1012-1016 (1989)

Fjellerup, J., E. Gjernes and L. Hansen "Pyrolysis and Combustion of Pluverized Wheat Straw in a Pressurized Entrained Flow Reactor", Energy & Fuels **10**, 649-651 (1996)

Geankoplis, C. Transport Processes and Unit Operations, Prentice-Hall, Toronto (1993)

Goh, Y., R. Siddall, V. Nasserzadeh, R. Zakaria, J. Swithbank, D. Lawrence, N. Goarrod and B. Jones "Mathematical modelling of the burning bed of a waste incinerator" Journal of the Institute of Energy **71**, 110-118 (1998)

Goh, R., Y. Yang, R. Zahkaria, R. Siddall, V. Nasserzadeh and J. Swithenbank "Development of an incinerator bed model for municipal solid waste incineration" combustion Science & Technology **162**, 37-58 (2001)

Gort, R., and J. Brouwers "Theoretical Analysis of the Propagation of a Reaction Front in a Packed Bed" Combustion and Flame **124**, 1-13 (2001)

Grønli, M., M. Antal and G. Várheyi "A Round-Robin Study of Cellulose Pyrolysis Kinetics by Thermogravimetry" Ind. Eng. Chem. Res. **38**, 2238-2244 (1999)

Grønli, M., and M. Melaaen "Mathematical Model for Wood Pyrolysis-Comparison of Experimental Measurements with Model Predictions" Energy & Fuels **14**, 791-800 (2000)

Gupta, M., J. Yang and C. Roy "Specific heat and thermal conductivity of softwood bark and softwood char particles" Fuel **82**, 919-927 (2003)

Hagge, M., and K. Bryden "Modeling the impact of shrinkage on the pyrolysis of dry biomass" Chemical Engineering Science **57**, 2881-2823 (2002)

Hajaligol, M. B. Waymack and D. Kellogg "Low temperature formation of aromatic hydrocarbon from pyrolysis of cellulosic materials" Fuel **80**, 1799-1807 (2001)

Hallett, W. "Combustion in Diffusion Systems" Lecture Notes for MCG 5192, University of Ottawa, Chapter 4 (1997)

Hastaoglu, M. and T. Al-Khalid "Treatment of Wood Pyrolysis Data via a Multiple Gas-Solid Reaction Model" Ind. Eng. Chem. Res. **40**, 1845-1851 (2001)

Hastaoglu, M., R. Kahraman and M. Syed "Pellet Breakup Due to Pressure Generated during Wood Pyrolysis" Ind. Eng. Chem. Res. **39**, 3255-3263 (2000)

Holman, J. Heat Transfer, McGraw-Hill, Toronto (1976)

Huang, C. "The Packed Bed Combination of Wood Cylinders", Thirteenth Annual Energy – Sources Technology Conference & Exhibition, p.17 (1987)

Jones, J.M., M. Pourkashanian and A. Williams "Biomass combustion modelling" International Journal of Ambient Energy **21**, n.3, 115-123 (2000)

Kaiser Gas Phase Chromatography, London : Butterworths, pp. 86-111 (1963)

Kanuary, A. "Combustion Characteristics of Biomass Fuels", Combustion Science and Technology **97**, 469-491 (1994)

Khan, A. and J. Bowen "Analysis of fixed bed reactors using a diffuse interface single pellet model" Trans IchemE **77**, part A, 47-54 (1999)

Koufopanos C.A., N. Papayannakos, G. Maschio and A. Lucchesi "Modelling of the Pyrolysis of Biomass Particles. Studies on Kinetics, Thermal and Heat Transfer Effects." The Canadian Journal of Chemical Engineering, **69**, 907-915 (1991)

Kuo, J. "Estimation of Burning Rates in Solid Waste Combustion Furnaces" Combust. Sci. and Tech. **137**, 1-29 (1998)

Larfelt, J., B. Leckner and M. C. Melaaen "Modelling and Measurements of the pyrolysis of large wood particles" Fuel **79**, 1637-1643 (2000)

Larfelt, J., B. Leckner and M. C. Melaaen "Modelling and measurements of heat transfer in charcoal from pyrolysis of large wood particles" Biomass and Bioenergy **18**, 507-514 (2000b)

Liang, X. and J. Kozinski "Numerical modeling of combustion and pyrolysis of cellulosic biomass in thermogravimetric systems" Fuel **79**, 1477-1486 (2000)

Löffler, G., V. Wargadalam and F. Winter "Catalytic effect of biomass ash on CO, $CH_4$ and HCN oxidation under fluidized bed combustor conditions" Fuel **81**, 711-717 (2002)

McCabe,W., J.Smith and P. Harriot Unit Operations of Chemical Engineering, Fifth Edition, McGraw-Hill, New York (1993)

Miller, R. and J. Bellan "Tar Yeild and Collection from the Pyrolysis of Large Biomass Particles" Combust. Sci. and Tech. **127**, 97-118 (1997)

Milosavljevic, I., V. Oja and E. Suuberg "Thermal Effects in Cellulose Pyrolysis: Relationship to Char Formation Processes", Ind. Eng. Chem. Res. **35**, 653-662 (1996)

Morf, P., P. Hasler and T. Nussbaumer "Mechanisms and kinetics of homogeneous secondary reaction of tar from continuous pyrolysis of wood chips" Fuel **81**, 843-853 (2002)

Niksa, S. "Predicting the Rapid Devolatilization of Diverse Forms of Biomass with bio-FLASHCHAIN", Proceedings of the Combustion Institute **28**, 2727-2733 (2000)

Oasmaa, A. and S. Czernik "Fuel Oil Quality of Biomass Pyrolysis Oils-State of the Art for End Users" Energy & Fuels **13**, 914-921 (1999)

Oesch, P., E. Leppämäki and P. Ståhlberg "Sampling and characterization of high-molecular-weight polyaromatic tar compounds formed in the pressurized fluidized-bed gasification of biomass" Fuel **75**, no. 12, 1406-1412 (1996)

Oman, J., M. Tacer and M. Tuma "Overfeed fixed-bed combustion of wood" Bioresource Technology **67**, 139-147 (1999)

Òrfao, J, F. Antunes and J. Figueiredo "Pyrolysis kinetics of lignocellulosic materials – Three independent reactions model" Fuel **78**, 349-358 (1999)

Ouedraogo, A., J. Mulligan and J. Cleland "A Quasi-steady Shrinking Core Analysis of Wood Combustion" Comb. and Flame **114**, 1-12 (1998)

Padban, N., Wang, W, Ye Z., Berjle I., Odenbrand I., "Tar Formation in Pressurized Fluidized Bed Air Gasification of Woody Biomass" Energy & Fuels **14**, 603-611 (2000)

Park, B., J. W. Bozzelli and M.R. Booty "Pyrolysis and Oxidation of Cellulose in a Continuous-Feed and Flow Reactor: Effects of NaCl" Ind. Eng. Chem. Res. **41**, 3526-3539 (2002b)

Patankar Numerical Heat Transfer and Fluid Flow, Hemisphere Publishing Corporation, Washington (1980)

Peters, B. "Classification of Combustion Regimes in a Packed Bed of Particles Based on the Relevant Time and Length Scales" Comb. and Flame **116**, 297-301 (1998)

Peters, B. "Extinction of burning particles due to unstable combustion modes" Fuel **81**, 391-396 (2002)

Peters, B., and C. Bruch "A flexible and stable numerical method for simulating the thermal decomposition of wood particles", Chemosphere **42**, 481-490 (2001)

Pyle, D. and C. Zaror "Heat transfer and kinetics in the low temperature pyrolysis of solids" Chemical Engineering Science **39**, no. 1, 147-158 (1984)

Rath, J. and G. Staudinger "Cracking reactions of tar from pyrolysis of spruce wood" Fuel **80**, 1379-1389 (2001)

Reina, J., E. Velo and L. Puigjaner "Kinetic Study of the Pyrolysis of Waste Wood" Ind. Eng. Chem. Res. **37**, 4290-4295 (1998)

Reynolds, J. and A. Burnham "Pyrolysis Decomposition Kinetics of Cellulose-Based Materials by Constant Heating Rate Micropyrolysis" Energy & Fuels **11**, 88-97 (1997)

Ryan, J., Char Combustion in Packed Bed Reactor, Masters Thesis, Department of Chemical Engineering, University of Ottawa (2000)

Ryan, J.S., Hallett, W.L.H., "Packed Bed Combustion of Char Particle: Experiments and an ash model" Chemical Eng. Science **57**, 3873-3882 (2002)

Ryan, J.S., Hallett, W.L.H., and Di Iorio, J., "Experiments on Solid Fuel Combustion in an Overfeed Bed" Combustion Inst. Canadian Sect. 1999 Meeting 21-1, 21-9 (1999)

Saade, R. and J. Koziński "Numerical modeling and TGA/FTIR/GCMS investigation of fibrous residue combustion" Biomass and Bioenergy **18**, 391-404 (2000)

Saastamoinen, J. and J. Richard "Simultaneous Drying and Pyrolysis of Solid Fuel Particles" Combustion and Flame **106**, 288-300 (1996)

Saastamoinen, J. J., R. Taipale, M. Horttanainen and P. Sarkomaa "Propagation of the Ignition Front in Beds of Wood Particles" Combustion and Flame **123**, 214-226 (2000)

Salzmann, R. and T. Nussbaumer "Fuel Staging for NOx Reduction in Biomass Combustion: Experiments and Modeling" Energy & Fuels **15**, 575-582 (2001)

Schwartz, C. and J. Smith "Flow Distribution in Packed Beds" Industrial and Chemical Engineering **45**, 1209-1218 (1953)

Sensöz, S., D. Angun and S. Yorgun "Influence of particle size on the pyrolysis of rapeseed (Brassica napus L.): fuel properties of bio-oil" Biomass and Bioenergy **19**, 271-279 (2000)

Sensöz, S. and M. Can "Pyrolysis of Pine (Pinus Brutia Ten.) Chips: 1. Effect of Pyrolysis Temperature and Heating Rate on the Product Yeilds" Energy Sources **24**, 347-355 (2002)

Sensöz, S. and M. Can "Pyrolysis of Pine (Pinus Brutia Ten.) Chips : 2. Structural Analysis of Bio-oil" Energy Sources **24**, 357-364 (2002)

Shin, D., S. Choi "The Combustion of Simulated Waste Particles in a Fixed Bed" Comb. and Flame **121**, 167-180 (2000)

Simell, P., P. Ståhlberg, E. Kurkela, J. Albrecht, S. Deutsch and K. Sjöström "Provisional protocol for the sampling and analysis of tar and particulates in the gas from large-scale biomass gasifiers. Version 1998" Biomass and Bioenergy **18**, 19-38 (2000)

Sipla, K., Kuoppala E., L. Fagerna and A. Oasmaa "Characterization of biomass-basd Flash Pyrolysis Oils" Biomass and Bioenergy **14** No. 2, 103-113 (1998)

Sørum, L., M. Grønli and J. Hustad "Pyrolysis characteristics and kinetics of municipal solid wastes" Fuel **80**, 1217-1227 (2001)

Sørum, L., O. Skyreiberg, P. Glaborg, A. Jensen and K. Dam-Johansen "Formation of NO From Combustinon of Volatiles From Municipal Wastes" Comb. and Flame **123**, 195-212 (2000)

Thomas, L. C. Heat Transfer, Prentice-Hall, Toronto (1992)

Thunman, H. and B. Leckner "Ignition and propagation of a reaction front in cross-current bed combustion of wet biofuels" Fuel **80**, 473-481 (2001)

United States Environmental Protection Agency "Greenhouse gas Emissions From Management of Selected Materials in Municipal Solid Waste", EPA Report 530-R-98-013 (1998)

van der Lans, R. P., L. Pedersen, A. Jensen, P.Glarborg and K. Dam-Johansen "Modelling and experiments of straw combustion in a grate furnace" Biomass and Bioenergy **19**, 199-208 (2000)

World Bank "Energy from Biomass" Technical Paper No. 422 (1999)

Wornat, M., R. Hurt, N. Yang and T. Headley "Structural and Compositional Transformations of Biomasss Chars during Combustion" Combustion and Flame **100**, 131-143 (1995)

Wright, G. Fundamentals of Air Sampling, CRC Press, Ann Arbor Press, New York (1994)

Wu, C., C. Chang and C. Tseng "Pyrolysis products of uncoated printing and writing paper of MSW" Fuel **81**, 719-725 (2002)

Xie, M. and X. Liang "Numerical Simulation of Combustion and Ignition-Quenching Behavior of Carbon Packed Bed" Combust. Sci. and Tech. **125**, 1-24 (1997)

Yu, Q., C. Brage, G. Chen and K. Sjöström "Temperature impact on the formation of tar from biomass pyrolysis in a free-fall reactor" Journal of Analytical and Applied Pyrolysis **40-41**, 481-489 (1997)

Zaror, C., I. Hutchings, D. Pyle, H. Stiles and R. Kandiyoti "Secondary char formation in the catalytic pyrolysis of biomass" Fuel **64,** 990-994 (1985)

Zevenhoven, R., E. Axelsen and M. Hupa "Pyrolysis of waste-derived fuel mixtures containing PVC" Fuel **81**, 507-510 (2002)

# APPENDIX A:

# COMBUSTION MODEL PROGRAM CODE

```
*       PROGRAM CHARVOL
*
*       CALCULATES TEMPERATURE AND CONCENTRATION PROFILES FOR BURNING
*       FIXED BEDS OF BIOMASS
************************************************************************

        PARAMETER (N=50)
        DIMENSION TG(N),TGI(N),TGO(N),TS(N),TSI(N),TSO(N)
        DIMENSION FE(N),XB(N),DXN(N)
        DIMENSION AKG(N),AKAG(N),AKAS(N),AKY(N,4),DEFF(N,4),H(N)
        DIMENSION CPG(N),AMWG(N),RE(N),CPGO(N)
        DIMENSION WC(N),WS(N),VOIDO(N),XCO(N),RHOSO(N),APHI(N),APHIO(N)
        DIMENSION RCO(N),RCOB(N)
        DIMENSION VOID(N),SLAB(N),SSB(N),SSBO(N),RHOS(N),G(N),DZETA(N)
        DIMENSION DIAMC(N),SSC(N),SSCO(N),XC(N)
        DIMENSION WG(N),RHOG(N),RHOGO(N)
        DIMENSION Y8O2(N),Y8CO2(N),Y8CO(N),Y8N2(N),Y8O2O(N),Y8CO2O(N)
        DIMENSION Y8COO(N),Y8N2O(N),Y8P(N),Y8PO(N)
        DIMENSION YRO2(N),YRCO2(N),YRCO(N),YRN2(N),YRP(N)
        DIMENSION G1(N),G2(N),X(N),S(N)
        DIMENSION TESTTG(N),TESTTS(N),TESTCO(N),TESTYW(N),TESTP(N)
        DIMENSION CPGREG(N),WCO(N)
        DIMENSION VG(N),VS(N),VC(N)
        DIMENSION DIFF(N,4)
        DIMENSION GV(N),RP(N),W(N),WO(N),yrh2o(n)
        DIMENSION  RHOF(N),YW(N),YCHAR(N),YWO(N)
        DIMENSION RHOFO(N),AMASSC(N),SCP(N)
        common/water/xh2o,rhow,yrh2o
        COMMON/DEBUB/AMASSC,ALEFF,SCP
        COMMON/DEVOL/GV,AVV,EVV,RP,COVOL,CO2VOL,HPYRO
        COMMON/BED/VOID,E,SLAB,SSB,SSBO,RHOS,G,DHTDT,DZETA
        COMMON/WCHAR/CARB,DIAMC,RHOC,VOIDC,SPHERC,SSC,SSCO,XC
        COMMON/ASH/ASH,DIAMA,RHOA,VOIDA,SPHERA,IBUILD
        COMMON/GAS/WG,RHOG,RHOGO
        COMMON/Y/Y8O2,Y8CO2,Y8CO,Y8N2,Y8O2O,Y8CO2O,Y8COO,Y8N2O,Y8P,Y8PO
        COMMON/YR/YRO2,YRCO2,YRCO,YRN2,YRP
        COMMON/INFO/WTN2,WTO2,WTCO2,WTCO,R,P,BETA,GAMMA,THI,WTP,TREF
        COMMON/STOIC/SCO2,SCO,S3,S2,DH1,DH2,DH3,DH4
        COMMON/GE/A,A1,ER,E1,ALPHA1,ALPHA2
        COMMON/PORE/IFIELD,IEFFECT,SSP,TAU,VOIDP
        COMMON/REACT/G1,G2,X,S,IREACT
        COMMON/RAD/TSG,TSB,TSW,HRG,HRB,HRW,F12B,BOLTZ,TCOAL
        COMMON/FLUXES/FO2,FC,FCO2,FP,FTG,FTS
        COMMON/GRATE/GRATE,GRTSOL,GRTBAR,IGMOD,GRTRHO,GRTPD,GRTSPACE
        COMMON/TIME/IFLAG,ITIME,ITERNS,TURNS,IB,IG,ICOB,TIMES,DT
        COMMON/TEST/TESTTG,TESTTS,TESTCO,CRIT,TESTYW,TESTP
        COMMON/EXTRA/CPGREG
        COMMON/V/VG,VS,VC


*       READ IN SYSTEM PARAMETERS
```

```
c       OPEN (1,FILE='RUN13dec.DAT',STATUS='OLD')
        OPEN (1,FILE='RUNEGX.DAT',STATUS='OLD')
        OPEN (2,FILE='CONSTEG.DAT',STATUS='OLD')
        OPEN (3,FILE='CHARVOL.OUT')
        open (8,file='crap.out')
        OPEN (9,FILE='PRODMASS.OUT')

*       PROGRAMME CONTROL:
*           IFLAG:    = 2 - KEEP ITERATING
*                     = 3 - NEXT TIME STEP
*                     = 4 - HALT X, END OF ALLOTTED TIME
*           IREACT:   = 0 - TURNS OFF ALL REACTIONS
*                     = 1 - TURNS OFF CO2 REDUCTION
*                     = 2 - ALL REACTIONS ON
*           IRXN:     = 1980 - WESTBROOK AND DRYER CO KINETICS
*                     = 1970 - HOWARD AND FINE CO KINETICS
*           ICOB:     = 0 - TURNS OFF REVERSE CO (EQUIL'M) RXN
*                     = 1 - TURNS ON REVERSE CO (EQUIL'M) RXN
*           IHTTR: CONTROLS SELECTION OF GAS/SOLID HT. TR. CORRELATION
*                     = 1970 - BATMAN AND PEI 1974
*                     = 1960 - YOSHIDA ET AL. 1962
*                     = 1950 - CHU
*           IGMOD: SELECTS GRATE MODEL
*                = 1 - PACKED BED OF POROUS MEDIUM, PARTICLE DIA.
*                     = 2 - STEEL BARS, SPECIFIED WIDTH (GRTBAR), DEPTH
*                     (GRATE) AND SOLIDITY (GRTSOL)
*         IBUILD:SELECTS THE ASH MOVEMENT
*                     = 0 - ASH FALLS THROUGH THE GRATE
*                = 1 - ASH BUILDS UP IN THE BED
*         IFEED: SELECTS THE FUEL FEEDING RATE
*                = 0 - NO FUEL FEEDING (THE BED HEIGHT DECREASES)
*                = 1 - CONSTANT FUEL FEEDING (MAINTAINS BED HEIGHT)
*         IZONE: SELECTS THE IGNITION METHOD
*                = 0 - A HOT LAYER OF A GIVEN THICKNESS (ALYATER) &
*                    TEMPERATURE (TIGNIT) AT THE BOTTOM OF THE BED
*                = 1 - A HOT LAYER OF A GIVEN THICKNESS (ALYATER) &
*                    TEMPERATURE (TIGNIT) AT THE TOP OF THE BED
*                = 2 - RADIATION FROM ABOVE THE BED
*                    (TS(IT) = TIGNIT)
*
*       TIME STEP INCREASED BY FACTOR OF ITCUT TIMES BEFORE END
*
*       VARIABLES:
*          CURRENT VALUES: TG,TS,Y802...
*          PREVIOUS ITERATION: TGI,TSI,Y8O2I...
*          PREVIOUS TIME STEP: TGO,TSO,Y8O2O...

        IFLAG = 2
        IFLAG3 = 0
        ITIME = 0
        ITERNS = 1
        ITSTEP = 0
        ICNT = 1
        ICNTN = 100
        icntn = 10
        IN = 0
```

```
      TCGONE = 0.0
      CRIT = 2.0
      TREF = 273.15
      CALL READER(1,2,TG,TS,U,US,TIGNIT,ALAYER,HT,IHTTR,IRXN,ITCUT,
     &              TLIMIT,IEND,IGRID,IGRAPH,IFEED,IZONE)
      CALL DIVIDE(HT,FE,XB,DXN,IGRID)
      CALL SETUP(TG,TGO,TS,TSO,U,US,WS,WC,TIGNIT,ALAYER,HT,APHIO,VOIDO,
     &       XCO,RHOSO,IFEED,RHOBO,IZONE,XB,APHI,W,RHOF,RHOFO
     &     ,YW,YWO,WO)

      TIMES = 0.0
      IF (IGRAPH.EQ.1) THEN
       OPEN(4,FILE='GRAPH.OUT')
       WRITE(4,100)
100    FORMAT('TIME',6X,'X'6X,'O2',5X,'CO2',5X,'CO',5X,'TG',5X,'TS')
       WRITE(4,101)
101    FORMAT('MIN',6X,'CM')
      ENDIF
      WRITE(3,131)
131   FORMAT('PROFILES FOR OVERFEED FUEL BED')
      WRITE(3,132)
132   FORMAT(/,'OPERATING CONDITIONS:')
      WRITE(3,133)HT*100,WG(1),TG(1)
133   FORMAT(F8.2,' CM DEEP BED WITH',F7.5,' KG/M2 S AIR AT ',F5.0,'
K')
      IF (IFEED.EQ.1) THEN
       WRITE(3,*)'THE BED HEIGHT IS CONSTANT'
      ENDIF
      IF (IFEED.EQ.0) THEN
       WRITE(3,*)'THE BED HEIGHT DECREASES WITH TIME'
      ENDIF
      IF (IBUILD.EQ.0) THEN
       WRITE(3,*)'ASH FALLS THROUGH THE GRATE'
      ENDIF
      IF (IBUILD.EQ.1) THEN
       WRITE(3,*)'ASH BUILDS UP IN THE BED'
      ENDIF
      WRITE(3,134)100.*CARB,100.*ASH,RHOF(IB+IG)
134   FORMAT(' FUEL: ',F4.1,'% FIXED CARBON, ',F5.2,'% ASH, DENSITY '
     1F6.1,' KG/M3')
      WRITE(3,135)DIAMC(IG+IB)*100.0,VOIDC,SPHERC
135   FORMAT(' FUEL PARTICLES: ',F4.2,' CM DIAMETER,',F4.2,
     & ' VOID FRACTION, ',F3.2,' SPHERICITY')
      WRITE(3,136)DIAMA*100.0,VOIDA,SPHERA
136   FORMAT(' ASH PARTICLES: ',F4.2,' CM DIAMETER,',F4.2,
     &' VOID FRACTION, ',F3.2,' SPHERICITY')
      WRITE(3,163)AVV,EVV,HPYRO/1000.
163   FORMAT(/,'PYROLYSIS KINETICS: A = ',E10.2,' E = ',F9.1,'
KJ/KMOL,'
     &,' ENTHALPY OF PYROLYSIS ',F6.1,' KJ/KG FUEL')
      WRITE(3,164)COVOL,CO2VOL,(1.-COVOL-CO2VOL)
164   FORMAT('   PRODUCTS: CO ',F6.4,', CO2',F6.4,', TAR AND HC ',F6.4,
     &' KG/KG FUEL')
      IF (IGMOD.EQ.1) THEN
       WRITE(3,141)GRATE,GRTPD
141      FORMAT(/,'GRATE MODEL 1: PACKED BED ',F4.0,' MM THICK, PARTIC
     &          LE SIZE ',F5.2,' MM, CONDUCTIVITY ',F7.4,' W/MK')
```

```
      ENDIF
      IF (IGMOD.EQ.2) THEN
       WRITE(3,142)GRATE,GRTBAR,GRTSOL*100.
142      FORMAT(/,'GRATE MODEL 2: STEEL BARS ',F4.0,' MM DEEP X ',
     &       F4.0,' MM WIDE, SOLIDITY 'F5.1,'%')
      ENDIF
      IF (IRXN.EQ.1980.AND.ICOB.NE.0)THEN
         WRITE(*,*)'WD WITH EQUILIBRIUM'
       WRITE(3,144)
144      FORMAT('WESTBROOK AND DRYER KINETICS FOR CO OXIDATION WITH
     &          REVERSE RXN. FOR EQUILIBRIUM')
      ENDIF
      IF (IRXN.EQ.1980.AND.ICOB.EQ.0)THEN
         WRITE(*,*)'WD, ONE STEP (NO REVERSE)'
       WRITE(3,149)
149      FORMAT('WESTBROOK AND DRYER KINETICS FOR CO OXIDATION',
     &         ' WITHOUT REVERSE RXN.')
      ENDIF
      IF (IRXN.EQ.1970.AND.ICOB.EQ.0)THEN
         WRITE(*,*)'HF ONE STEP (NO REVERSE)'
       WRITE(3,145)
145      FORMAT('HOWARD AND FINE KINETICS FOR CO OXIDATION ',
     &          'WITHOUT REVERSE REACTION')
      ENDIF
      IF (IRXN.EQ.1970.AND.ICOB.NE.0)THEN
         WRITE(*,*)'HF WITH EQUILIBRIUM'
       WRITE(3,150)
150      FORMAT('HOWARD AND FINE KINETICS FOR CO OXIDATION ',
     &          'WITH REVERSE REACTION (EQUILIBRIUM)')
      ENDIF
      IF (IFIELD.EQ.0) THEN
       WRITE(3,161)
161    FORMAT('C OXIDATION CALCULATED FROM THE EFFECTIVENESS')
      ELSE
       WRITE(3,162)
162    FORMAT('C OXIDATION CALCULATED USING THE FIELD EQUATION')
      ENDIF
      WRITE(3,160)A1,E1
160   FORMAT('CO2 REDUCTION RATE COEFFICIENTS: A = ',E9.2,', E =
',F9.1)
      IF (IHTTR.EQ.1970)THEN
       WRITE(3,146)
146      FORMAT('BHATTACHARYA AND PEI HEAT TR. COEFFICIENT')
      ENDIF
      IF (IHTTR.EQ.1960)THEN
       WRITE(3,147)
147      FORMAT('YOSHIDA ET AL. HEAT TR. COEFFICIENT')
      ENDIF
      IF (IHTTR.EQ.1950)THEN
       WRITE(3,148)
148      FORMAT('CHU HEAT TR. COEFFICIENT')
      ENDIF
      WRITE(3,140)
140   FORMAT(/,'ALL GAS CONCENTRATIONS ON TAR-FREE BASIS, TAR IS G
TAR/G
     & GAS WITHOUT TAR')
```

```
*************************************************************************
*
*      RECURSION OF MAIN TIME LOOP
*
*************************************************************************
*
66     CONTINUE
       IF ((TIMES.GE.TLIMIT).AND.(IFLAG3.EQ.5)) THEN
        IFLAG = 4

        WRITE(*,138) WG(1),TG(1)
138     FORMAT(6X,F7.5,'KG/M2 S AIR AT ',F5.0,'K')
        AVGCGONE = TCGONE/IN
        WRITE(*,199) AVGCGONE*3600.0
199     FORMAT(6X,'AVERAGE BURNING RATE: ',F7.2,' KG/M2 HR ')

        CALL PRINT(3,TG,TS,WS,WC,AKAS,CGONE,VGONE,XB,RHOF,
     &                    YW,W)
          CALL ENERGY(TG,TS,WS,CPG,ERROR,RHOF,YW)
        WRITE(3,44) ERROR
        GO TO 111
       ENDIF

       IF (ITERNS.EQ.IEND) THEN
        WRITE(3,*) 'THE DAMN THING DNCV'
          GO TO 111
       ENDIF

       IF ((IFEED.EQ.0).AND.(ITERNS.EQ.1)) THEN
        CALL DIVIDE(HT,FE,XB,DXN,IGRID)
       ENDIF

       CALL WESTMAN(VOIDO)
       CALL BEDCOND(RHOF,W)
       CALL STOICH(TS)
       CALL GEE(TG,TSO,AMWG,DIFF,WO,RHOF(IG+IB),VOIDO,YWO)
       CALL DEE(WC,APHI,APHIO,VOIDO,XCO,HT,RHOF,RHOFO)

       IF ((ITERNS.EQ.1).OR.(ITIME.EQ.0).OR.(ITIME.EQ.1))THEN
       CALL GPROP(IHTTR,TG,TS,RE,CPG,AKG,AKAG,AKY,DEFF,H,DIFF)
       ENDIF
       CALL GFLUX(VOIDO,XB,HT)
       CALL SFLUX(3,WS,VOIDO,RHOSO,ISTOP,IFEED,XB,HT)
       CALL CFLUX(WS,WC,XB,HT,RHOF)
       IF (ISTOP.GT.0) THEN
          GO TO 111
       ENDIF

       IF ((ITERNS.EQ.1).OR.(ITIME.EQ.0).OR.(ITIME.EQ.1))THEN
          CALL COND(TG,TS,AKG,AKAS,RHOF,YW)
       ENDIF

       CALL PCONC(AKY)
       CALL TDMACN(TGO,VOIDO,DEFF,IRXN,RCO,RCOB,DXN,FE)
       CALL TDMATG(TG,TGI,TGO,TS,VOIDO,CPG,CPGO,AKAG,H,RCO,RCOB,DXN,FE)
       CALL TDMATS(TG,TS,TSI,TSO,VOIDO,RHOSO,WS,AKAS,H,DXN,FE,RHOF
     & ,RHOFO,YW,YWO)
```

```
      CALL TDMAYW(WC,YW,YWO,VOIDO,XCO,HT,W,YCHAR
     &                  ,RHOF,RHOFO)

      IF (IFEED.EQ.0) THEN
       CALL HEIGHT(HT,RHOB,RHOBO)
      ENDIF
      CALL STOCK(TG,TGI,TGO,TS,TSO,TSI,APHI,APHIO,VOIDO,RHOSO,
     &          XCO,CGONE,VGONE,DTEMP,HT,HTO,RHOB,RHOBO,RHOFO,W,RHOF,WO,
     &          YWO,YW,WC,WCO,CPG,CPGO)

*     NEED ANOTHER ITERATION
      IF (IFLAG.EQ.2) THEN
         ITERNS = ITERNS+1
         GO TO 66
      ENDIF

*     PROCEED TO THE NEXT TIMESTEP
      IF (IFLAG.EQ.3) THEN
       IN = IN+1
         TCGONE = TCGONE+CGONE+VGONE
*     FULL PRINTOUT EVERY ICNTN TIME STEPS
       IF (ICNT.EQ.ICNTN) THEN
          CALL PRINT(3,TG,TS,WS,WC,AKAS,CGONE,VGONE,XB,RHOF,
     &                    YW,W)
          IF (IGRAPH.EQ.1) THEN
             CALL GRAPHING(4,XB,AMWG,TG,TS)
          ENDIF

            CALL ENERGY(TG,TS,WS,CPG,ERROR,RHOF,YW)
          WRITE(3,44) ERROR
          WRITE(*,44) ERROR
            ICNT = 0
       ENDIF
       ITEST = INT(ICNT/5)*5-ICNT
       ICNT = ICNT+1
       IF (ITEST.EQ.0) THEN
          WRITE (*,170) TIMES,TG(20),TS(20),DTEMP/(IB+IG)/2.,ITERNS
       ENDIF

170      FORMAT(1X,'TIME ',F6.0,' S; TG20 ',F5.0,'  TS20 ',F5.0,
     &          '  DTEMP/IT ',F5.1,'  ITERNS',I3)
         ITIME = ITIME+1
       IF ((ABS(DTEMP).LE.2.0*2.*(IB+IG)).AND.(ITSTEP.LT.ITCUT)) THEN
          DT = DT*2.0
          ITSTEP = ITSTEP+1
       ENDIF
       TIMES = TIMES+DT
       ITERNS = 1
       IFLAG3 = 5
       GO TO 66
      ENDIF
*************************************************************************
*
*     END OF MAIN TIME LOOP
*
*************************************************************************
*
```

```
43     FORMAT(/,'TIME ELAPSED IS :',F10.1)
44     FORMAT(/,' ENERGY ERROR FROM STEADY STATE BALANCE IS:',
      &F8.1,'%')

111    STOP
       END

*************************************************************************

       SUBROUTINE READER(IRUN,ICONST,TG,TS,U,US,TIGNIT,ALAYER,HT,
      &                  IHTTR,IRXN,ITCUT,TLIMIT,IEND,IGRID,IGRAPH,
      &                  IFEED,IZONE)

*      READS IN ALL SYSTEM BOUNDARIES

       CHARACTER*72 TITLE
       PARAMETER (N=50)
       DIMENSION TG(N),TS(N)
       DIMENSION VOID(N),SLAB(N),SSB(N),SSBO(N),RHOS(N),G(N),DZETA(N)
       DIMENSION DIAMC(N),SSC(N),SSCO(N),XC(N)
       DIMENSION Y8O2(N),Y8CO2(N),Y8CO(N),Y8N2(N),Y8O2O(N),Y8CO2O(N)
       DIMENSION Y8COO(N),Y8N2O(N),Y8P(N),Y8PO(N)
       DIMENSION G1(N),G2(N),X(N),S(N)
       DIMENSION GV(N),RP(N),yrh2o(n)
       common/water/xh2o,rhow,yrh2o
       COMMON/DEVOL/GV,AVV,EVV,RP,COVOL,CO2VOL,HPYRO
       COMMON/BED/VOID,E,SLAB,SSB,SSBO,RHOS,G,DHTDT,DZETA
       COMMON/WCHAR/CARB,DIAMC,RHOC,VOIDC,SPHERC,SSC,SSCO,XC
       COMMON/ASH/ASH,DIAMA,RHOA,VOIDA,SPHERA,IBUILD
       COMMON/Y/Y8O2,Y8CO2,Y8CO,Y8N2,Y8O2O,Y8CO2O,Y8COO,Y8N2O,Y8P,Y8PO
       COMMON/INFO/WTN2,WTO2,WTCO2,WTCO,R,P,BETA,GAMMA,THI,WTP,TREF
       COMMON/STOIC/SCO2,SCO,S3,S2,DH1,DH2,DH3,DH4
       COMMON/GE/A,A1,ER,E1,ALPHA1,ALPHA2
       COMMON/PORE/IFIELD,IEFFECT,SSP,TAU,VOIDP
       COMMON/REACT/G1,G2,X,S,IREACT
       COMMON/RAD/TSG,TSB,TSW,HRG,HRB,HRW,F12B,BOLTZ,TCOAL
       COMMON/GRATE/GRATE,GRTSOL,GRTBAR,IGMOD,GRTRHO,GRTPD,GRTSPACE
       COMMON/TIME/IFLAG,ITIME,ITERNS,TURNS,IB,IG,ICOB,TIMES,DT

       REWIND IRUN
       REWIND ICONST
       READ(IRUN,99) TITLE
       READ(IRUN,*) IB,IG,TLIMIT,DT,ITCUT,IEND
       IT = IG+IB
       read(irun,99) title
       read(irun,*) xh2o,rhow,covol,co2vol
       write(*,*) xh2o
       READ(IRUN,99) TITLE
       READ(IRUN,*) DIAMC(IT),CARB,RHOC,VOIDC,SPHERC,E,TCOAL
       READ(IRUN,99) TITLE
       READ(IRUN,*) DIAMA,ASH,RHOA,VOIDA,SPHERA
       READ(IRUN,99) TITLE
       READ(IRUN,*) HT,U,P
       READ(IRUN,99) TITLE
       READ(IRUN,*) A1,E1,A,ER
       READ(IRUN,99) TITLE
```

```
      READ(IRUN,*) IREACT,IHTTR,IRXN,ICOB,IBUILD,IFEED
      READ(IRUN,99) TITLE
      READ(IRUN,*) TS(1),TG(1),TG(IT),TS(IT),TIGNIT,ALAYER,IZONE
      READ(IRUN,99) TITLE
      READ(IRUN,*) IGRAPH,IGRID
      READ(IRUN,99) TITLE
      READ(IRUN,*) IFIELD,IEFFECT,SSP,TAU,VOIDP
      READ(IRUN,99) TITLE
      READ(IRUN,*) AVV,EVV,HPYRO
      READ(ICONST,99) TITLE
      READ(ICONST,*) R,BOLTZ,WTN2,WTO2,WTCO2,WTCO,WTP,wth2o
      READ(ICONST,99) TITLE
      READ(ICONST,*) BETA,GAMMA,THI,ALPHA1,ALPHA2
      READ(ICONST,99) TITLE
      READ(ICONST,*) SCO,SCO2,S3,S2,DH1,DH2,DH3,DH4
      READ(ICONST,99) TITLE
      READ(ICONST,*) US,G(1),G(IT)
      READ(ICONST,99) TITLE

READ(ICONST,*)Y8O2(1),Y8CO(1),Y8CO2(1),Y8O2(IT),Y8CO(IT),Y8CO2(IT)
      READ(ICONST,99) TITLE
      READ(ICONST,*) IGMOD,GRATE,GRTPD,GRTSPACE,GRTBAR,GRTRHO
      READ(ICONST,99) TITLE
      READ(ICONST,*) Y8P(1),Y8P(IT)
99    FORMAT(A72)
      Y8N2(1)=1.-Y8O2(1)-Y8CO2(1)-Y8CO(1)-Y8P(1)
      Y8N2(IT)=1.-Y8O2(IT)-Y8CO2(IT)-Y8CO(IT)-Y8P(IT)
      RETURN
      END

*****************************************************************************

      SUBROUTINE DIVIDE(HT,FE,XB,DXN,IGRID)

*     GENERATES THE GRID

      PARAMETER (N=50)
      DIMENSION FE(N),XB(N),DXN(N)
      DIMENSION VOID(N),SLAB(N),SSB(N),SSBO(N),RHOS(N),G(N),DZETA(N)
      COMMON/BED/VOID,E,SLAB,SSB,SSBO,RHOS,G,DHTDT,DZETA
      COMMON/GRATE/GRATE,GRTSOL,GRTBAR,IGMOD,GRTRHO,GRTPD,GRTSPACE
      COMMON/TIME/IFLAG,ITIME,ITERNS,TURNS,IB,IG,ICOB,TIMES,DT

*****************************************************************************
*     COORDINATE SYSTEM: ORIGIN IS AT TOP OF GRATE. NODES 1 TO IG ARE
*     GRATE NODES, IG+1 TO IB+IG ARE THE BED ITSELF. THE COORDINATE
*     XB LOCATES THE NORTH (TOP) INTERFACE OF THE CELL. SLAB IS THE
*     CELL THICKNESS AND DXN THE DISTANCE FROM NODE I TO NODE I+1. THE
*     TOP OF THE BED IS AT THE NORTH FACE OF CELL (IG+IB-1). NODES ARE
*     CENTRED IN THE CELLS. AT PRINTOUT, COORDS ARE TRANSFORMED SO THAT
*     THE X COORDINATE BECOMES THE NODE LOCATION.
*****************************************************************************

*     EVENLY SPACED GRID POINTS
      IF (IGRID.EQ.0) THEN
       XB(IG) = 0.0
       SLAB(IG) = GRATE/(IG-1.0)*0.001
```

```
      DO 20 I=IG+1,IG+IB
        SLAB(I) = HT/(IB-1.0)
        XB(I) = SLAB(I)+XB(I-1)
20    CONTINUE
      DO 21 I=IG-1,1,-1
        SLAB(I) = GRATE/(IG-1.0)*0.001
        XB(I) = XB(I+1)-SLAB(I)
21    CONTINUE

*     EXPONENTIALLY SPACED GRID POINTS
      ELSE
       DEL1 = LOG(HT+1.0)/(IB-1)
       DEL2 = LOG(GRATE+1.0)/(IG-1)
       DO 10 I=IG+1,IB+IG
          XB(I) = (EXP((I-IG)*DEL1)-1.0)
10     CONTINUE
       DO 11 I=1,IG
          XB(IG-I+1) = -(EXP((I-1)*DEL2)-1.0)*0.001
11     CONTINUE
       DO 12 I=1,IB+IG
          IF (I.EQ.1) THEN
             SLAB(I) = ABS(XB(I+1)-XB(I))
          ELSE
             SLAB(I) = ABS(XB(I)-XB(I-1))
          ENDIF
12     CONTINUE
      ENDIF

      DO 13 I=1,IB+IG-1
         DXN(I) = ABS(SLAB(I)+SLAB(I+1))/2.0
       FE(I) = 0.5*SLAB(I)/DXN(I)
       IF (I.GT.IG) THEN
          DZETA(I) = SLAB(I)/HT
       ELSE
          DZETA(I) = 0.0
       ENDIF
13    CONTINUE
      RETURN
      END

*****************************************************************************

      SUBROUTINE SETUP(TG,TGO,TS,TSO,U,US,WS,WC,TIGNIT,ALAYER,HT,APHIO,
     &         VOIDO,XCO,RHOSO,IFEED,RHOBO,IZONE,XB,APHI,W,RHOF,RHOFO
     &     ,YW,YWO,WO)

*     CALCULATES THE INITIAL PROFILES AND BOUNDARIES

      PARAMETER (N=50)
      PARAMETER (PI=3.141592654)
      DIMENSION TG(N),TGO(N),TS(N),TSO(N)
      DIMENSION WS(N),WC(N),APHIO(N),VOIDO(N),XCO(N),RHOSO(N),APHI(N)
      DIMENSION VOID(N),SLAB(N),SSB(N),SSBO(N),RHOS(N),G(N),DZETA(N)
      DIMENSION DIAMC(N),SSC(N),SSCO(N),XC(N)
      DIMENSION WG(N),RHOG(N),RHOGO(N)
      DIMENSION Y8O2(N),Y8CO2(N),Y8CO(N),Y8N2(N),Y8O2O(N),Y8CO2O(N)
      DIMENSION Y8COO(N),Y8N2O(N),Y8P(N),Y8PO(N)
```

```
      DIMENSION YRO2(N),YRCO2(N),YRCO(N),YRN2(N),YRP(N)
      DIMENSION G1(N),G2(N),X(N),S(N)
      DIMENSION SSA(N),XB(N)
      DIMENSION GV(N),RP(N),W(N),WO(N)
      DIMENSION RHOF(N),RHOFO(N)
      DIMENSION YWO(N),YW(N)
      COMMON/DEVOL/GV,AVV,EVV,RP,COVOL,CO2VOL,HPYRO
      COMMON/BED/VOID,E,SLAB,SSB,SSBO,RHOS,G,DHTDT,DZETA
      COMMON/WCHAR/CARB,DIAMC,RHOC,VOIDC,SPHERC,SSC,SSCO,XC
      COMMON/ASH/ASH,DIAMA,RHOA,VOIDA,SPHERA,IBUILD
      COMMON/GAS/WG,RHOG,RHOGO
      COMMON/Y/Y8O2,Y8CO2,Y8CO,Y8N2,Y8O2O,Y8CO2O,Y8COO,Y8N2O,Y8P,Y8PO
      COMMON/YR/YRO2,YRCO2,YRCO,YRN2,YRP
      COMMON/REACT/G1,G2,X,S,IREACT
      COMMON/RAD/TSG,TSB,TSW,HRG,HRB,HRW,F12B,BOLTZ,TCOAL
      COMMON/GRATE/GRATE,GRTSOL,GRTBAR,IGMOD,GRTRHO,GRTPD,GRTSPACE
      COMMON/TIME/IFLAG,ITIME,ITERNS,TURNS,IB,IG,ICOB,TIMES,DT

      IT = IB+IG

*  ALLOWS THE PROGRAM TO BE RUN WITH NO VOLATILES
      IF(CARB.EQ.0)THEN
        YW(IT) =1E-38
        W(IT) = 1E-38
        RHOF(IT) = RHOC
      ELSE
        YW(IT) = 1.0
        W(IT) = 1.0
        RHOF(IT) = RHOC/CARB
      END IF

      DO 10 I=2,IT-1
       RHOF(I) = RHOF(IT)
       RHOFO(I) = RHOF(I)
       W(I)=W(IT)
* SETS INITIAL TEMPERATURE VALUES
       TS(I) = TS(IT)
         TG(I) = TG(1)
         Y8O2(I) = Y8O2(1)
         Y8CO2(I)= Y8CO2(1)
       Y8CO(I) = Y8CO(1)
         Y8P(I) = Y8P(1)
         Y8N2(I)=Y8N2(1)
*  ADD YW INITIALIZATION
       IF (I.GE.IG+1) THEN
         YW(I) = YW(IT)
       ELSE
         YW(I) = 0
       END IF
       YWO(I) = YW(I)
       WO(I) =YWO(I)*CARB/(1-YWO(I)*(1-CARB))
10     CONTINUE


*      SETS UP TEMPERATURES IN THE IGNITION ZONE
*      IGNITION AT THE BOTTOM OF THE BED
       IF (IZONE.EQ.0) THEN
```

```
      DO 9 I=IG+1,IT
         ZONE = XB(I)
         IF (ZONE.LT.ALAYER) THEN
            IIGNIT = I
         ENDIF
9     CONTINUE
      DO 8 I=IG+1,IIGNIT
         TS(I) = TIGNIT
8     CONTINUE
      ENDIF
*     IGNITION AT THE TOP OF THE BED
      IF (IZONE.EQ.1) THEN
      DO 11 I=IT-1,IG+1,-1
         ZONE = HT-XB(I)
         IF (ZONE.LT.ALAYER) THEN
            IIGNIT = I
         ENDIF
11    CONTINUE
      DO 12 I=IT-1,IIGNIT,-1
         TS(I) = TIGNIT
12    CONTINUE
      ENDIF
*     IGNITION BY RADIATION
      IF (IZONE.EQ.2) THEN
      TS(IT) = TIGNIT
      ENDIF

      DO 13 I=1,IT
         RHOG(I) = DENS(TG(I),I)
         RHOGO(I) = RHOG(I)
      G1(I) = G(IT)
         G2(I) = G(IT)
         YRO2(I) = Y8O2(I)
         YRCO2(I) = Y8CO2(I)
      YRCO(I) = Y8CO(I)
      YRP(I) = Y8P(I)

      YRN2(I) = 1.0-YRO2(I)-YRCO2(I)-YRCO(I)-YRP(I)
         TGO(I) = TG(I)
         TSO(I) = TS(I)
         Y8O2O(I) = Y8O2(I)
         Y8CO2O(I) = Y8CO2(I)
      Y8COO(I) = Y8CO(I)
      Y8PO(I) = Y8P(I)
         IF ((I.LE.IG).AND.(IBUILD.EQ.1)) THEN
          WS(I) = 0.0
      ELSE
         WS(I) = US*RHOF(I)
         WC(I) = US*RHOF(I)
      ENDIF
      WG(I) = U*RHOG(I)
13    CONTINUE

      IF (IFEED.EQ.0) THEN
      WS(IT) = 0.0
      ENDIF
```

```
      RHOBO = 0.0
      DO 14 I=IG+1,IT-1
       DIAMC(I) = DIAMC(IT)
       APHI(I) = 6.0/(PI*RHOF(I)*DIAMC(IT)**3.0)
       APHIO(I) = APHI(I)
         VOID(I) = VOIDC
         VOIDO(I) = VOID(I)
       XC(I) = 1.0/(1.0+RHOF(I)/RHOA*ASH
     &              *(DIAMC(IT)**3.0/DIAMC(I)**3.0-1.0))
         XCO(I) = XC(I)
       RHOS(I) = XC(I)*RHOF(I)+(1.0-XC(I))*RHOA
       RHOSO(I) = RHOS(I)
       RHOBO = RHOBO+RHOS(I)*(1.0-VOID(I))*DZETA(I)
       SSC(I) = 6.0/(DIAMC(I)*SPHERC)*XC(I)*(1.0-VOID(I))
         SSCO(I) = SSC(I)
         SSA(I) = 6.0/(DIAMA*SPHERA)*(1.0-XC(I))*(1.0-VOID(I))
         SSB(I) = SSC(I)+SSA(I)
       SSBO(I) = SSB(I)
14    CONTINUE

      DHTDT = 0.0
      RHOS(IT) = RHOF(I-1)
      VOID(IT) = VOIDC
      SSB(IT) = SSB(IT-1)
      SSC(IT) = SSC(IT-1)
      XC(IT) = XC(IT-1)

      IF (IGMOD.EQ.1) THEN
         DO 15 I = 1,IG
            VOID(I) = VOIDA
            DIAMC(I) = GRTPD/1000.0
            SSB(I) = 6.0*(1.0-VOID(I))/DIAMC(I)/SPHERA
15       CONTINUE
      ENDIF

      IF (IGMOD.EQ.2) THEN
         GRTSOL = GRTBAR/(GRTSPACE+GRTBAR)
         DO 16 I = 1,IG
            SSB(I) = 2.0*GRTSOL/(GRTBAR/1000.0)
            SSBO(I) = SSB(I)
            VOID(I) = 1.0-GRTSOL
            VOIDO(I) = VOID(I)
            DIAMC(I) = 6.0*(1.0-VOID(I))/SSB(I)
            RHOS(I) = GRTRHO
            RHOSO(I) = RHOS(I)
16       CONTINUE
         SSB(2) = SSB(2)+GRTSOL/SLAB(2)
         SSBO(2) = SSB(2)
      ENDIF

*     RADIATION
*     GRATE TO ASHPAN
      TSG = (TS(1)+TS(2))/2.0
      HRG = BOLTZ*(TS(1)**2.0+TSG**2.0)*(TS(1)+TSG)*GRTSOL
*     BED TO ASHPAN
      TSB = (TS(IG)+TS(IG+1))/2.0
      RH = GRATE/GRTSPACE
```

```
      F12B = SQRT(1.0+RH**2.0)-RH
      F12B = 1.0/(2.0/(1.0+F12B)+1.0/E-1.0)
      HRB = BOLTZ*F12B*(TSB**2.0+TS(1)**2.0)*(TSB+TS(1))
*     BED TO WALLS
      TSW = (TS(IT-1)+TS(IT))/2.0
      HRW = BOLTZ*F12W(HT)*(TS(IT)**2.0+TSW**2.0)*(TS(IT)+TSW)
*     volatiles to bed from flames
      RETURN
      END

*************************************************************************

      SUBROUTINE WESTMAN(VOIDO)

*     CALCULATES THE BED VOID FRACTION USING THE WESTMAN EQUATION

      PARAMETER (N=50)
      DIMENSION VOID(N),SLAB(N),SSB(N),SSBO(N),RHOS(N),G(N),DZETA(N)
      DIMENSION DIAMC(N),SSC(N),SSCO(N),XC(N)
      COMMON/BED/VOID,E,SLAB,SSB,SSBO,RHOS,G,DHTDT,DZETA
      COMMON/WCHAR/CARB,DIAMC,RHOC,VOIDC,SPHERC,SSC,SSCO,XC
      COMMON/ASH/ASH,DIAMA,RHOA,VOIDA,SPHERA,IBUILD
      COMMON/TIME/IFLAG,ITIME,ITERNS,TURNS,IB,IG,ICOB,TIMES,DT

      DO 10 I=IG+1,IG+IB-1
       DIAML = DIAMC(I)
       DIAMS = DIAMA
       VOIDL = VOIDC
       VOIDS = VOIDA
       XL = XC(I)
       RATIO = DIAMS/DIAML
         RSTR = (1.0/VOIDL-1.0)*RATIO**3.0/(1.0-VOIDS)
         AK = -0.63
         GWEST = RSTR**AK+(1.0-VOIDL**(-AK))

*     TEST FOR PHYSICALLY REASONABLE SOLUTION
       SVL = 1.0/(1.0-VOIDL)
       SVS = 1.0/(1.0-VOIDS)
       VMIN = SVL*SVS/(SVL+SVS-1.0)
         XMIN = (1.0-VOIDL)/(1.0-VOIDL*VOIDS)
       VTEST1 = SVS+(VMIN-SVS)*XL/XMIN
         VTEST1 = 0.995*VTEST1
       VTEST2 = VMIN+(SVL-VMIN)*(XL-XMIN)/(1.0-XMIN)
         VTEST2 = 0.995*VTEST2

         CALL NEWTON(I,GWEST,VOIDO,V)
         IF ((V.LT.VTEST1).OR.(V.LT.VTEST2)) THEN
            VOIDO = AMAX1(VOIDC,VOIDA)
            CALL NEWTON(I,GWEST,VOIDO,V)
            PRINT*,'NEWTON CALLED AGAIN - V =',V
         ENDIF
         IF ((V.LT.VTEST1).OR.(V.LT.VTEST2)) THEN
            PRINT*,'UNREASONABLE VOID FRACTION'
            STOP
         ENDIF
         VOID(I) = 1.0-1.0/V
10    CONTINUE
```

```
      RETURN
      END

*****************************************************************************
*

      SUBROUTINE NEWTON(I,GWEST,VOIDO,V)

*     SOLVES THE WESTMAN EQUATION USING THE NEWTON-RAPHSON METHOD

      PARAMETER (N=50)
      DIMENSION VOIDO(N)
      DIMENSION DIAMC(N),SSC(N),SSCO(N),XC(N)
      COMMON/WCHAR/CARB,DIAMC,RHOC,VOIDC,SPHERC,SSC,SSCO,XC
      COMMON/ASH/ASH,DIAMA,RHOA,VOIDA,SPHERA,IBUILD

      J = 0
      JMAX = 100
      TOL = 1.0E-6
      VOLD = 1.0/(1.0-VOIDO(I))
1     CONTINUE
      IF (J.LE.JMAX) THEN
         VNEW = VOLD-F(VOLD,I,GWEST)/DF(VOLD,I,GWEST)
         J = J+1
         IF (DABS(VNEW-VOLD).LT.TOL) THEN
            V = (VNEW+VOLD)*0.5
            RETURN
         ELSE
            VOLD = VNEW
         ENDIF
         GO TO 1
      ENDIF
      IF (J.GT.JMAX) THEN
         PRINT*,'MAXIMUM NUMBER OF ITERATIONS EXCEEDED IN NEWTON'
         STOP
      ENDIF
      RETURN
      END

*****************************************************************************

      SUBROUTINE BEDCOND(RHOF,W)

*     CALCULATES THE BED CONDITIONS

      PARAMETER (N=50)
      DIMENSION VOID(N),SLAB(N),SSB(N),SSBO(N),RHOS(N),G(N),DZETA(N)
      DIMENSION DIAMC(N),SSC(N),SSCO(N),XC(N)
      DIMENSION SSA(N)
      DIMENSION RHOF(N),W(N)
      COMMON/BED/VOID,E,SLAB,SSB,SSBO,RHOS,G,DHTDT,DZETA
      COMMON/WCHAR/CARB,DIAMC,RHOC,VOIDC,SPHERC,SSC,SSCO,XC
      COMMON/ASH/ASH,DIAMA,RHOA,VOIDA,SPHERA,IBUILD
      COMMON/TIME/IFLAG,ITIME,ITERNS,TURNS,IB,IG,ICOB,TIMES,DT

      IF (CARB.NE.0) THEN
       DO 16 I=IG+1,IG+IB-1
```

```
                RHOF(I)=RHOF(IB+IG) * ( W(I)+carb* (1-W(I)) )

16      CONTINUE
        END IF

        DO 10 I=IG+1,IG+IB-1
           XC(I) = 1.0/(1.0+RHOF(IG+IB)/RHOA*ASH
     &              * (DIAMC(IB+IG)**3.0/DIAMC(I)**3.0-1.0))
          RHOS(I) = XC(I)*RHOF(I)+(1.0-XC(I))*RHOA
           SSC(I) = 6.0/(DIAMC(I)*SPHERC)*XC(I)*(1.0-VOID(I))
           SSA(I) = 6.0/(DIAMA*SPHERA)*(1.0-XC(I))*(1.0-VOID(I))
          SSB(I) = SSC(I)+SSA(I)
10      CONTINUE
        RETURN
        END

*************************************************************************

        SUBROUTINE STOICH(TS)

*       CALCULATES THE CO/CO2 RATIO AND MASS C BURNED PER CO+CO2 PRODUCT
*       from char combustion

        PARAMETER (N=50)
        DIMENSION TS(N)
        DIMENSION G1(N),G2(N),X(N),S(N)
        COMMON/INFO/WTN2,WTO2,WTCO2,WTCO,R,P,BETA,GAMMA,THI,WTP,TREF
        COMMON/STOIC/SCO2,SCO,S3,S2,DH1,DH2,DH3,DH4
        COMMON/REACT/G1,G2,X,S,IREACT
        COMMON/TIME/IFLAG,ITIME,ITERNS,TURNS,IB,IG,ICOB,TIMES,DT

        S(1) = 0.0
        X(1) = 0.0
        DO 10 I=2,IG+IB-1
         X(I) = 2500.0*EXP(-6240.0/TS(I))*WTCO/WTCO2
         X(I) = 1.0/(1.0+X(I))
         S(I) = (1.0+SCO2)*(1.0+SCO)
           S(I) = S(I)/(X(I)*(1.0+SCO)+(1.0-X(I))*(1.0+SCO2))
           S(I) = S(I)-1.0
10      CONTINUE
        S(IB+IG) = 0.0
        X(IB+IG) = 0.0
        RETURN
        END

*************************************************************************

        SUBROUTINE GEE(TG,TSO,AMWG,DIFF,WO,RHOFW,VOIDO,YWO)

*       CALCULATES THE CARBON CONSUMPTION RATES

        PARAMETER (N=50)
        DIMENSION TG(N),TSO(N),AMWG(N),DIFF(N,4)
        DIMENSION VOID(N),SLAB(N),SSB(N),SSBO(N),RHOS(N),G(N),DZETA(N)
        DIMENSION DIAMC(N),SSC(N),SSCO(N),XC(N)
        DIMENSION WG(N),RHOG(N),RHOGO(N)
        DIMENSION YRO2(N),YRCO2(N),YRCO(N),YRN2(N),YRP(N)
```

```
      DIMENSION G1(N),G2(N),X(N),S(N)
      DIMENSION GV(N),RP(N),WO(N),YWO(N)
      DIMENSION VOIDO(N)
      COMMON/DEVOL/GV,AVV,EVV,RP,COVOL,CO2VOL,HPYRO
      COMMON/BED/VOID,E,SLAB,SSB,SSBO,RHOS,G,DHTDT,DZETA
      COMMON/WCHAR/CARB,DIAMC,RHOC,VOIDC,SPHERC,SSC,SSCO,XC
      COMMON/ASH/ASH,DIAMA,RHOA,VOIDA,SPHERA,IBUILD
      COMMON/GAS/WG,RHOG,RHOGO
      COMMON/YR/YRO2,YRCO2,YRCO,YRN2,YRP
      COMMON/INFO/WTN2,WTO2,WTCO2,WTCO,R,P,BETA,GAMMA,THI,WTP,TREF
      COMMON/GE/A,A1,ER,E1,ALPHA1,ALPHA2
      COMMON/PORE/IFIELD,IEFFECT,SSP,TAU,VOIDP
      COMMON/REACT/G1,G2,X,S,IREACT
      COMMON/TIME/IFLAG,ITIME,ITERNS,TURNS,IB,IG,ICOB,TIMES,DT

      G1(1) = 0.0
      G2(1) = 0.0
      DO 10 I=2,IG
         G(I) = 0.0
         G1(I) = 0.0
         G2(I)= 0.0
10    CONTINUE
      DO 11 I=1,IB+IG-1
         AMWG(I) = RHOG(I)*R*TG(I)/P
11    CONTINUE
      DO 12 I=IG+1,IB+IG-1
*     SET PARTIAL PRESSURES OF GASES IN THE BED SLABS (IN KPA)
         IF (IREACT.GT.0) THEN
          PO2 = P*YRO2(I)*AMWG(I)/WTO2

          PCO = P*YRCO(I)*AMWG(I)/WTCO
          PCO2 = P*YRCO2(I)*AMWG(I)/WTCO2

*     CHAR OXIDATION RXN
          IF (IFIELD.EQ.0) THEN
             AKIP = 678.0*EXP(-179400.0/(R*TSO(I)))
             AKIM = AKIP*R*TSO(I)/12.0
             IF (TIMES.EQ.0.0) THEN
              DIFF(I,1) = 0.000247
             ENDIF
             DEFFP = DIFF(I,1)*VOIDP/TAU
             THIELE = DIAMC(I)/2.0*SQRT(AKIM*SSP/DEFFP)
             EFFECT = 3.0/(THIELE**2.0)
     &                   *(THIELE*(TANH(THIELE))**(-1.0)-1.0)
             AKP = DIAMC(I)/6.0*EFFECT*SSP*AKIP
             G1(I) = AKP*PO2
          ELSE
             G1(I) = A*EXP(-ER/TSO(I))*PO2
          ENDIF
          G2(I) = 0.0

*     CHAR REDUCTION RXN
          IF (IREACT.GT.1) THEN
             AK1 = A1*EXP(-E1/(R*TSO(I)))
             IF (IEFFECT.EQ.0) THEN
              G2(I) = AK1*PCO2
             ELSE
```

```
                AKIP = AK1
                AKIM = AKIP*R*TSO(I)/12.0
                IF (TIMES.EQ.0.0) THEN
                   DIFF(I,2) = 0.000199
                ENDIF
                DEFFP = DIFF(I,2)*VOIDP/TAU
                    THIELE = DIAMC(I)/2.0*SQRT(AKIM*SSP/DEFFP)
                    EFFECT = 3.0/(THIELE**2.0)
     &                    *(THIELE*(TANH(THIELE))**(-1.0)-1.0)
                AKP = DIAMC(I)/6.0*EFFECT*SSP*AKIP
                G2(I) = AKP*PCO2
               ENDIF
             ENDIF
             IF (DIAMC(I).LT.DIAMC(IG+IB)/1000.0) THEN
                G1(I) = 0.0
                G2(I) = 0.0
             ENDIF
             G(I) = G1(I)+G2(I)
            ELSE
             G1(I) = 0.0
             G2(I) = 0.0
             G(I) = G1(I)+G2(I)
           ENDIF
12         CONTINUE

C      TRANSITION FROM DEVOL'N TO CHAR COMBUSTION
C      GSCALE = 0 if less than 2% is pyrolyzed, then ramped up to 1
C      between 2% and 5% pyrolyzed
        GSCALEUP=0.98
        GSCALEDN=0.95
        GSLOPE=1./(GSCALEUP-GSCALEDN)

       DO 155 I=IG+1,IG+IB-1
        IF(YWO(I).GE.GSCALEUP)THEN
            GSCALE=0.
        ELSE
            IF(YWO(I).LT.GSCALEDN)THEN
            GSCALE=1.
            ELSE
            GSCALE=1.-GSLOPE*(YWO(I)-GSCALEDN)
        ENDIF
        ENDIF
        G(I)=GSCALE*G(I)
        G1(I)=GSCALE*G1(I)
        G2(I)=GSCALE*G2(I)
155    CONTINUE

*******CALCULATES THE FUEL CONSUMPTION DUE TO THE DEVOLATILIZATION
ASSUMING
*      IT OCCURS ONLY AT THE SURFACE OF THE PARTICLE
        DO 15 I=IG+1,IG+IB-1
         IT=IG+IB
         RP(I) = -EVV/(R*TSO(I))
         RP(I) = AVV * exp(RP(I))

*   USE VOID AND W FROM LAST TIME STEP, WOOD DENSITY FROM FEED
         RP(I) = (1.-CARB)*(1.-VOIDO(I))*RHOFW*RP(I)*WO(I)
```

```
       GV(I) = 1./SSCO(I) * RP(I)
15     CONTINUE

*      BACK TO PREVIOUS MASS CALCULATIONS
       G1(IB+IG) = 0.0
       G2(IB+IG) = 0.0
       RETURN
       END

*****************************************************************************

       SUBROUTINE DEE(WC,APHI,APHIO,VOIDO,XCO,HT,RHOF,RHOFO)

*      CALCULATES THE CHAR PARTICLE DIAMETER

       PARAMETER (N=50)
       PARAMETER (PI=3.141592654)
       DIMENSION VOID(N),SLAB(N),SSB(N),SSBO(N),RHOS(N),G(N),DZETA(N)
       DIMENSION DIAMC(N),SSC(N),SSCO(N),XC(N)
       DIMENSION PD(N),QD(N),AMASSC(N)
       DIMENSION SCP(N),RHOF(N),RHOFO(N)
       DIMENSION WC(N),APHIO(N),VOIDO(N),XCO(N),APHI(N)
       dimension GV(N),RP(N)
       COMMON/DEVOL/GV,AVV,EVV,RP,COVOL,CO2VOL,HPYRO
       COMMON/BED/VOID,E,SLAB,SSB,SSBO,RHOS,G,DHTDT,DZETA
       COMMON/WCHAR/CARB,DIAMC,RHOC,VOIDC,SPHERC,SSC,SSCO,XC
       COMMON/DEBUB/AMASSC,ALEFF,SCP
       COMMON/ASH/ASH,DIAMA,RHOA,VOIDA,SPHERA,IBUILD
       COMMON/TIME/IFLAG,ITIME,ITERNS,TURNS,IB,IG,ICOB,TIMES,DT

       AD = 1.0
       BD = 0.0
       CD = 0.0
       DD = 6.0/(PI*RHOF(IB+IG)*DIAMC(IB+IG)**3.0)
       PD(IB+IG) = BD/AD
       QD(IB+IG) = DD/AD

       DO 10 I=IB+IG-1,IG+1,-1
        AOD = RHOF(I)*XC(I)*(1.0-VOID(I))*SLAB(I)
        AD = AOD+AMAX1(WC(I)*DT,0.0)+AMAX1(-WC(I-1)*DT,0.0)
        BD = AMAX1(-WC(I)*DT,0.0)
        CD = AMAX1(WC(I-1)*DT,0.0)
        DD = RHOFO(I)*XCO(I)*(1.0-VOIDO(I))*APHIO(I)
      &           * DZETA(I)*(HT-DHTDT*DT)
        PD(I) = CD/(AD-BD*PD(I+1))
        QD(I) = (BD*QD(I+1)+DD)/(AD-BD*PD(I+1))

10     CONTINUE

       APHI(IG+1) = QD(IG+1)
       AMASSC(IG+1) = 1.0/APHI(IG+1)
       DIAMC(IG+1) = (6.0*AMASSC(IG+1)/(RHOF(IG+1)*PI))**(1.0/3.0)

       DO 11 I=IG+2,IG+IB-1
        APHI(I) = PD(I)*APHI(I-1)+QD(I)
        AMASSC(I) = 1.0/APHI(I)
```

```
       DIAMC(I) = (6.0*AMASSC(I)/(RHOF(I)*PI))**(1.0/3.0)
11     CONTINUE
       RETURN
       END

*****************************************************************************

       SUBROUTINE GPROP(IHTTR,TG,TS,RE,CPG,AKG,AKAG,AKY,DEFF,H,DIFF)

*      CALCULATES THE GAS PROPERTIES

       PARAMETER (N=50)
       DIMENSION TG(N),TS(N),RE(N),CPG(N),AKG(N),AKAG(N),AKY(N,4)
       DIMENSION DEFF(N,4),H(N)
       DIMENSION VOID(N),SLAB(N),SSB(N),SSBO(N),RHOS(N),G(N),DZETA(N)
       DIMENSION DIAMC(N),SSC(N),SSCO(N),XC(N)
       DIMENSION WG(N),RHOG(N),RHOGO(N)
       DIMENSION Y8O2(N),Y8CO2(N),Y8CO(N),Y8N2(N),Y8O2O(N),Y8CO2O(N)
       DIMENSION Y8COO(N),Y8N2O(N),Y8P(N),Y8PO(N)
       DIMENSION YRO2(N),YRCO2(N),YRCO(N),YRN2(N),YRP(N)
       DIMENSION CPGREG(N)
       DIMENSION EKAI(4),SIGMI(4),WT(4),DIFF(N,4),SCHM(4),AMWG(N)
       DIMENSION GV(N),RP(N),BM(N),CORRKY(N)
       COMMON/DEVOL/GV,AVV,EVV,RP,COVOL,CO2VOL,HPYRO
       COMMON/BED/VOID,E,SLAB,SSB,SSBO,RHOS,G,DHTDT,DZETA
       COMMON/WCHAR/CARB,DIAMC,RHOC,VOIDC,SPHERC,SSC,SSCO,XC
       COMMON/ASH/ASH,DIAMA,RHOA,VOIDA,SPHERA,IBUILD
       COMMON/Y/Y8O2,Y8CO2,Y8CO,Y8N2,Y8O2O,Y8CO2O,Y8COO,Y8N2O,Y8P,Y8PO
       COMMON/GAS/WG,RHOG,RHOGO
       COMMON/YR/YRO2,YRCO2,YRCO,YRN2,YRP
       COMMON/INFO/WTN2,WTO2,WTCO2,WTCO,R,P,BETA,GAMMA,THI,WTP,TREF
       COMMON/STOIC/SCO2,SCO,S3,S2,DH1,DH2,DH3,DH4
       COMMON/GRATE/GRATE,GRTSOL,GRTBAR,IGMOD,GRTRHO,GRTPD,GRTSPACE
       COMMON/TIME/IFLAG,ITIME,ITERNS,TURNS,IB,IG,ICOB,TIMES,DT
       COMMON/EXTRA/CPGREG

       AV = 1.16145
       BV = 0.14874
       CV = 0.52487
       DV = 0.77320
       EV = 2.16178
       FV = 2.43787

       AD = 1.06036
       BD = 0.15610
       CD = 0.19300
       DD = 0.47635
       ED = 1.03587
       FD = 1.52996
       GD = 1.76474
       HD = 3.89411

       SIGN2 = 3.798
       EKAN2 = 71.4
       SIGMI(1) = 3.467
       EKAI(1) = 106.7
       WT(1) = WTO2
```

```
      SIGMI(2) = 3.941
      EKAI(2) = 195.2
      WT(2) = WTCO2
      SIGMI(3) = 3.690
      EKAI(3) = 91.7
      WT(3) = WTCO
C TAR PROPERTIES ASSUMED EQUIVALENT TO THOSE FOR LEVOGLUCOSAN
      SIGMI(4) = 5.043
      EKAI(4) = 1087.
      WT(4) = WTP

      DO 10 I=1,IB+IG
       IF (I.LE.IG) THEN
          DIAM = DIAMC(I)
       ELSE
          DIAM = 1.0/(XC(I)/DIAMC(I)+(1.0-XC(I))/DIAMA)
       ENDIF


*      CALCULATION OF THERMAL CONDUCTIVITY
       TASTA = TG(I)/EKAN2
       OMEGN2 = AV/TASTA**BV+CV/EXP(DV*TASTA)+EV/EXP(FV*TASTA)
       AMU = 2.6693E-06*SQRT(WTN2*TG(I))/((SIGN2**2.0)*OMEGN2)
         CPG(I) = CPGBAR(TG(I),I)
         AMWG(I) = RHOG(I)*TG(I)*R/P
       AKG(I) = (CPGREG(I)+(5.0/4.0)*(R/AMWG(I)*1000.0))*AMU

*      CALCULATION OF COMPONENT DIFFUSIVITIES (M2/S)
          PATM = P/101.3
       DO 11 J=1,4
            SNI = (SIGN2+SIGMI(J))/2.0
            EKNI = (EKAN2*EKAI(J))**(1.0/2.0)
            TASTA = TG(I)/EKNI
            OMEGAD = AD/TASTA**BD+CD/EXP(DD*TASTA)+ED/EXP(FD*TASTA)
     &                + GD/EXP(HD*TASTA)
            DIFF(I,J) = 1.858E-3*TG(I)**(3.0/2.0)*((WTN2+WT(J))
     &                  / (WTN2*WT(J)))**(1.0/2.0)
     &                  / (PATM*SNI**2.0*OMEGAD)*1.0E-4
            SCHM(J) = AMU/RHOG(I)/DIFF(I,J)
11     CONTINUE

C CORRECTION TO MASS AND HEAT TRANSFER COEFFS. FOR HIGH MASS TR. RATES
      IF(CARB.EQ.0) THEN
       ALEFF = 1.0
      ELSE
       ALEFF = RHOG(I)*DIFF(I,4)*CPGREG(I)/AKG(I)
      END IF

       GTOT=G(I)+GV(I)
         IF(ITIME.EQ.0)THEN
             DO 23 J=1,4
 23          BM(J)=0.
             GOTO22
         ENDIF
         IF(GTOT.GT.0.)THEN
         CHIO2=YRO2(I)+AKY(I,1)*(YRO2(I)-Y8O2(I))/GTOT
         CHICO2=YRCO2(I)+AKY(I,2)*(YRCO2(I)-Y8CO2(I))/GTOT
```

```
          CHICO=YRCO(I)+AKY(I,3)*(YRCO(I)-Y8CO(I))/GTOT
          CHIP=YRP(I)+AKY(I,4)*(YRP(I)-Y8P(I))/GTOT
          BM(1)=(YRO2(I)-Y8O2(I))/(CHIO2-YRO2(I))
          BM(2)=(YRCO2(I)-Y8CO2(I))/(CHICO2-YRCO2(I))
          BM(3)=(YRCO(I)-Y8CO(I))/(CHICO-YRCO(I))
          BM(4)=(YRP(I)-Y8P(I))/(CHIP-YRP(I))
          ELSE
          CHIO2=YRO2(I)
          CHICO2=YRCO2(I)
          CHICO=YRCO(I)
          CHIP=YRP(I)
          DO 21 J=1,4
 21       BM(J)=0.
          ENDIF
 22    CONTINUE
          DO 15 J=1,4
          IF (ABS(BM(J)).LE.1.0E-2) THEN
             CORRKY(J) = 1.0
          ELSE
             CORRKY(J) = (LOG(1.0+BM(J)))/BM(J)
          ENDIF
 15       CONTINUE
          BT = ((1.0+BM(4))**ALEFF)-1.0
          IF ((BT.LE.1.0E-3).OR.(ABS(BM(4)).LT.1.0E-3)) THEN
             CORRH = 1.0
          ELSE
             CORRH = (LOG(1.0+BT))/BT
          ENDIF
        RE(I) = WG(I)/(AMU*SSB(I))
          AR = (DIAM**3.0)*9.8*RHOG(I)*(RHOS(I)-RHOG(I))/(AMU**2.0)
        PR = AMU*CPGREG(I)/AKG(I)

*     BHATTACHARYA AND PEI HEAT TR OPTION
          IF (IHTTR.EQ.1970) THEN
             AJH = 0.018*(AR/(RE(I)*RE(I)*36.0))**(0.25)
          ENDIF

*     YOSHIDA AND WEN OPTION
          IF (IHTTR.EQ.1960) THEN
             IF (RE(I).LT.50.0) THEN
                AJH = 0.91*(RE(I)**(-0.51))
             ELSE
                AJH = 0.61*(RE(I)**(-0.41))
             ENDIF
          ENDIF

*     CHU OPTION
          IF (IHTTR.EQ.1950) THEN
             AJH = 1.77*(RE(I)*6.0)**(-0.44)
             AJD = 5.7*(RE(I)*6.0)**(-0.78)
          ELSE
             AJD = AJH
          ENDIF

          FVOID = 1.0-VOIDA/VOID(I)*(1.0-VOID(I))/(1.0-VOIDA)*(1.0-
XC(I))
          DO 12 J=1,4
```

```
            IF ((I.EQ.1).OR.(I.EQ.IB+IG)) THEN
               AKY(I,J) = 0.0
            ELSE
               AKY(I,J) = (AJD*WG(I)/(SCHM(J)**(0.66)))*CORRKY(J)
             AKY(I,J) = AKY(I,J)*FVOID
            ENDIF
            DDEFF = 1.0+(9.7*VOID(I)*RHOG(I)*DIFF(I,J)/(WG(I)*DIAM))
          DDEFF = 0.73*DIFF(I,J)+0.5*WG(I)*DIAM/VOID(I)/RHOG(I)/DDEFF
            DEFF(I,J) = DDEFF*VOID(I)
12        CONTINUE
         AKAG(I) = 1.0+(9.7*VOID(I)*AKG(I)/(WG(I)*DIAM*CPGREG(I)))
          AKAG(I) = 0.73*VOID(I)*AKG(I)
     &                +0.5*WG(I)*DIAM*CPGREG(I)/AKAG(I)
          IF ((I.EQ.1).OR.(I.EQ.IB+IG)) THEN
             H(I) = 0.0
          ELSE
           H(I) = AJH*CORRH*CPGREG(I)*WG(I)/(PR**(0.66))
          ENDIF
10      CONTINUE

*       CALCULATE HEAT TRANSFER COEFFICIENT TO GRATE BARS
*       PROPERTIES, ETC. BASED ON NODE 3
        IF (IGMOD.EQ.2) THEN
           TFILM = (TG(3)+TS(3))/2.0
           AMU = 2.6693E-06*SQRT(WTN2*TFILM)/((SIGN2**2.0)*OMEGN2)
         REGRT = WG(3)*GRTBAR/1000.0/AMU
           AKGGRT = (CPGREG(3)+(5.0/4.0)*(R/AMWG(3)*1000.0))*AMU
           PR = AMU*CPGREG(3)/AKGGRT
           XNU = (0.43+0.5*REGRT**0.5)*PR**0.38
           HGRT = AKGGRT*XNU/(GRTBAR/1000.0)
           DO 13 I=1,IG
              RE(I) = REGRT
              AKAG(I) = (1.0-GRTSOL)*AKG(I)
              H(I) = HGRT
            DO 14 J=1,4
                 DEFF(I,J) = (1.0-GRTSOL)*DIFF(I,J)
14             CONTINUE
13          CONTINUE
        ENDIF
        RETURN
        END

*************************************************************************

        SUBROUTINE GFLUX(VOIDO,XB,HT)

*       CALCULATES THE GAS MASS VELOCITIES THROUGH THE BED SLABS

        PARAMETER (N=50)
        DIMENSION VOIDO(N),XB(N)
        DIMENSION VOID(N),SLAB(N),SSB(N),SSBO(N),RHOS(N),G(N),DZETA(N)
        DIMENSION DIAMC(N),SSC(N),SSCO(N),XC(N)
        DIMENSION WG(N),RHOG(N),RHOGO(N)
        DIMENSION VG(N),VS(N),VC(N)
        DIMENSION GV(N),RP(N)
        COMMON/DEVOL/GV,AVV,EVV,RP,COVOL,CO2VOL,HPYRO
        COMMON/BED/VOID,E,SLAB,SSB,SSBO,RHOS,G,DHTDT,DZETA
```

```
      COMMON/WCHAR/CARB,DIAMC,RHOC,VOIDC,SPHERC,SSC,SSCO,XC
      COMMON/GAS/WG,RHOG,RHOGO
      COMMON/TIME/IFLAG,ITIME,ITERNS,TURNS,IB,IG,ICOB,TIMES,DT
      COMMON/V/VG,VS,VC

*     THE VARIABLE WG IS ACTUALLY THE MASS FLUX RHOG*WG

      DO 10 I = 2,IB+IG-1
       WG(I) = (G(I)+GV(I))*SLAB(I)*SSCO(I)
     &             -(VOID(I)*RHOG(I)-VOIDO(I)*RHOGO(I))*SLAB(I)/DT
     &             -VOID(I)*RHOG(I)*DHTDT*DZETA(I)
       WG(I) = WG(I)+WG(I-1)
10    CONTINUE
      WG(IB+IG) = WG(IB+IG-1)

      DO 11 I=1,IG+IB
       IF (I.LE.IG) THEN
          VG(I) = WG(I)
       ELSE
          ZETA = XB(I)/HT
          VG(I) = WG(I)+ZETA*VOID(I)*DHTDT*RHOG(I)
      ENDIF
11    CONTINUE
      RETURN
      END

*****************************************************************************

      SUBROUTINE SFLUX(IO,WS,VOIDO,RHOSO,ISTOP,IFEED,XB,HT)

*     CALCULATES THE SOLID (CHAR+ASH) MASS VELOCITIES THROUGH THE BED
SLABS

      PARAMETER (N=50)
      DIMENSION WS(N),VOIDO(N),RHOSO(N),XB(N)
      DIMENSION VOID(N),SLAB(N),SSB(N),SSBO(N),RHOS(N),G(N),DZETA(N)
      DIMENSION DIAMC(N),SSC(N),SSCO(N),XC(N)
      DIMENSION WG(N),RHOG(N),RHOGO(N)
      DIMENSION VG(N),VS(N),VC(N)
      DIMENSION GV(N),RP(N)
      COMMON/DEVOL/GV,AVV,EVV,RP,COVOL,CO2VOL,HPYRO
      COMMON/V/VG,VS,VC
      COMMON/BED/VOID,E,SLAB,SSB,SSBO,RHOS,G,DHTDT,DZETA
      COMMON/WCHAR/CARB,DIAMC,RHOC,VOIDC,SPHERC,SSC,SSCO,XC
      COMMON/ASH/ASH,DIAMA,RHOA,VOIDA,SPHERA,IBUILD
      COMMON/GAS/WG,RHOG,RHOGO
      COMMON/GRATE/GRATE,GRTSOL,GRTBAR,IGMOD,GRTRHO,GRTPD,GRTSPACE
      COMMON/TIME/IFLAG,ITIME,ITERNS,TURNS,IB,IG,ICOB,TIMES,DT


*     THE VARIABLE WS IS ACTUALLY THE MASS FLUX RHOS*WS

      ISTOP = 0
      ICOUNT = 0

*     IF THE ASH FALLS THROUGH THE GRATE
      IF (IBUILD.EQ.0) THEN
```

```
*     RESET A GUESS FUEL INLET MASS VELOCITY UNTIL CONVERGENCE
333      DO 10 I=2,IB+IG-1
          WS(I) = -(G(I)+GV(I))*SLAB(I)*SSCO(I)
     &                -((1.0-VOID(I))*RHOS(I)
     &                -(1.0-VOIDO(I))*RHOSO(I))*SLAB(I)/DT
          WS(I) = WS(I)+WS(I-1)
10       CONTINUE
         IF (ASH.GT.0.0)THEN
          WS(IB+IG) = WS(1)/ASH
         ELSE
          WS(IB+IG) = WS(IG+IB-1)
         ENDIF
*     CONVERGENCE CRITERION FOR FEED FLOW RATE IS BASED ON INLET
*     AIR FLOW RATE/6 (ROUGHLY STOICH. AIR FOR C TO CO) AS A REFERENCE
*     SOLID FLUX. THIS IS DONE BECAUSE DURING BED STARTUP ACTUAL SOLIDS
*     FLUX MAY BECOME 0. TIGHTENING CONVERGENCE CRITERION FROM 1E-3 TO
*     1E-4 INCREASED ITERATIONS WITHOUT IMPROVING ACCURACY.
       VCHK = ABS(WS(IB+IG)-WS(IB+IG-1))
       VCRIT = WG(1)/6.0
         IF ((VCHK/VCRIT).GT.1.0E-03) THEN
          WS(1) = WS(IB+IG-1)*ASH
            ICOUNT = ICOUNT+1
            IF (ICOUNT.GT.100) THEN
             WRITE(IO,*) 'RESULTS INVALID - WS DNCNV'
               WRITE(IO,*) VCHK
               ISTOP = 1
               GO TO 33
            ENDIF
            GO TO 333
         ENDIF
       ENDIF

*      IF THE ASH BUILDS UP IN THE BED
       IF (IBUILD.EQ.1) THEN
          DO 11 I=1,IG
           WS(I) = 0.0
11      CONTINUE
        DO 12 I=IG+1,IG+IB-1
          WS(I) = -(G(I)+GV(I))*SLAB(I)*SSCO(I)
     &                -((1.0-VOID(I))*RHOS(I)
     &                -(1.0-VOIDO(I))*RHOSO(I))*SLAB(I)/DT
     &                -(1.0-VOID(I))*RHOS(I)*DHTDT*DZETA(I)
          WS(I) = WS(I)+WS(I-1)
12      CONTINUE
        IF (IFEED.EQ.0) THEN
          WS(IG+IB) = 0.0
        ELSE
          WS(IG+IB) = WS(IG+IB-1)
        ENDIF
       ENDIF

       DO 13 I=1,IG+IB
        IF (I.LE.IG) THEN
          VS(I) = 0.0
        ELSE
          ZETA = XB(I)/HT
          VS(I) = WS(I)+ZETA*(1.0-VOID(I))*DHTDT*RHOS(I)
```

```
      ENDIF
13    CONTINUE
33    RETURN
      END
*************************************************************************

      SUBROUTINE CFLUX(WS,WC,XB,HT,RHOF)

*     CALCULATES THE CHAR VELOCITIES THROUGH THE BED SLABS

      PARAMETER (N=50)
      DIMENSION WS(N),WC(N)
*      ,APHIO(N),VOIDO(N),XCO(N),RHOSO(N),APHI(N)
      DIMENSION XB(N)
      DIMENSION VOID(N),SLAB(N),SSB(N),SSBO(N),RHOS(N),G(N),DZETA(N)
      DIMENSION DIAMC(N),SSC(N),SSCO(N),XC(N)
      DIMENSION VG(N),VS(N),VC(N)
      DIMENSION GV(N),RP(N)
      DIMENSION RHOF(N)
      COMMON/DEVOL/GV,AVV,EVV,RP,COVOL,CO2VOL,HPYRO
      COMMON/BED/VOID,E,SLAB,SSB,SSBO,RHOS,G,DHTDT,DZETA
      COMMON/WCHAR/CARB,DIAMC,RHOC,VOIDC,SPHERC,SSC,SSCO,XC
      COMMON/ASH/ASH,DIAMA,RHOA,VOIDA,SPHERA,IBUILD
      COMMON/TIME/IFLAG,ITIME,ITERNS,TURNS,IB,IG,ICOB,TIMES,DT
      COMMON/V/VG,VS,VC

*     THE VARIABLE WC IS ACTUALLY THE MASS FLUX RHOC*WC

      DO 12 I=IG+1,IG+IB-1
       WC(I) = RHOF(I)/RHOS(I)*XC(I)*WS(I)
12    CONTINUE

      DO 13 I=1,IG+IB
       IF (I.LE.IG) THEN
          VC(I) = 0.0
       ELSE
          ZETA = XB(I)/HT
          VC(I) = WC(I)+ZETA*(1.0-VOID(I))*DHTDT*XC(I)*RHOF(I)
      ENDIF
13    CONTINUE
      RETURN
      END

*************************************************************************

      SUBROUTINE COND(TG,TS,AKG,AKAS,RHOF,YW)

*     CALCULATES THE EFFECTIVE CONDUCTIVITY OF THE SOLID PHASE

      PARAMETER (N=50)
      DIMENSION TG(N),TS(N),AKG(N),AKAS(N),RHOF(N),YW(N)
      DIMENSION VOID(N),SLAB(N),SSB(N),SSBO(N),RHOS(N),G(N),DZETA(N)
      DIMENSION DIAMC(N),SSC(N),SSCO(N),XC(N)
      DIMENSION TC(N),GRATEK(N)
      COMMON/BED/VOID,E,SLAB,SSB,SSBO,RHOS,G,DHTDT,DZETA
      COMMON/WCHAR/CARB,DIAMC,RHOC,VOIDC,SPHERC,SSC,SSCO,XC
      COMMON/ASH/ASH,DIAMA,RHOA,VOIDA,SPHERA,IBUILD
```

```
      COMMON/INFO/WTN2,WTO2,WTCO2,WTCO,R,P,BETA,GAMMA,THI,WTP,TREF
      COMMON/GRATE/GRATE,GRTSOL,GRTBAR,IGMOD,GRTRHO,GRTPD,GRTSPACE
      COMMON/TIME/IFLAG,ITIME,ITERNS,TURNS,IB,IG,ICOB,TIMES,DT

      DO 10 I=1,IG
         TC(I) = TS(I)-273.0
         IF (IGMOD.EQ.2) THEN
            GRATEK(I) = 0.0137*TC(I)+15.086
          AKAS(I) = GRTSOL*GRATEK(I)
         ENDIF
10    CONTINUE

      DO 11 I=IG+1,IB+IG
         TC(I) = TS(I)-273.0
         TM = (TS(I)+TG(I))/2.0
*     EFFECTIVE ASH CONDUCTIVITY
       EA = E
         AKSA = 1.09
        HRSA = 0.2268*(EA/(2.0-EA))*((TM/100.0)**3.0)
        HRVA = 0.2268/(1.0+(0.5*VOIDA/(1.0-VOIDA))*((1.0-EA)/EA))
     &             *((TM/100.0 )**3.0)
        AKASA = BETA*(1.0-VOIDA)
     &              /(GAMMA/AKSA+1.0/(AKG(I)/THI+HRSA*DIAMA))
     &              +VOIDA*BETA*DIAMA*HRVA
        VCHAR = XC(I)*(1.0-VOID(I))
        CHECK = (1.0-VOIDC)/(1.0-VOIDC*VOIDA)
        IF (XC(I).LE.CHECK) THEN
           CHIA = 1.0
        ELSE
           CHIA = (1.0-VOIDC)/(1.0-VOIDA)*(1.0-XC(I))/(VOIDC*XC(I))
        ENDIF

*     EFFECTIVE BED CONDUCTIVITY
C     EQUATION OF MERRICK FOR THERMAL CONDUCTIVITY OF COKE
C         AKS = ((RHOF(I)/4511.0)**3.5)*TS(I)**0.5
      RHOFUEL=RHOF(I)
C     MODEL OF LARFELDT ET AL. 2000 FOR CONDUCTIVITY OF WOOD CHAR
         AKCG = 9.0037E-03+5.6263E-05*TS(I)
         AKCHAR = 0.1
         POROS = 1.-CARB
         POROSMAC = 0.6
         DPORE = 0.35E-03
         SIGMA = 5.669E-8
         EMISPORE=0.9
         AKCRAD = 4.*POROSMAC*SIGMA*EMISPORE*DPORE*TS(I)**3
         AKC = (1.-POROS)*AKCHAR+POROS*AKCG+AKCRAD
C     MODEL OF KOUFOPANOS ET AL. 1991 FOR CONDUCTIVITY OF WOOD
         AKW = 0.13+3.E-4*(TS(I)-273.)
C     OVERALL CONDUCTIVITY OF WOOD PLUS CHAR
         AKS = YW(I)*AKW+(1.-YW(I))*AKC
C         WRITE(8,*)I,TS(I),AKW,AKC,YW(I),AKS
         HRS = 0.2268*(E/(2.0-E))*((TM/100.0)**3.0)
       HRV = 0.2268/(1.0+(0.5*VOID(I)/(1.0-VOID(I)))*((1.0-E)/E))
     &             *((TM/100.0)**3.0)

        AKAS(I) = VCHAR*BETA
     &               /(GAMMA/AKS+1.0/(AKG(I)/THI+HRS*DIAMC(I)))
```

```
     &                +(1.0-VCHAR)*(1-CHIA)*BETA*DIAMC(I)*HRV
     &                +(1.0-VCHAR)*CHIA*AKASA

11     CONTINUE
       RETURN
       END

*************************************************************************

       SUBROUTINE PCONC(AKY)

*      CALCULATES THE GAS CONCENRATIONS AT THE PARTICLE SURFACE

       PARAMETER (N=50)
       DIMENSION AKY(N,4)
       DIMENSION VOID(N),SLAB(N),SSB(N),SSBO(N),RHOS(N),G(N),DZETA(N)
       DIMENSION Y8O2(N),Y8CO2(N),Y8CO(N),Y8N2(N),Y8O2O(N),Y8CO2O(N)
       DIMENSION Y8COO(N),Y8N2O(N),Y8P(N),Y8PO(N)
       DIMENSION YRO2(N),YRCO2(N),YRCO(N),YRN2(N),YRP(N)
       DIMENSION G1(N),G2(N),X(N),S(N)
       DIMENSION YRCO2I(N),YRCOI(N),YRO2I(N),YRPI(N)
       DIMENSION GV(N),RP(N),yrh2o(n)
       DIMENSION WG(N),RHOG(N),RHOGO(N)
       common/water/xh2o,rhow,yrh2o
       COMMON/DEVOL/GV,AVV,EVV,RP,COVOL,CO2VOL,HPYRO
       COMMON/BED/VOID,E,SLAB,SSB,SSBO,RHOS,G,DHTDT,DZETA
       COMMON/Y/Y8O2,Y8CO2,Y8CO,Y8N2,Y8O2O,Y8CO2O,Y8COO,Y8N2O,Y8P,Y8PO
       COMMON/YR/YRO2,YRCO2,YRCO,YRN2,YRP
       COMMON/STOIC/SCO2,SCO,S3,S2,DH1,DH2,DH3,DH4
       COMMON/REACT/G1,G2,X,S,IREACT
       COMMON/TIME/IFLAG,ITIME,ITERNS,TURNS,IB,IG,ICOB,TIMES,DT
       COMMON/GAS/WG,RHOG,RHOGO

       DO 10 I=2,IG+IB-1
          YRCO2I(I) = YRCO2(I)
        YRO2I(I) = YRO2(I)
          YRCOI(I) = YRCO(I)
          YRPI(I) = YRP(I)
        FACTOR = G(I)+GV(I)+(S(I)*G1(I))/YRO2I(I)
          YRO2(I) = Y8O2(I)/(1.0+(1.0/AKY(I,1))*FACTOR)
          YRCO2(I) = (X(I)*(1.0+S(I))*G1(I)+COVOL*GV(I))/AKY(I,2)
     &               +Y8CO2(I)
        YRCO2(I) = YRCO2(I)/(1.0+(1.0/AKY(I,2))*(G(I)+GV(I)
     &                +S2*G2(I)/YRCO2I(I)))
          ADD = (1.0-X(I))*(1.0+S(I))*G1(I)+AKY(I,3)*Y8CO(I)+COVOL*GV(I)
          YRCO(I) = ((1.0+S2)*G2(I)+ADD)/(G(I)+GV(I)+AKY(I,3))
        YRP(I)=((1.-COVOL-CO2VOL)*GV(I))+AKY(I,4)*Y8P(I)
        YRP(I)=YRP(I)/(G(I)+GV(I)+AKY(I,4))

          IF (YRCO(I).LE.1.0E-38) THEN
             YRCO(I) = 1.0E-38
          ENDIF
          IF (YRO2(I).LE.1.0E-38) THEN
             YRO2(I) = 1.0E-38
          ENDIF
          IF (YRCO2(I).LE.1.0E-38) THEN
             YRCO2(I) = 1.0E-38
```

```
        ENDIF
        IF (YRP(I).LE.1.0E-38) THEN
           YRP(I) = 1.0E-38
        ENDIF

10      CONTINUE
        RETURN
        END

*************************************************************************

        SUBROUTINE TDMACN(TGO,VOIDO,DEFF,IRXN,RCO,RCOB,DXN,FE)

*       CALCULATES THE SPECIES CONCENTRATION PROFILES

        PARAMETER (N=50)
        DIMENSION TGO(N),VOIDO(N),DEFF(N,4),RCO(N),RCOB(N),DXN(N),FE(N)
        DIMENSION DIAMC(N),SSC(N),SSCO(N),XC(N)
        DIMENSION VOID(N),SLAB(N),SSB(N),SSBO(N),RHOS(N),G(N),DZETA(N)
        DIMENSION WG(N),RHOG(N),RHOGO(N)
        DIMENSION Y8O2(N),Y8CO2(N),Y8CO(N),Y8N2(N),Y8O2O(N),Y8CO2O(N)
        DIMENSION Y8COO(N),Y8N2O(N),Y8P(N),Y8PO(N)
        DIMENSION G1(N),G2(N),X(N),S(N)
        DIMENSION TESTTG(N),TESTTS(N),TESTCO(N),TESTYW(N),TESTP(N)
        DIMENSION Y8CO2I(N),Y8COI(N),Y8O2I(N),Y8PI(N)
        DIMENSION AC(N),CC(N,4),QC(N),PC(N),CONC(N)
        DIMENSION FN(N),DN(N,4),FS(N),DS(N,4),PEN(N,4),PES(N,4)
        DIMENSION SPO2(N),SCOO2(N),SPCO(N),SCCO(N),SPCO2(N),SCCO2(N)
        DIMENSION SPP(N), SCP(N)
        DIMENSION GV(N),RP(N)
        DIMENSION RATE(N)
        COMMON/DEVOL/GV,AVV,EVV,RP,COVOL,CO2VOL,HPYRO
        COMMON/BED/VOID,E,SLAB,SSB,SSBO,RHOS,G,DHTDT,DZETA
        COMMON/WCHAR/CARB,DIAMC,RHOC,VOIDC,SPHERC,SSC,SSCO,XC
        COMMON/GAS/WG,RHOG,RHOGO
        COMMON/Y/Y8O2,Y8CO2,Y8CO,Y8N2,Y8O2O,Y8CO2O,Y8COO,Y8N2O,Y8P,Y8PO
        COMMON/INFO/WTN2,WTO2,WTCO2,WTCO,R,P,BETA,GAMMA,THI,WTP,TREF
        COMMON/STOIC/SCO2,SCO,S3,S2,DH1,DH2,DH3,DH4
        COMMON/REACT/G1,G2,X,S,IREACT
        COMMON/RAD/TSG,TSB,TSW,HRG,HRB,HRW,F12B,BOLTZ,TCOAL
        COMMON/FLUXES/FO2,FC,FCO2,FP,FTG,FTS
        COMMON/TIME/IFLAG,ITIME,ITERNS,TURNS,IB,IG,ICOB,TIMES,DT
        COMMON/TEST/TESTTG,TESTTS,TESTCO,CRIT,TESTYW,TESTP

*       NUMBERING OF GASES (J): 1=O2, 2=CO2, 3=CO, 4=PYROLYSIS GASES

        DO 10 I=2,IB+IG-1
         Y8O2I(I) = Y8O2(I)
         Y8CO2I(I) = Y8CO2(I)
         Y8COI(I) = Y8CO(I)
         Y8PI(I) = Y8P(I)
           IF (Y8CO2I(I).LE.1.0E-38) THEN
              Y8CO2I(I) = 1.0E-38
           ENDIF
           IF (Y8O2I(I).LE.1.0E-38) THEN
              Y8O2I(I) = 1.0E-38
         ENDIF
```

```
      IF (Y8PI(I).LE.1.0E-38) THEN
         Y8PI(I) = 1.0E-38
      ENDIF

      FN(I) = WG(I)*DT
      FS(I) = WG(I-1)*DT
      DO 11 J=1,4
           DN(I,J) = FE(I)*DEFF(I,J)+(1.0-FE(I))*DEFF(I+1,J)
           DN(I,J) = RHOG(I)*DN(I,J)*DT/DXN(I)
           DS(I,J) = FE(I-1)*DEFF(I-1,J)+(1.0-FE(I-1))*DEFF(I,J)
           DS(I,J) = RHOG(I-1)*DS(I,J)*DT/DXN(I-1)
           PEN(I,J) = FN(I)/DN(I,J)
           PES(I,J) = FS(I)/DS(I,J)
11      CONTINUE

*     WESTBROOK AND DRYER CO KINETICS OPTION
         IF (IRXN.EQ.1980) THEN
            IF ((IREACT.LT.2))THEN
               RCO(I) = 0.0
            ELSE
             RCO(I) =(Y8O2I(I)**0.25)*(1.8562E+10)*EXP(-20130./TGO(I))
               RCO(I) = RCO(I)*(RHOG(I)**1.75)*Y8COI(I)*VOID(I)
     &                  *SLAB(I)*DT

*     REVERSE REACTION FOR EQUILIBRIUM
               RCOB(I) = 9.74E12*RHOG(I)*Y8CO2I(I)*EXP(-46490.0/TGO(I))
*              RCOB(I) = 3.69E13*RHOG(I)*Y8CO2I(I)*EXP(-51566.0/TGO(I))
               RCOB(I) = RCOB(I)*VOID(I)*SLAB(I)*DT
             IF (ICOB.EQ.0)THEN
                RCOB(I) = 0.0
              ENDIF
            ENDIF
         ENDIF

*     HOWARD AND FINE CO KINETICS OPTION
         IF (IRXN.EQ.1970) THEN
            IF ((IREACT.LT.2))THEN
               RCO(I) = 0.0
            ELSE
               RCO(I) = (Y8O2I(I)**0.5)*(4.5319E+8)*EXP(-15098./TGO(I))
               RCO(I) = RCO(I)*(RHOG(I)**2.0)*Y8COI(I)*VOID(I)
     &                  *SLAB(I)*DT
            ENDIF
            RCOB(I) = 4.8E11*RHOG(I)*Y8CO2I(I)*EXP(-46500./TGO(I))
            RCOB(I) = RCOB(I)*VOID(I)*SLAB(I)*DT
            IF (ICOB.EQ.0)THEN
               RCOB(I) = 0.0
            ENDIF
         ENDIF

C       ECO2 = (Y8CO2I(I)+0.30)/2.0
        ECO2 = (Y8CO2I(I)+0.40)/2.0
       ECO = (Y8COI(I)+0.40)/2.0
        EO2 = (Y8O2I(I)+0.2322)/2.0

        RATE(I) =  RP(I)*SLAB(I)*DT
```

```
*  see Patankar, p 49 for explanation on S
          SPCO2(I) = -S2*G2(I)*SSCO(I)*SLAB(I)*DT/Y8CO2I(I)
        SPCO2(I) = SPCO2(I)-RCO(I)*(1.0+S3)/(ECO2-Y8CO2I(I))
          SPCO2(I) = SPCO2(I)-RCOB(I)*(1.0+S3)/Y8CO2I(I)
          SCCO2(I) = X(I)*(1.0+S(I))*G1(I)*SSCO(I)*SLAB(I)*DT
        SCCO2(I) = SCCO2(I)+(1.0+S3)*RCO(I)*ECO2/(ECO2-Y8CO2I(I))
        SCCO2(I) = SCCO2(I)+CO2VOL*RATE(I)
        SPO2(I) = (-S(I)*G1(I)*SSCO(I)*SLAB(I)*DT-S3*RCO(I))/Y8O2I(I)
          SPO2(I) = SPO2(I)-S3*RCOB(I)/(EO2-Y8O2I(I))
        SCOO2(I) = S3*RCOB(I)*EO2/(EO2-Y8O2I(I))
        SPCO(I) = -RCO(I)/Y8COI(I)
          SPCO(I) = SPCO(I)-RCOB(I)/(ECO-Y8COI(I))
          SCCO(I) = (1.0-X(I))*(1.0+S(I))*G1(I)
          SCCO(I) = (SCCO(I)+(1.0+S2)*G2(I))*SSCO(I)*SLAB(I)*DT
        SCCO(I) = SCCO(I)+RCOB(I)*ECO/(ECO-Y8COI(I))
        SCCO(I) = SCCO(I)+COVOL*RATE(I)
        SCP(I) = RATE(I)*(1.-covol-co2vol)
          SPP(I) = 0.
10     CONTINUE

        IF (IREACT.GT.0) THEN
        DO 12 J=1,4
             DO 13 I=2,IB+IG-1
                AC(1) = 1.0
                PC(1) = 0.0
                BC = DN(I,J)*AMAX1(0.0,(1.0-0.1*ABS(PEN(I,J)))**5.0)
                BC = BC+AMAX1(0.0,-FN(I))
                IF (I.EQ.IB+IG-1) THEN
                   BC = 0.0
                ENDIF
                CC(I,J) = DS(I,J)*AMAX1(0.0,(1.0-
0.1*ABS(PES(I,J)))**5.0)
                CC(I,J) = CC(I,J)+AMAX1(0.0,FS(I))
              AC(I) = VOID(I)*SLAB(I)*RHOG(I)+BC+CC(I,J)+FN(I)-FS(I)
     &                      +VOID(I)*RHOG(I)*DHTDT*DT*DZETA(I)
                IF (J.EQ.1) THEN
                   AC(I) = AC(I)-SPO2(I)
                   DDC = Y8O2(1)
                   DC = VOIDO(I)*SLAB(I)*RHOGO(I)*Y8O2O(I)+SCOO2(I)
                ENDIF
                IF (J.EQ.2) THEN
                   AC(I) = AC(I)-SPCO2(I)
                   DDC = Y8CO2(1)
               DC = VOIDO(I)*SLAB(I)*RHOGO(I)*Y8CO2O(I)+SCCO2(I)
                ENDIF
                IF (J.EQ.3) THEN
                   AC(I) = AC(I)-SPCO(I)
                   DDC = Y8CO(1)
                   DC = VOIDO(I)*SLAB(I)*RHOGO(I)*Y8COO(I)+SCCO(I)
              ENDIF
              IF (J.EQ.4) THEN
               AC(I) = AC(I)-SPP(I)
               DDC = Y8P(1)
                   DC = VOIDO(I)*SLAB(I)*RHOGO(I)*Y8PO(I)+SCP(I)
              ENDIF
              QC(1) = DDC/AC(1)
              PC(I) = BC/( AC(I)-CC(I,J)*PC(I-1))
```

```
            QC(I) =(CC(I,J)*QC(I-1)+DC)/(AC(I)-CC(I,J)*PC(I-1))
13        CONTINUE

          PC(IB+IG) = 0.0
            QC(IB+IG) = QC(IG+IB-1)/(1.0-PC(IG+IB-1))
            CONC(IB+IG) = QC(IB+IG)

            DO 14 I=IB+IG-1,2,-1
               CONC(I) = CONC(I+1)*PC(I)+QC(I)
               IF (J.EQ.1) THEN
                  Y8O2(IB+IG) = CONC(IB+IG)
                  Y8O2(I) = CONC(I)
               ENDIF
               IF (J.EQ.2) THEN
                  Y8CO2(IB+IG) = CONC(IB+IG)
                  Y8CO2(I) = CONC(I)
               ENDIF
               IF (J.EQ.3) THEN
                  Y8CO(IB+IG) = CONC(IB+IG)
                  Y8CO(I) = CONC(I)
              TESTCO(I) = ABS(Y8CO(I)-Y8COI(I))
             ENDIF
             IF (J.EQ.4) THEN
              Y8P(IB+IG) = CONC(IB+IG)
              Y8P(I) = CONC(I)
             ENDIF
14          CONTINUE
12       CONTINUE
        DO 16 I=1,IB+IG
16      Y8N2(I) = 1.0-Y8CO(I)-Y8O2(I)-Y8CO2(I)-Y8P(I)

         FLUXB = CC(2,1)
           FLUXA = CC(2,1)-AMAX1(FS(2),0.0)+AMAX1(-FS(2),0.0)
           FO2 = (FLUXB*Y8O2(1)-FLUXA*Y8O2(2))/DT
           FLUXB = CC(2,2)
           FLUXA = CC(2,2)-AMAX1(FS(2),0.0)+AMAX1(-FS(2),0.0)
           FCO2 = (FLUXB*Y8CO2(1)-FLUXA*Y8CO2(2))/DT
           FLUXB = CC(2,3)
           FLUXA = CC(2,3)-AMAX1(FS(2),0.0)+AMAX1(-FS(2),0.0)
         FC = (FLUXB*Y8CO(1)-FLUXA*Y8CO(2))/DT
         FLUXB = CC(2,4)
         FLUXA = CC(2,4)-AMAX1(FS(2),0.0)+AMAX1(-FS(2),0.0)
         FP = (FLUXB*Y8P(1)-FLUXA*Y8P(2))/DT
         ENDIF

         RETURN
         END

*************************************************************************

        SUBROUTINE TDMATG(TG,TGI,TGO,TS,VOIDO,CPG,CPGO,AKAG,H,RCO,RCOB,
       1DXN,FE)

*       CALCULATES THE GAS TEMPERATURE PROFILES

        PARAMETER (N=50)
        DIMENSION TG(N),TGI(N),TGO(N),TS(N),VOIDO(N),CPG(N),AKAG(N),H(N)
```

```
      DIMENSION RCO(N),RCOB(N),DXN(N),FE(N),CPGO(N),TGC(N)
      DIMENSION VOID(N),SLAB(N),SSB(N),SSBO(N),RHOS(N),G(N),DZETA(N)
      DIMENSION WG(N),RHOG(N),RHOGO(N)
      DIMENSION G1(N),G2(N),X(N),S(N)
      DIMENSION TESTTG(N),TESTTS(N),TESTCO(N),TESTYW(N),TESTP(N)
      DIMENSION FS(N),CGT(N),PGT(N),QGT(N)
      COMMON/BED/VOID,E,SLAB,SSB,SSBO,RHOS,G,DHTDT,DZETA
      COMMON/GAS/WG,RHOG,RHOGO
      COMMON/INFO/WTN2,WTO2,WTCO2,WTCO,R,P,BETA,GAMMA,THI,WTP,TREF
      COMMON/STOIC/SCO2,SCO,S3,S2,DH1,DH2,DH3,DH4
      COMMON/REACT/G1,G2,X,S,IREACT
      COMMON/RAD/TSG,TSB,TSW,HRG,HRB,HRW,F12B,BOLTZ,TCOAL
      COMMON/FLUXES/FO2,FC,FCO2,FP,FTG,FTS
      COMMON/TIME/IFLAG,ITIME,ITERNS,TURNS,IB,IG,ICOB,TIMES,DT
      COMMON/TEST/TESTTG,TESTTS,TESTCO,CRIT,TESTYW,TESTP

C ENTHALPY FORMULATED USING MEAN SPECIFIC HEATS AND CELSIUS TEMPERATURE
C TREF = 0C. TG IS KELVIN TEMPERATURE, TGC CELSIUS.

      AGT = 1.0
      BGT = 0.0
      TGC(1)=TG(1)-TREF
      DGT = TGC(1)
      PGT(1) = BGT/AGT
      QGT(1) = DGT/AGT
      DO 10 I=2,IB+IG-1
         TGI(I) = TG(I)
       FN = WG(I)*CPG(I)*DT
       FS(I) = WG(I-1)*CPG(I-1)*DT
         DN = (FE(I)*AKAG(I)+(1.0-FE(I))*AKAG(I+1))*DT/DXN(I)
         DS = (FE(I-1)*AKAG(I-1)+(1.0-FE(I-1))*AKAG(I))*DT/DXN(I-1)
         PEN = FN/DN
         PES = FS(I)/DS
         BGT = DN*AMAX1(0.0,(1.0-0.1*ABS(PEN))**5.0)
         BGT = (BGT+AMAX1(0.0,-FN))
         IF (I.EQ.IG+IB-1) THEN
            BGT = 0.0
         ENDIF
         CGT(I) = DS*AMAX1(0.0,(1.0-0.1*ABS(PES))**5.0)
         CGT(I) = (CGT(I)+AMAX1(0.0,FS(I)))
         SPT = -RCO(I)*DH4/(2600.0-TGI(I))
         SPT = SPT-RCOB(I)*DH4/(TGI(I)-TREF)
         SCT = RCO(I)*DH4*(2600.0-TREF)/(2600.0-TGI(I))
       AGT = VOID(I)*SLAB(I)*RHOG(I)*CPG(I)+BGT+CGT(I)
         AGT = AGT+(FN-FS(I))+H(I)*SSBO(I)*SLAB(I)*DT
         AGT = AGT-SPT+VOID(I)*RHOG(I)*CPGO(I)*DHTDT*DT*DZETA(I)
         DGT = VOIDO(I)*SLAB(I)*RHOGO(I)*CPGO(I)*(TGO(I)-TREF)
         DGT = DGT+H(I)*SSBO(I)*(TS(I)-TREF)*SLAB(I)*DT
       DGT = DGT+SCT
         PGT(I) = BGT/(AGT-CGT(I)*PGT(I-1))
         QGT(I) = CGT(I)*QGT(I-1)+DGT
         QGT(I) = QGT(I)/(AGT-CGT(I)*PGT(I-1))
10    CONTINUE
      CGT(IB+IG) = 0.0
      PGT(IG+IB) = 0.0
      QGT(IG+IB) = QGT(IG+IB-1)/(1.0-PGT(IB+IG-1))
      TGC(IB+IG) = QGT(IB+IG)
```

```
      TG(IB+IG) = TGC(IB+IG)+TREF

      DO 11 I=IB+IG-1,2,-1
         TGC(I) = PGT(I)*TGC(I+1)+QGT(I)
         TG(I)=TGC(I)+TREF
       TESTTG(I) = ABS(TG(I)-TGI(I))
       IF (TG(I).GT.3000.0) THEN
          TG(I) = 3000.0
            WRITE(*,*)'TG OVERFLOW AT NODE ',I
         ENDIF
11    CONTINUE
      FLUXB = CGT(2)/DT
      FLUXA = CGT(2)/DT-AMAX1(FS(2),0.0)/DT+AMAX1(-FS(2),0.0)/DT
      FTG = FLUXB*TGC(1)-FLUXA*TGC(2)
      RETURN
      END

*****************************************************************************

      SUBROUTINE TDMATS(TG,TS,TSI,TSO,VOIDO,RHOSO,WS,AKAS,H,DXN,FE,
     & RHOF,RHOFO,YW,YWO)

*     CALCULATES THE SOLID TEMPERATURE PROFILE

      PARAMETER (N=50)
      DIMENSION
TG(N),TS(N),TSI(N),TSO(N),VOIDO(N),RHOSO(N),WS(N),TSC(N)
      DIMENSION AKAS(N),H(N),DXN(N),FE(N)
      DIMENSION VOID(N),SLAB(N),SSB(N),SSBO(N),RHOS(N),G(N),DZETA(N)
      DIMENSION DIAMC(N),SSC(N),SSCO(N),XC(N)
      DIMENSION WG(N),RHOG(N),RHOGO(N)
      DIMENSION G1(N),G2(N),X(N),S(N)
      DIMENSION TESTTG(N),TESTTS(N),TESTCO(N),TESTYW(N),TESTP(N)
      DIMENSION PST(N),QST(N)
      DIMENSION GV(N),RP(N)
      DIMENSION RHOF(N),RHOFO(N),CPSB(N),CPSO(N),YW(N),YWO(N)
      COMMON/DEVOL/GV,AVV,EVV,RP,COVOL,CO2VOL,HPYRO
      COMMON/BED/VOID,E,SLAB,SSB,SSBO,RHOS,G,DHTDT,DZETA
      COMMON/WCHAR/CARB,DIAMC,RHOC,VOIDC,SPHERC,SSC,SSCO,XC
      COMMON/ASH/ASH,DIAMA,RHOA,VOIDA,SPHERA,IBUILD
      COMMON/GAS/WG,RHOG,RHOGO
      COMMON/INFO/WTN2,WTO2,WTCO2,WTCO,R,P,BETA,GAMMA,THI,WTP,TREF
      COMMON/STOIC/SCO2,SCO,S3,S2,DH1,DH2,DH3,DH4
      COMMON/REACT/G1,G2,X,S,IREACT
      COMMON/RAD/TSG,TSB,TSW,HRG,HRB,HRW,F12B,BOLTZ,TCOAL
      COMMON/FLUXES/FO2,FC,FCO2,FP,FTG,FTS
      COMMON/GRATE/GRATE,GRTSOL,GRTBAR,IGMOD,GRTRHO,GRTPD,GRTSPACE
      COMMON/TIME/IFLAG,ITIME,ITERNS,TURNS,IB,IG,ICOB,TIMES,DT
      COMMON/TEST/TESTTG,TESTTS,TESTCO,CRIT,TESTYW,TESTP

      IT = IB+IG
      AST = 1.0
      BST = 0.0
      CST = 0.0
      TSC(IT)=TS(IT)-TREF
      TSC(1)=TS(1)-TREF
      DST = TSC(1)
```

```
      EST = 0.0
      PST(1) = BST/AST
      QST(1) = DST/AST
      TSG = (2.0*AKAS(2)/SLAB(2))*TS(2)+HRG*TS(1)
      TSG = TSG/(2.0*AKAS(2)/SLAB(2)+HRG)
      HRG = BOLTZ*(TS(1)**2.0+TSG**2.0)*(TS(1)+TSG)*GRTSOL
      TSB = AKAS(IG+1)*TS(IG+1)+SLAB(IG+1)/2.0*HRB*TS(1)
      TSB = TSB/(AKAS(IG+1)+SLAB(IG+1)/2.0*HRB)
      HRB = BOLTZ*F12B*(TSB**2.0+TS(1)**2.0)*(TSB+TS(1))
      TSW = (2.0*AKAS(IT-1)/SLAB(IT-1))*TS(IT-1)+HRW*TS(IT)
      TSW  = TSW/(2.0*AKAS(IT-1)/SLAB(IT-1)+HRW)
      HRW = BOLTZ*F12W(HT)*(TS(IT)**2.0+TSW**2.0)*(TS(IT)+TSW)
      DO 12 I=1,IT
12    CPSB(I)=CPS(TS(I),I,RHOF(I),YW(I))
      DO 13 I=1,IT-1
13    CPSO(I)=CPS(TSO(I),I,RHOFO(I),YWO(I))
      DO 10 I=2,IT-1
       TSI(I) = TS(I)
         FN = WS(I)*CPSB(I+1)*DT
         FS = WS(I-1)*CPSB(I)*DT
       IF (I.EQ.2) THEN
            FS = WS(I-1)*CPS(TSG,I,RHOF(I),YW(I))*DT
       ENDIF
         IF (I.EQ.IT-1) THEN
            T = TCOAL
            FN = WS(I)*CPS(T,I,RHOF(I),YW(I))*DT
       ENDIF
         DN = ((1.0-FE(I))/AKAS(I)+FE(I)/AKAS(I+1))**(-1.0)
       DN = DN*DT/DXN(I)
         DS = ((1.0-FE(I-1))/AKAS(I-1)+FE(I-1)/AKAS(I))**(-1.0)
         DS = DS*DT/DXN(I-1)
         PEN = FN/DN
       PES = FS/DS
         BST = DN*AMAX1(0.0,(1.0-0.1*ABS(PEN))**5.0)
         BST = (BST+AMAX1(0.0,-FN))
         IF (I.EQ.IT-1) THEN
            BST = (AKAS(I)*DT)/(SLAB(I)/2.0)
            BST = BST*(1.0/(1.0+2.0*AKAS(I)/(SLAB(I)*HRW)))
       ENDIF
         CST = DS*AMAX1(0.0,(1.0-0.1*ABS(PES) )**5.0)
         CST = (CST+AMAX1(0.0,FS))
         IF (I.EQ.2) THEN
            CST= (AKAS(I)*DT)/(SLAB(2)/2.0)
            CST = CST*(1.0/(1.0+2.0*AKAS(I)/(SLAB(2)*HRG)))
         ENDIF
         DENOM= X(I)*12.0/44.0+(1.0-X(I))*12.0/28.0
         SC = (DH1*X(I)*12.0/44.0)/DENOM
         SC = SC+(DH2*(1.0-X(I))*12.0/28.0)/DENOM
       SC = (G1(I)*SC)*SSCO(I)*SLAB(I)*DT
       DST = (1.0-VOIDO(I))*SLAB(I)*RHOSO(I)*CPSO(I)*(TSO(I)-TREF)
       DST = DST+H(I)*SSBO(I)*(TG(I)-TSI(I))*SLAB(I)*DT+SC
C   NOTE: ENTHALPY OF PYROLYSIS IS PER UNIT MASS FUEL, NOT PRODUCT
       DST = DST+RP(I)*HPYRO/(1.-CARB)*DT*SLAB(I)
         IF (I.EQ.IG+1) THEN
            DST = DST-(1.0-GRTSOL)*HRB*(TSB-TS(1))*DT
         ENDIF
         AST = (1.0-VOID(I))*RHOS(I)*SLAB(I)*CPSB(I)
```

```
     &         +(1.0-VOID(I))*RHOS(I)*CPSB(I)*DHTDT*DT*DZETA(I)
        SP = G2(I)*DH3*SSCO(I)*SLAB(I)*DT
          IF ((I.NE.IT-1).AND.(I.NE.2)) THEN
C              AST = AST+BST+CST+FN-FS-SP/TSI(I)
             AST = AST+BST+CST+FN-FS-SP/(TSI(I)-TREF)
          ENDIF
          IF (I.EQ.IT-1) THEN
           AST = AST+BST+CST-FS-SP/(TSI(I)-TREF)
             DST = DST-FN*(TCOAL-TREF)
          ENDIF
          IF (I.EQ.2) THEN
           AST = AST+BST+CST+FN-SP/(TSI(I)-TREF)
           DST = DST+FS*(TSG-TREF)
          ENDIF
          PST(I) = BST/(AST-CST*PST(I-1))
          QST(I) = CST*QST(I-1)+DST
        QST(I) = QST(I)/(AST-CST*PST(I-1))
10     CONTINUE
       DO 11 I=IT-1,2,-1
        TSC(I) = PST(I)*TSC(I+1)+QST(I)
          TS(I)=TSC(I)+TREF
          TESTTS(I) = ABS(TS(I)-TSI(I))
11     CONTINUE
       RETURN
       END

*************************************************************************
       SUBROUTINE TDMAYW(WC,YW,YWO,VOIDO,XCO,HT,W,YCHAR
      &                  ,RHOF,RHOFO)

*      CALCULATES THE MASS FRACTION OF UNCONVERTED WOOD

       PARAMETER (N=50)
       PARAMETER (PI=3.141592654)
       DIMENSION VOID(N),SLAB(N),SSB(N),SSBO(N),RHOS(N),G(N),DZETA(N)
       DIMENSION TESTTG(N),TESTTS(N),TESTCO(N),TESTYW(N),TESTP(N)
       DIMENSION DIAMC(N),SSC(N),SSCO(N),XC(N)
       DIMENSION PYW(N),QYW(N),YW(N),RHOF(N),RHOFO(N)
       DIMENSION WC(N),YWO(N),VOIDO(N),XCO(N),YCHAR(N),YWI(N)
       DIMENSION GV(N),RP(N),W(N)
       COMMON/DEVOL/GV,AVV,EVV,RP,COVOL,CO2VOL,HPYRO
       COMMON/BED/VOID,E,SLAB,SSB,SSBO,RHOS,G,DHTDT,DZETA
       COMMON/WCHAR/CARB,DIAMC,RHOC,VOIDC,SPHERC,SSC,SSCO,XC
       COMMON/ASH/ASH,DIAMA,RHOA,VOIDA,SPHERA,IBUILD
       COMMON/TIME/IFLAG,ITIME,ITERNS,TURNS,IB,IG,ICOB,TIMES,DT
       COMMON/TEST/TESTTG,TESTTS,TESTCO,CRIT,TESTYW,TESTP

       DO 9 I=1,IG+IB-1
       YWI(I) = YW(I)
       IF (YWI(I).EQ.0.0) YWI(I) = 1.0E-6
9      CONTINUE

C  THESE VALUES ARE USED TO CALCULATE THE INITIAL VALUES AT THE TOP OF
C  THE BED.
          AYW = 1.0
          BYW = 0.0
          CYW = 0.0
```

```
C THIS DYW SETS YW IN FEED (FEED ASSUMED PURE WOOD UNLESS PURE C
SPECIFIED)
      IF(CARB.NE.0) THEN
        DYW = 1.0
      ELSE
        DYW=0.
      END IF
      PYW(IB+IG) = BYW/AYW
      QYW(IB+IG) = DYW/AYW

      DO 10 I=IB+IG-1,IG+1,-1
         SCYW = 0.0
         SPYW = -RP(I)/((1-CARB)*YWI(I))
       SPYW = SPYW*SLAB(I)*DT
       AOYW = RHOF(I)*XC(I)*(1.0-VOID(I))*SLAB(I)
       AYW = AOYW-SPYW+AMAX1(WC(I)*DT,0.0)
     &              +AMAX1(-WC(I-1)*DT,0.0)
       BYW = AMAX1(-WC(I)*DT,0.0)
       CYW = AMAX1(WC(I-1)*DT,0.0)
       DYW1 = RHOFO(I)*XCO(I)*(1.0-VOIDO(I))*YWO(I)
     &           * DZETA(I)*(HT-DHTDT*DT)
       DYW = DYW1 +SCYW
       PYW(I) = CYW/(AYW-BYW*PYW(I+1))
       QYW(I)=(BYW*QYW(I+1)+DYW)
       QYW(I)=QYW(I)/(AYW-BYW*PYW(I+1))
10    CONTINUE

      YW(IG+1) = QYW(IG+1)
      YCHAR(IG+1) = 1.0-YW(IG+1)
      W(IG+1) = YW(IG+1)*CARB/(1-YW(IG+1)*(1-CARB))

      DO 11 I=IG+2,IG+IB-1
       YW(I) = PYW(I)*YW(I-1)+QYW(I)
       YCHAR(I) = 1.0-YW(I)
       W(I) = YW(I)*CARB/(1-YW(I)*(1-CARB))
11    CONTINUE
      RETURN
      END

*****************************************************************************

      SUBROUTINE HEIGHT(HT,RHOB,RHOBO)

*     CALCULATES THE CHANGE IN THE BED HEIGHT

      PARAMETER (N=50)
      DIMENSION VOID(N),SLAB(N),SSB(N),SSBO(N),RHOS(N),G(N),DZETA(N)
      DIMENSION DIAMC(N),SSC(N),SSCO(N),XC(N)
      DIMENSION GV(N),RP(N)
      COMMON/DEVOL/GV,AVV,EVV,RP,COVOL,CO2VOL,HPYRO
      COMMON/BED/VOID,E,SLAB,SSB,SSBO,RHOS,G,DHTDT,DZETA
      COMMON/WCHAR/CARB,DIAMC,RHOC,VOIDC,SPHERC,SSC,SSCO,XC
      COMMON/TIME/IFLAG,ITIME,ITERNS,TURNS,IB,IG,ICOB,TIMES,DT

      CGONE = 0.0
      VGONE = 0.0
      DO 9 I=IG+1,IG+IB-1
```

```
      CGONE = CGONE+G(I)*SSC(I)*DZETA(I)
        VGONE = VGONE+GV(I)*SSC(I)*DZETA(I)
9     CONTINUE
      CGONE = CGONE*HT
      VGONE = VGONE*HT
      RHOB = 0.0
      DO 11 I=IG+1,IG+IB-1
      RHOB = RHOB+RHOS(I)*(1.0-VOID(I))*DZETA(I)
11    CONTINUE
      DHTDT = -1.0/RHOBO*(CGONE+VGONE+HT*(RHOB-RHOBO)/DT)
      RETURN
      END

*****************************************************************************

      SUBROUTINE STOCK(TG,TGI,TGO,TS,TSO,TSI,APHI,APHIO,VOIDO,RHOSO,
     &          XCO,CGONE,VGONE,DTEMP,HT,HTO,RHOB,RHOBO,RHOFO,W,RHOF,WO,
     &          YWO,YW,WC,WCO,CPG,CPGO)

      PARAMETER (N=50)
      DIMENSION TG(N),TGI(N),TGO(N),TS(N),TSO(N),TSI(N),CPG(N),CPGO(N)
      DIMENSION WC(N),VOIDO(N),XCO(N),RHOSO(N),APHI(N),APHIO(N)
      DIMENSION VOID(N),SLAB(N),SSB(N),SSBO(N),RHOS(N),G(N),DZETA(N)
      DIMENSION DIAMC(N),SSC(N),SSCO(N),XC(N)
      DIMENSION WG(N),RHOG(N),RHOGO(N)
      DIMENSION Y8O2(N),Y8CO2(N),Y8CO(N),Y8N2(N),Y8O2O(N),Y8CO2O(N)
      DIMENSION Y8COO(N),Y8N2O(N),Y8P(N),Y8PO(N)
      DIMENSION TESTTG(N),TESTTS(N),TESTCO(N),TESTYW(N),TESTP(N)
      DIMENSION GV(N),RP(N),W(N),WO(N)
      DIMENSION RHOF(N),RHOFO(N)
      DIMENSION YWO(N),YW(N),WCO(N)
      COMMON/DEVOL/GV,AVV,EVV,RP,COVOL,CO2VOL,HPYRO
      COMMON/BED/VOID,E,SLAB,SSB,SSBO,RHOS,G,DHTDT,DZETA
      COMMON/WCHAR/CARB,DIAMC,RHOC,VOIDC,SPHERC,SSC,SSCO,XC
      COMMON/GAS/WG,RHOG,RHOGO
      COMMON/Y/Y8O2,Y8CO2,Y8CO,Y8N2,Y8O2O,Y8CO2O,Y8COO,Y8N2O,Y8P,Y8PO
      COMMON/GE/A,A1,ER,E1,ALPHA1,ALPHA2
      COMMON/TIME/IFLAG,ITIME,ITERNS,TURNS,IB,IG,ICOB,TIMES,DT
      COMMON/TEST/TESTTG,TESTTS,TESTCO,CRIT,TESTYW,TESTP

      IFLAG = 3
      DO 10 I=2,IG+IB-1
       CRIT = AMAX1(TESTTS(I),TESTTG(I))/(IG+IB)
       IF (CRIT.GT.0.02) THEN
          IFLAG = 2

         ENDIF
         CRITCO = TESTCO(I)/(IG+IB)
       IF (CRITCO.GT.1.0E-5) THEN
*      IF (CRITCO.GT.0.5E-05) THEN
            IFLAG = 2
       ENDIF
10    CONTINUE

      IF ((IFLAG.EQ.3).OR.(IFLAG.EQ.4)) THEN
*     CALCULATE THE CARBON CONSUMPTION AND DEVOL. RATE
         CGONE = 0.0
```

```
        VGONE = 0.0
       DO 9 I=IG+1,IG+IB-1
            CGONE = CGONE+(G(I))*SSC(I)*DZETA(I)
            VGONE = VGONE+(GV(I))*SSC(I)*DZETA(I)
9      CONTINUE
        CGONE = CGONE*HT
        VGONE = VGONE*HT
*     CALCULATE THE NEW BED HEIGHT
       IF (ITIME.EQ.0) THEN
          HTO = HT
       ENDIF
       HT = HTO+DHTDT*DT
       RHOBO = RHOB
       HTO = HT

        TURNS = ITERNS
        DTEMP = 0.0
       DO 12 I=1,IG+IB
            DTEMP = DTEMP+ABS(TG(I)-TGO(I))+ABS(TS(I)-TSO(I))
            TGO(I) = TG(I)
            Y8O2O(I) = Y8O2(I)
            Y8CO2O(I) = Y8CO2(I)
            Y8COO(I) = Y8CO(I)
            Y8PO(I)=Y8P(I)
          RHOGO(I) = RHOG(I)
            RHOFO(I) = RHOF(I)
            CPGO(I)=CPG(I)
12     CONTINUE

       DO 13 I=2,IG+IB-1
          TSO(I)=TS(I)
          XCO(I) = XC(I)
13     CONTINUE
       DO 14 I=IG+1,IG+IB-1
          SSBO(I) = SSB(I)
            SSCO(I) = SSC(I)
            APHIO(I) = APHI(I)
            VOIDO(I) = VOID(I)
          RHOSO(I) = RHOS(I)
          WO(I) = W(I)
          YWO(I) = YW(I)
          WCO(I) = WC(I)
14     CONTINUE
      ELSE
       DO 15 I=2,IG+IB-1
            TG(I) = ALPHA1*TG(I)+(1.0-ALPHA1)*TGI(I)
          TS(I) = ALPHA2*TS(I)+(1.0-ALPHA2)*TSI(I)
15     CONTINUE
       IFLAG = 2
      ENDIF

*     UPDATE DENSITY
      DO 16 I=2,IG+IB
       RHOG(I) = DENS(TG(I),I)
16    CONTINUE
      RETURN
      END
```

```
************************************************************************

      SUBROUTINE PRINT(IO,TG,TS,WS,WC,AKAS,CGONE,VGONE,XB,RHOF,
     &                 YW,W)

      PARAMETER (N=50)
      DIMENSION TG(N),TS(N),WS(N),WC(N),AKAS(N),XB(N)
      DIMENSION VOID(N),SLAB(N),SSB(N),SSBO(N),RHOS(N),G(N),DZETA(N)
      DIMENSION DIAMC(N),SSC(N),SSCO(N),XC(N)
      DIMENSION WG(N),RHOG(N),RHOGO(N)
      DIMENSION Y8O2(N),Y8CO2(N),Y8CO(N),Y8N2(N),Y8O2O(N),Y8CO2O(N)
      DIMENSION Y8COO(N),Y8N2O(N),Y8P(N),Y8PO(N)
      DIMENSION Y8O2PR(N),Y8COPR(N),Y8C2PR(N)
      DIMENSION YRO2(N),YRCO2(N),YRCO(N),YRN2(N),YRP(N)
      DIMENSION Y8O2M(N),Y8CO2M(N),Y8COM(N),Y8PM(N),Y8N2M(N)
      DIMENSION XN(N),UNBURNTC(N)
      DIMENSION VG(N),VS(N),VC(N)
      DIMENSION GV(N),RP(N),W(N),yrh2o(n)
      DIMENSION AMASSC(N)
      DIMENSION SCP(N)
      DIMENSION RHOF(N),YW(N),y8ppr(n)
      common/water/xh2o,rhow,yrh2o
      COMMON/DEBUB/AMASSC,ALEFF,SCP
      COMMON/DEVOL/GV,AVV,EVV,RP,COVOL,CO2VOL,HPYRO
      COMMON/BED/VOID,E,SLAB,SSB,SSBO,RHOS,G,DHTDT,DZETA
      COMMON/WCHAR/CARB,DIAMC,RHOC,VOIDC,SPHERC,SSC,SSCO,XC
      COMMON/GAS/WG,RHOG,RHOGO
      COMMON/Y/Y8O2,Y8CO2,Y8CO,Y8N2,Y8O2O,Y8CO2O,Y8COO,Y8N2O,Y8P,Y8PO
      COMMON/YR/YRO2,YRCO2,YRCO,YRN2,YRP
      COMMON/INFO/WTN2,WTO2,WTCO2,WTCO,R,P,BETA,GAMMA,THI,WTP,TREF
      COMMON/TIME/IFLAG,ITIME,ITERNS,TURNS,IB,IG,ICOB,TIMES,DT
      COMMON/V/VG,VS,VC

      TIMEH = AINT(TIMES/3600.0)
      TIMEM = (TIMES/3600.0-TIMEH)*60.0
C     SET IMFLAG TO 1 FOR GAS CONCS. IN MASS FRACTION, TO 0 FOR VOL.
      IMFLAG = 1
      WRITE(IO,132) TIMES,TIMEH,TIMEM
132   FORMAT(/,'     TIME = ',F6.0,' SEC.;  ',F3.0,' HOURS ',F4.1,
     &       ' MIN.')
      WRITE(IO,130)
      IF(IMFLAG.EQ.0)THEN
      WRITE(IO,134)
      ELSE
      WRITE(IO,139)
      ENDIF
      DO 10 J=1,IB+IG
         XN(J) = (XB(J)-0.5*SLAB(J))
      IF(IMFLAG.EQ.0)THEN
C CALCULATE VOLUME FRACTIONS OF GAS SPECIES WITHOUT TAR FOR PRINTOUT
         AMW=Y8O2(J)/WTO2+Y8CO2(J)/WTCO2+Y8CO(J)/WTCO+Y8N2(J)/WTN2
         AMW=AMW/(Y8O2(J)+Y8CO2(J)+Y8CO(J)+Y8N2(J))
         AMW=1./AMW
         Y8O2PR(J) = Y8O2(J)*AMW/WTO2
         Y8C2PR(J) = Y8CO2(J)*AMW/WTCO2
         Y8COPR(J) = Y8CO(J)*AMW/WTCO
```

```
      ELSE
C CALCULATE MASS FRACTIONS OF GAS SPECIES WITHOUT TAR FOR PRINTOUT
         YMTOTAL=Y8O2(J)+Y8CO2(J)+Y8CO(J)+Y8N2(J)
         Y8O2PR(J) = Y8O2(J)/YMTOTAL
         Y8C2PR(J) = Y8CO2(J)/YMTOTAL
         Y8COPR(J) = Y8CO(J)/YMTOTAL
       ENDIF
C TAR QUANTITY PER UNIT FUEL
C       Y8PPR(J)=Y8P(J)*WG(J)/(-VS(IB+IG))
C     TAR MASS PER UNIT MASS OF GASEOUS PRODUCTS (WITHOUT TAR)
        Y8PPR(J)=Y8P(J)/(1.-Y8P(J))
       IF (J.LE.IG) THEN
          UNBURNTC(J) = 0.0
       ELSE
C            UNBURNTC(J) = DIAMC(J)**3.0/DIAMC(IG+IB)**3.0
           UNBURNTC(J) = RHOF(J)*DIAMC(J)**3.0/RHOF(IB+IG)/
     &DIAMC(IG+IB)**3.0
       ENDIF
      WRITE(IO,135)
J,XN(J)*100.,Y8O2PR(J),Y8C2PR(J),Y8COPR(J),y8ppr(j),
     &          XC(J),UNBURNTC(J),
     &
G(J),GV(J),TG(J),TS(J),DIAMC(J)*100.0,VOID(J),VG(J),AKAS(J),
     &   CPS(TS(J),J,RHOF(J),YW(J)),SSB(J),WC(J),(VG(J)+WS(J)),SSCO(J),
     &      W(J),RHOF(J),Y8P(J),YRP(J),
     &          YW(J)
10    CONTINUE
      WRITE(*,137) VGONE,VGONE*3600.0,VGONE*2.2*0.0929*3600.0
      WRITE(IO,137) VGONE,VGONE*3600.0,VGONE*2.2*0.0929*3600.0
137   FORMAT(6X,'PYROLYSIS RATE: ',F7.5,' KG/M2 S; ',F7.2,' KG/M2 HR;
',
     &       F7.2,' LB/FT2 HR')
      WRITE(*,136) CGONE,CGONE*3600.0,CGONE*2.2*0.0929*3600.0
      WRITE(IO,136) CGONE,CGONE*3600.0,CGONE*2.2*0.0929*3600.0
136   FORMAT(6X,'CHAR BURNING RATE: ',F7.5,' KG/M2 S; ',F7.2,' KG/M2
HR;
     & ', F7.2,' LB/FT2 HR')
      WRITE(*,138) -VS(IG+IB),-VS(IG+IB)*3600.,-VS(IG+IB)*2.2*0.0929
     &*3600.
      WRITE(IO,138) -VS(IG+IB),-VS(IG+IB)*3600.,-VS(IG+IB)*2.2*0.0929
     &*3600.
138   FORMAT(6X,'FUEL FEED RATE: ',F7.5,' KG/M2 S; ',F7.2,' KG/M2 HR;
     & ', F7.2,' LB/FT2 HR')
130   FORMAT(/,3X,'I',6X,'X',7X,'O2',6X,'CO2',5X,'CO',7X,'TAR',6x,
     &   'XF',4X,'UNBURNT F',6X,'G',9X,'GV',
     &   10X,'TG',8X,'TS',6X,'DIAM',5X,'VOID',5X,'VG',6X,'AKAS',6X,
     &   'CPS',6X,'SSAB',6X,'WC',6X,'VG+WS',7X,'SSCO',8X,'W',
     &   7X,'RHOF',6X,'Y8P',5X,'YRP',
     &       7X,'YW')
134   FORMAT(10X,'CM',6X,'VOL. FRACT. W/O TAR',3X,'KG/KG GAS ',21X,
     &   'KG/M2S',5X,'KG/M2S',7X,'K',9X,'K',9X,'CM ',13X,'KG/M2S',3X,
     &   'W/M K',3X,'J/KG K',75X,'MASS FRACT.')
139   FORMAT(10X,'CM',6X,'MASS FRACT. W/O TAR',3X,'KG/KG GAS ',21X,
     &   'KG/M2S',5X,'KG/M2S',7X,'K',9X,'K',9X,'CM ',13X,'KG/M2S',3X,
     &   'W/M K',3X,'J/KG K',75X,'MASS FRACT.')
135   FORMAT(1X,I3,3X,F7.2,3X,F5.4,3X,F5.4,3X,F5.4,2X,F6.4,3x
     &       ,F7.5,3X,F7.5
```

```
     &    ,1X,E9.1,3X,E10.2 ,3X,F7.1,3X,F7.1
     &    ,3X,F6.4,3X,F5.3,3X,F7.5,3X,F6.3,3X,F6.1,3X,F6.1,3X,F7.5,
     &        3X,F7.5,3X
     &        ,E10.2,3X,F6.3,1X,F6.1,3X,F8.3,1X,F8.3
     &        ,3X,F10.5,3x,F10.5)
      SUMDEVOL=0.
      SUMDEV2=0.
      DO 141 J = 1,IB+IG
      SUMDEVOL=SUMDEVOL+RP(J)*SLAB(J)
      SUMDEV2=SUMDEV2+GV(J)*SLAB(J)*SSCO(J)
 141  CONTINUE
 140  FORMAT(1X,I3,5(1X,F8.5),F7.5,3(E10.3))
C CALCULATE PRODUCT QUANTITIES NORMALIZED BY FUEL FEED RATE
C NOTE THAT THESE ARE CONVECTION TERMS ONLY - SINCE THEY DON'T INCLUDE
C DIFFUSION, THEY MAY APPEAR TO VIOLATE A MASS BALANCE (BUT THEY DON'T)
      WRITE(9,132) TIMES,TIMEH,TIMEM
      WRITE(9,151)
151   FORMAT(/,'PRODUCT QUANTITIES IN KG PER KG FUEL FIRED')
      WRITE(9,152)
152   FORMAT(/,3X,'I',6X,'X',6X,'O2',6X,'CO2',5X,'CO',7X,'TAR',7x,
     &       'N2',6X,'SUM',5X,'UNBURNT F',7X,'DIAM',5X,'YW')
      DO 11 J=1,IB+IG
      FACTOR=WG(J)/(-VS(IB+IG))
      Y8O2M(J)=Y8O2(J)*FACTOR
      Y8CO2M(J)=Y8CO2(J)*FACTOR
      Y8COM(J)=Y8CO(J)*FACTOR
      Y8PM(J)=Y8P(J)*FACTOR
      Y8N2M(J)=Y8N2(J)*FACTOR
      SUMYM=Y8O2M(J)+Y8CO2M(J)+Y8COM(J)+Y8PM(J)+Y8N2M(J)
      WRITE(9,150) J,XN(J)*100.,Y8O2M(J),Y8CO2M(J),Y8COM(J),Y8PM(J),
     &Y8N2M(J),SUMYM,UNBURNTC(J),DIAMC(J)*100.0,YW(J)
11    CONTINUE
150   FORMAT(1X,I3,3X,F7.2,6(2X,F6.3),
     &       3X,F7.5,3X,F7.1,3X,F10.5)
      RETURN
      END

*****************************************************************************

      SUBROUTINE GRAPHING(IO,XB,AMWG,TG,TS)

      PARAMETER (N=50)
      DIMENSION XB(N),AMWG(N),TG(N),TS(N)
      DIMENSION VOID(N),SLAB(N),SSB(N),SSBO(N),RHOS(N),G(N),DZETA(N)
      DIMENSION Y8O2(N),Y8CO2(N),Y8CO(N),Y8N2(N),Y8O2O(N),Y8CO2O(N)
      DIMENSION Y8COO(N),Y8N2O(N),Y8P(N),Y8PO(N)
      COMMON/BED/VOID,E,SLAB,SSB,SSBO,RHOS,G,DHTDT,DZETA
      COMMON/Y/Y8O2,Y8CO2,Y8CO,Y8N2,Y8O2O,Y8CO2O,Y8COO,Y8N2O,Y8P,Y8PO
      COMMON/INFO/WTN2,WTO2,WTCO2,WTCO,R,P,BETA,GAMMA,THI,WTP,TREF
      COMMON/TIME/IFLAG,ITIME,ITERNS,TURNS,IB,IG,ICOB,TIMES,DT

*     NOTE: THESE EQUATIONS ARE DIFFERENT FOR EACH EXPERIMENT

      XS = 6.0045-0.0527*TIMES/60.0
      IF (XS.LT.2.9) THEN
       XS = 3.6358-0.0116*TIMES/60.0
      ENDIF
```

```
      DO 10 I=IG+1,IG+IB
       DELTA = SLAB(I)/2.0*100.0
       X = XB(I)*100.0-DELTA
       IF ((X.GT.(XS-DELTA)).AND.(X.LT.(XS+DELTA))) THEN
          O2PLOT = Y8O2(I)*AMWG(I)/WTO2*100.0
          CO2PLOT = Y8CO2(I)*AMWG(I)/WTCO2*100.0
          COPLOT = Y8CO(I)*AMWG(I)/WTCO*100.0
          TGPLOT = TG(I)
          TSPLOT = TS(I)
          WRITE(IO,100) TIMES/60.0,XS,O2PLOT,CO2PLOT,COPLOT,TGPLOT,
     &              TSPLOT
       ENDIF
10     CONTINUE
100    FORMAT(1X,F5.1,3X,F6.3,3X,F5.2,3X,F5.2,3X,F5.2,3X,F6.1,3X,F6.1)
       RETURN
       END

*****************************************************************************

       SUBROUTINE ENERGY(TG,TS,WS,CPG,ERROR,RHOF,YW)

       PARAMETER (N=50)
       DIMENSION TG(N),TS(N),WS(N),CPG(N),RHOF(N)
       DIMENSION WG(N),RHOG(N),RHOGO(N)
       DIMENSION Y8O2(N),Y8CO2(N),Y8CO(N),Y8N2(N),Y8O2O(N),Y8CO2O(N)
       DIMENSION Y8COO(N),Y8N2O(N),Y8P(N),Y8PO(N),YW(N)
       COMMON/GAS/WG,RHOG,RHOGO
       COMMON/Y/Y8O2,Y8CO2,Y8CO,Y8N2,Y8O2O,Y8CO2O,Y8COO,Y8N2O,Y8P,Y8PO
       COMMON/RAD/TSG,TSB,TSW,HRG,HRB,HRW,F12B,BOLTZ,TCOAL
       COMMON/GRATE/GRATE,GRTSOL,GRTBAR,IGMOD,GRTRHO,GRTPD,GRTSPACE
       COMMON/FLUXES/FO2,FC,FCO2,FP,FTG,FTS
       COMMON/TIME/IFLAG,ITIME,ITERNS,TURNS,IB,IG,ICOB,TIMES,DT
       COMMON/INFO/WTN2,WTO2,WTCO2,WTCO,R,P,BETA,GAMMA,THI,WTP,TREF

       IT = IB+IG
       T = TCOAL
       ENIN = FTG+BOLTZ*(TS(1)**4.0-TSG**4.0)*GRTSOL
      &           +BOLTZ*F12B*(TS(1)**4.0-TSB**4.0)
       IF (WS(1).LT.0.0) THEN
          ENIN = ENIN+WS(1)*(TSG-TREF)*CPS(TSG,I,RHOF(1),YW(1))
       ENDIF
       ENOUT = WG(IT)*CPG(IT)*(TG(IT)-TREF)+BOLTZ*F12W(HT)
      &          * (TSW**4.0-TS(IT)**4.0)
       ENOUT = ENOUT+WS(IT)*(TCOAL-TREF)*CPS(T,I,RHOF(IT),YW(IT))
       ENB = ENOUT-ENIN
       ENR = (WG(IT)*Y8CO(IT)-FC)*9.3E06*12.0/28.0
       ENR = ENR+(WG(IT)*Y8CO2(IT)-FCO2)*32.8E06*12.0/44.0
       ERROR = 100.0*(ENB-ENR)/AMIN1(ENB,ENR)
       RETURN
       END

*****************************************************************************

       REAL FUNCTION F(V,I,GWEST)

*      WESTMAN EQUATION
```

```
      PARAMETER (N=50)
      DIMENSION DIAMC(N),SSC(N),SSCO(N),XC(N)
      COMMON/WCHAR/CARB,DIAMC,RHOC,VOIDC,SPHERC,SSC,SSCO,XC
      COMMON/ASH/ASH,DIAMA,RHOA,VOIDA,SPHERA,IBUILD

      VOIDL = VOIDC
      VOIDS = VOIDA
      XL = XC(I)
      XS = 1.0-XC(I)
      SVL = 1.0/(1.0-VOIDL)
      SVS = 1.0/(1.0-VOIDS)
      F = ((V-SVL*XL)/SVS)**2.0
     &         +2.0*GWEST*((V-SVL*XL)/SVS)*((V-XL-SVS*XS)/(SVL-1.0))
     &         +((V-XL-SVS*XS)/(SVL-1.0))**2.0-1.0
      RETURN
      END

*************************************************************************

      REAL FUNCTION DF(V,I,GWEST)

*     DERIVATIVE OF THE WESTMAN EQUATION

      PARAMETER (N=50)
      DIMENSION DIAMC(N),SSC(N),SSCO(N),XC(N)
      COMMON/WCHAR/CARB,DIAMC,RHOC,VOIDC,SPHERC,SSC,SSCO,XC
      COMMON/ASH/ASH,DIAMA,RHOA,VOIDA,SPHERA,IBUILD

      VOIDL = VOIDA
      VOIDS = VOIDC
      XL = 1.0-XC(I)
      XS = XC(I)
      SVL = 1.0/(1.0-VOIDL)
      SVS = 1.0/(1.0-VOIDS)
      DF = 2.0*((V-SVL*XL)/SVS)*(1.0/SVS)
     &         +2.0*GWEST*((V-SVL*XL)/SVS)*(1.0/(SVL-1.0))
     &         +2.0*GWEST*(1.0/SVS)*((V-XL-SVS*XS)/(SVL-1.0))
     &         +2.0*((V-XL-SVS*XS)/(SVL-1.0))*(1.0/(SVL-1.0))
      RETURN
      END

*************************************************************************

      REAL FUNCTION DENS(T,I)

*     CALCULATES THE GAS DENSITY

      PARAMETER (N=50)
      DIMENSION Y8O2(N),Y8CO2(N),Y8CO(N),Y8N2(N),Y8O2O(N),Y8CO2O(N)
      DIMENSION Y8COO(N),Y8N2O(N),Y8P(N),Y8PO(N)
      COMMON/Y/Y8O2,Y8CO2,Y8CO,Y8N2,Y8O2O,Y8CO2O,Y8COO,Y8N2O,Y8P,Y8PO
      COMMON/INFO/WTN2,WTO2,WTCO2,WTCO,R,P,BETA,GAMMA,THI,WTP,TREF

      STORE = (Y8O2(I)/WTO2)+(Y8CO(I)/WTCO)+(Y8CO2(I)/WTCO2)
      STORE = 1.0/(STORE+(Y8N2(I)/WTN2)+(Y8P(I)/WTP))
      DENS = P*STORE/(R*T)
```

```
      RETURN
      END

*****************************************************************************

      REAL FUNCTION CPS(T,I,RHOFU,YW)

*     CALCULATES THE SOLID HEAT CAPACITIES

      PARAMETER (N=50)
      DIMENSION DIAMC(N),SSC(N),SSCO(N),XC(N)
      COMMON/WCHAR/CARB,DIAMC,RHOC,VOIDC,SPHERC,SSC,SSCO,XC
      COMMON/ASH/ASH,DIAMA,RHOA,VOIDA,SPHERA,IBUILD
      COMMON/GRATE/GRATE,GRTSOL,GRTBAR,IGMOD,GRTRHO,GRTPD,GRTSPACE
      COMMON/INFO/WTN2,WTO2,WTCO2,WTCO,R,P,BETA,GAMMA,THI,WTP,TREF
      COMMON/TIME/IFLAG,ITIME,ITERNS,TURNS,IB,IG,ICOB,TIMES,DT
C MEAN SPECIFIC HEAT DEFINED FOR TEMPERATURES IN CELSIUS
      TC = T-273.15
      IF ((IGMOD.EQ.1).AND.(I.LE.IG)) THEN
         CPS = 754.0+0.293*TC
      ELSE IF ((IGMOD.EQ.2).AND.(I.LE.IG)) THEN
         CPS = 0.2087*TC+492.74
      ELSE
C     EXPRESSION FOR MEAN SP. HT. OF COKE
C         A = 1.0/12.0
C         X1 = 380.0/TREF
C         X1 = 1.0/(EXP(X1)-1.0)
C         X2 = 1800.0/TREF
C         X2 =  1.0/(EXP(X2)-1.0)
C         HCREF = (1000.0)*(R*A)*(380.0*X1+3600.0*X2)
C         X1 = 380.0/T
C         X1 = 1.0/(EXP(X1)-1.0)
C         X2 = 1800.0/T
C         X2 =  1.0/(EXP(X2)-1.0)
C         HC = (1000.0)*(R*A)*(380.0*X1+3600.0*X2)
C         IF(ABS(T-TREF).LT.5)THEN
C         CPC = (1000.0/T/T)*(R*A)*(380.0**2*(X1+X1**2)
C     1         +2.*1800.0**2*(X2+X2**2))
C         ELSE
C         CPC = (HC-HCREF)/(T-TREF)
C         ENDIF
C         CPC = (1000.0/T)*(R*A)*(380.0*X1+3600.0*X2)
C     EXPRESSION FOR MEAN SP. HEAT OF WOOD - GUPTA ET AL 2003
C      CPW = 2.73*(T+TREF)-524.77
C     EXPRESSION FOR MEAN SP. HEAT OF WOOD - GRONLI ET AL 2000
      CPW = 1500+0.5*(T+TREF)
C     EXPRESSION FOR MEAN SP. HEAT OF WOOD CHAR - LARFELDT 2000
      HC = 1430.*T+(0.355/2.)*T*T+7.32E07/T
      HCREF = 1430.*TREF+(0.355/2.)*TREF*TREF+7.32E07/TREF
         IF(ABS(T-TREF).LT.5)THEN
           CPC = 1430.+0.355*T-(7.32E07/T**2)
         ELSE
         CPC = (HC-HCREF)/(T-TREF)
         ENDIF
         CPA = 754.0+0.293*TC
         CPF = YW*CPW+(1.-YW)*CPC
         CPS = (RHOFU*XC(I)*CPF+RHOA*(1.0-XC(I))*CPA)
```

```
     &          /(RHOFU*XC(I)+RHOA*(1.0-XC(I)))
C       WRITE(8,*)T,CPW,CPC,YW,CPF
C          CPS = (RHOFU*XC(I)*CPC+RHOA*(1.0-XC(I))*CPA)
C     &          /(RHOFU*XC(I)+RHOA*(1.0-XC(I)))
      ENDIF
      RETURN
      END

*************************************************************************

      REAL FUNCTION CPGBAR(T,I)

*     CALCULATES THE SPECIFIC HEATS

      PARAMETER (N=50)
      DIMENSION Y8O2(N),Y8CO2(N),Y8CO(N),Y8N2(N),Y8O2O(N),Y8CO2O(N)
      DIMENSION Y8COO(N),Y8N2O(N),Y8P(N),Y8PO(N)
      DIMENSION G1(N),G2(N),X(N),S(N)
      DIMENSION CPGREG(N)
      COMMON/Y/Y8O2,Y8CO2,Y8CO,Y8N2,Y8O2O,Y8CO2O,Y8COO,Y8N2O,Y8P,Y8PO
      COMMON/INFO/WTN2,WTO2,WTCO2,WTCO,R,P,BETA,GAMMA,THI,WTP,TREF
      COMMON/STOIC/SCO2,SCO,S3,S2,DH1,DH2,DH3,DH4
      COMMON/REACT/G1,G2,X,S,IREACT
      COMMON/EXTRA/CPGREG

      Y8N2(I) = 1.0-Y8O2(I)-Y8CO(I)-Y8CO2(I)-Y8P(I)

*     VAN WYLEN AND SONNTAG SPECIFIC HEAT EXPRESSIONS.
*     THESE BEHAVE VERY STRANGELY BELOW 200 K,
*     SO THAT ONE MUST CALCULATE (h - h298) AND THEN ADD h AT 298 K
*     FROM PERFECT GAS TABLES TO GET CORRECT VALUES OF CP BAR.

      THET = T/100.0
      CPO2 = 37.432+0.020102*THET**1.5-178.57/(THET**1.5)
      CPO2 = (CPO2+236.88/THET/THET)/WTO2*1000.0
      CPCO = 69.145-0.70463*THET**0.75-200.77/(THET**0.5)
      CPCO = (CPCO+176.76/(THET**0.75))/WTCO*1000.0
      CPCO2 = -3.7357+30.529*THET**0.5-4.1034*THET
      CPCO2 = (CPCO2+0.024198*THET*THET)/WTCO2*1000.0
      CPN2 = 39.060-512.79/(THET**1.5)+1072.7/THET/THET
      CPN2 = (CPN2-820.40/(THET**3))/WTN2*1000.
* SPECIFIC HEAT FOR LEVOGLUCOSAN USING JOBACK CORRELATION
      CPP = (-26.539+0.8319*T-5.431E-4*T**2+1.4E-7*T**3)/WTP*1000.

      HO2 = 37.432*THET+0.020102/2.5*THET**2.5+178.57*2./(THET**0.5)
      HO2 = (HO2-236.88/THET)
      HCO = 69.145*THET-0.70463/1.75*THET**1.75-200.77*2.*(THET**0.5)
      HCO = (HCO+176.76*4.*(THET**0.25))
      HCO2 = -3.7357*THET+30.529/1.5*THET**1.5-4.1034/2.*THET**2
      HCO2 = (HCO2+0.024198/3.*THET**3)
      HN2 = 39.060*THET+512.79*2./(THET**0.5)-1072.7/THET
      HN2 = (HN2+820.40/2./(THET**2))
      HPP = -26.539*T+0.8319/2*T**2-5.431E-4/3*T**3+1.4E-7/4*T**4

      THT3 = TREF/100.
      HO23 = 37.432*THT3+0.020102/2.5*THT3**2.5+178.57*2./(THT3**0.5)
      HO23 = (HO23-236.88/THT3)
```

```
      HCO3 = 69.145*THT3-0.70463/1.75*THT3**1.75-200.77*2.*(THT3**0.5)
      HCO3 = (HCO3+176.76*4.*(THT3**0.25))
      HCO23 = -3.7357*THT3+30.529/1.5*THT3**1.5-4.1034/2.*THT3**2
      HCO23 = (HCO23+0.024198/3.*THT3**3)
      HN23 = 39.060*THT3+512.79*2./(THT3**0.5)-1072.7/THT3
      HN23 = (HN23+820.40/2./(THT3**2))
      HP3 = -26.539*TREF+0.8319/2*TREF**2-5.431E-4/3*TREF**3+
     1 1.4E-7/4*TREF**4
C MEAN SPECIFIC HEAT CPG BASED ON CELSIUS TEMPERATURE
      TC=T-TREF
      IF(ABS(TC).LT.10.)THEN
      CPO2B = CPO2
      CPCOB = CPCO
      CPCO2B = CPCO2
      CPN2B = CPN2
      ELSE
      CPO2B = ((HO2-HO23)*100.)/TC/WTO2*1000.0
      CPCOB = ((HCO-HCO3)*100.)/TC/WTCO*1000.0
      CPCO2B = ((HCO2-HCO23)*100.)/TC/WTCO2*1000.0
      CPN2B = ((HN2-HN23)*100.)/TC/WTN2*1000.0
      CPPB = (HPP-HP3)/TC/WTP*1000.0
      ENDIF

      CPEFF = (1.0+S(I))*CPCO-S(I)*CPO2
      CPGBAR = Y8O2(I)*CPO2B+Y8CO2(I)*CPCO2B
      CPGBAR = CPGBAR+Y8N2(I)*CPN2B+Y8CO(I)*CPCOB
      CPGBAR = CPGBAR + Y8P(I)*CPPB
      CPGREG(I) = Y8O2(I)*CPO2+Y8CO2(I)*CPCO2
      CPGREG(I) = CPGREG(I)+Y8N2(I)*CPN2+Y8CO(I)*CPCO
      CPGREG(I) = CPGREG(I)+Y8P(I)*CPP
      RETURN
      END

*****************************************************************************

      REAL FUNCTION F12W(HT)

*     EFFECTIVE VIEW FACTOR

      PARAMETER (N=50)
      DIMENSION VOID(N),SLAB(N),SSB(N),SSBO(N),RHOS(N),G(N),DZETA(N)
      COMMON/BED/VOID,E,SLAB,SSB,SSBO,RHOS,G,DHTDT,DZETA

      RH = 4.5/(8.0-(HT*100.0)/2.54)
      RX = 1.0+(1.0+RH**2.0)/RH**2.0
      F12 = 0.5*(RX-(RX**2.0-4.0)**0.5)
      F12W = 1.0/(2.0/(1.0+F12)+1.0/E-1.0)
      RETURN
      END
```

# RUN DATA INPUT FILE CODE

```
**********************************************************************
*RUN.DAT FILE
**********************************************************************
*****
IB  IG      TLIMIT  DT   ITCUT      IEND
30  10      18.E03 4.0   2          200
Mois  Rhow     COvol   CO2vol
0.064 998.0       .3      .3
DIAMC(M)    CARB   RHOC  VOIDC  SPHERC   E   TCOAL
0.028       0.15  79.8  0.47   0.77    0.8  300.0
DIAMA(M)    ASH   RHOA        VOIDA       SPHERA
0.00095     0.001 1030.0      0.45        0.60
HT(M)   U(1)     P(KPA)
0.22  0.025       101.92
A1        E1          A    ER
1.8e-4      100000.0 860.0 18000.0
IREACT IHTTR  IRXN  ICOB  IBUILD IFEED
  2   1970   1970   1      1    1
TS(1)  TG(1) TG(N)  TS(N) TIGNIT  ALAYER(M) IZONE
350.0  294.0  950.0  700.0  1200.0  0.1    0
IGRAPH IGRID
   1   0
IFIELD      IEFFECT   AI      TAU   VOIDP
  1 .         1   1.0E6       2     0.1
AV     EV     HEAT OF PYROLYSIS (J/KG)
0.05  20000       -5.38E05
```

# PROGRAM CONSTANT INPUT FILE CODE

```
**********************************************************************
* CONST.DAT FILE
**********************************************************************
R      BOLTZ   WTN2  WTO2  WTCO2  WTCO     WTP    WTh20
8.314  5.67E-08  28.0  32.0  44.0   28.0  162.0  33.0
BETA  GAMMA   THI   ALPHA1  ALPHA2
1.0    1.0   0.05   0.25   0.5
SCO      SCO2      S3     S2      DH1      DH2      DH3       DH4
1.3333  2.66667  0.571  3.667  32.79E06  9.21E06 -14.37E06  10.11E06
US(1)    G(1) G(N)
-0.0011  0.0   0.0
Y8O2(1)  Y8CO(1)  Y8CO2(1) Y8O2(N)  Y8CO(N)  Y8CO2(N)
0.232    0.001    0.003     0.232     0.001    0.003
IGMOD  GRATE(MM)  GRTPD(MM)  GRTSPACE(MM)  GRTBAR(MM)  GRTRHO
  2    19.05        13.7           3.3        3.05      7920.0
Y8P(1)       Y8P(N)
0.0          0.000
```

## Appendix B: Notes on Probe Design Calculations

This section provides further details on the probe design calculations. The goal of these calculations were to determine the amount of tar that could be cooled by the filter. A two dimensional axial heat transfer calculation was performed on the sample filter, as per the method of Patankar (1980). The inlet gas temperature and flowrate were set to 1200 K and 0.03 kg/m$^2$s, respectively. The cooling water temperature was set to 323 K. The filter properties (diameter, material, height) were modified to obtain the desired outlet gas temperature. The boundary conditions are shown in **Figure A1** below.

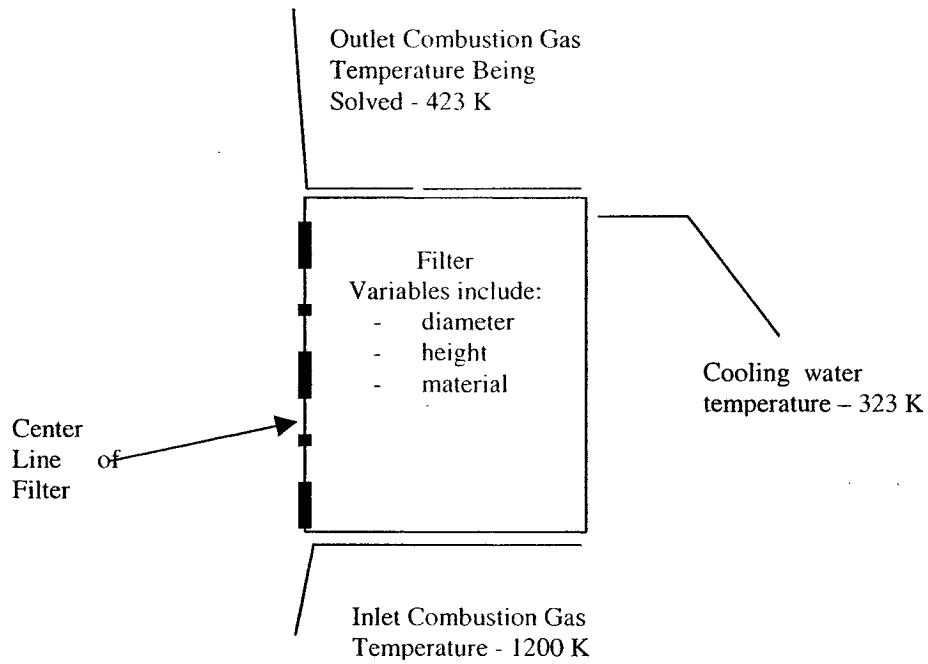


**Figure A-1: Boundary Conditions**

The thermal conductivity data used were those reported in Geankopolis (1993) for steel wool, ceramic and copper and stainless steel. For the nickel-chrome metal foam, the supplier thermal conductivity data was questionable (a linear relationship was shown from 0 to 900 K) but experimental calculation of thermal conductivities would produce results with greater uncertainty[1]. Therefore a thermal conductivity of 10% of the parent metal (0.19 W/mK) was used. This assumption overestimates the heat transfer resistance and therefore the actual heat transfer will be higher than that reported below. The range of thermal conductivities in the relevant range was 0.3 to 1 W/mK.

The heat transfer correlations for forced convection through a packed bed as proposed by Eckert and Goldstein (1976) and Bhattacharya and Pei (1975) were both tested to select the material. The heat transfer coefficient from Pei was calculated to be 1.12 and from Eckert to be between 2.60 to 4.46. Using the Eckert value and the average of the high and low temperatures at the top of the filter, h was calculated to be 3.57. This resulted in an outlet gas temperature of 390 to 453 K for a 1.13 cm diameter filter of 7 mm thickness when a cooling rate of 3.6 L/min was used. These preliminary calculations were based on a constant temperature height through a 0.7mm thickness of filter since this was the thickness of one sheet of Retimet (the metal-foam filter material). Two sheet thicknesses were determined to be required in the final design.

The design was then fine-tuned to determine the diameter and filter height to use in combination with various readily available tubing dimensions. The selected tubing dimensions have previously been described. The effect of changing the diameter from 1.13 cm to 1 cm was shown to only marginally decrease the outlet temperature from 883

[1] A method proposed of contacting solid spheres would result significant inaccuracies due to difficulties in measuring the solid temperature, accounting for the solid interface resistance, etc...

to 827 K. Maintaining the water temperature above 50°C and assuming an inlet gas temperature of 1000C, the sample gas should be cooled down to about 150 to 115°C as it exits the top of the filter[2].

[2] Calculations reported used a Geankoplis thermal conductivity constant. If the thermal conductivity by Pei was used the exit temperature estimate would increase to 400C.

## Appendix C: Radiation Calculation Method

For a single thermocouple, the energy equation is

$$h\,(T_g - T) = \sigma \varepsilon_T\,(T^4 - T_{2\infty}^4)$$

where h is the heat transfer coefficient for convection, $T_g$ is the gas temperature, T is the thermocouple temperature, $\sigma$ is the Stefan-Boltzmann constant = $5.76*10^{-8}$W/m$^2$K$^4$, $\varepsilon_T$ is the total emissivity of the thermocouple and, $T_2$ is the effective radiating temperature of the surroundings. Adding this equation for two different diameter thermocouples we obtain:

$$(h_1 - h_2)T_g + h_2T_2 - h_1T_1 = \sigma \varepsilon_T\,(T_1^4 - T_2^4)$$

This equation can then be solved for the gas temperature $T_g$ by using the heat transfer coefficient calculated at thermocouple tip conditions and the properties of the gas at the bed exit. For example during run 072202, the volume percent concentration of nitrogen measurement was 47% $N_2$.

Temperature readings taken above the bed using the radiation thermocouple are shown in **Table 5.4**. The readings from the two different diameter thermocouples profiles were very similar and ranged between 88°C to 350°C during the course of the experiment. The wide range in temperature readings could be due to the effect of the non-uniform volatile flame behaviour above the bed.

By using the measured nitrogen concentration from a gas sample taken near the top of the bed, the increase in gas mass at the top of the bed could be estimated. Using this corrected gas mass flow rate the Reynolds, Re, and Prandtl, Pr, numbers, the heat transfer coefficient, h, for a cylinder in a cross-flow could be calculated.

$$h = \frac{k}{d} C\,Re^n Pr^{1/3}$$

where k is thermal conductivity, d is the diameter of the thermocouple, C and n are constants depending on the Renoylds number for heat transfer to cylinders with axis perpendicular to flow as given by Geankoplis (1993).

Also in order to determine the radiation gas temperature the following energy balance was used, where $T_r$ is the radiation temperature:

$$h_A(T_A - T_g) = \sigma\varepsilon_T T_r^4 - \sigma\varepsilon_T (T_r^4 - T_A^4)$$

where $h_A$ and $T_A$ are the heat transfer coefficient and temperature reading of the 0.020 cm thermocouples.

And therefore for two thermocouples:

$$h_B T_B + h_A T_A - (h_A + h_B) T_g = 2\sigma\varepsilon_T T_r^4 - \sigma\varepsilon_T (T_A^4 - T_B^4)$$

where $h_B$ and $T_B$ are the heat transfer coefficient and temperature reading of the 0.038 cm thermocouples.